5-2018

Programming of Retention Capacity and Release Capabilities of Propargyl Acrylate Nanoparticles Decorated with Poloxamer Copolymer

Oleksandr Klep
Clemson University, oleksandrklep@gmail.com

PROGRAMMING OF RETENTION CAPACITY AND RELEASE CAPABILITIES OF PROPARGYL ACRYLATE NANOPARTICLES DECORATED WITH POLOXAMER COPOLYMER

A Dissertation
Presented to
the Graduate School of
Clemson University

In Partial Fulfillment
of the Requirements for the Degree
Doctor of Philosophy
Materials Science and Engineering

---

by
Oleksandr Klep
May 2018

Accepted by:
Dr. Stephen H. Foulger, Committee Chair
Dr. Konstantin Kornev
Dr. Igor Luzinov
Dr. Thompson Mefford

Abstract

Nanoparticle based drug delivery offers an advantage over free drug delivery as it allows the manufacturer to introduce various control mechanisms either for targeted delivery or for the controlled release profile of the drug. Systems capable to encapsulate different active molecules, ranging from dyes to drugs, gained a lot of attention in recent years. It was shown that it is possible to create a programmable device that can serve multiple functions ranging from enhanced imaging techniques to cancer treatment along with extended drug delivery applications. Therefore methods for fabrication and characterization of the devices that can be used in the medical field is in high demand. Proposed is a device build around propargyl acrylate nanoparticle along with a set of methods to fully characterize the final nanocomposite composition. The release rate of the active molecules from the proposed nanocomposite is compared to the composition of the device. The ability to program the release rate and set a burst release temperature for the device is essential for future advances in drug delivery application.

F*ö*rster Resonance Energy Transfer (FRET) was used to investigate the changes in the surface configuration. To do this, pair of dyes with good spectral overlap was attached to the propargyl acrylate core. The donor dye was immobilized on the surface of the core, while the acceptor dye was attached to the free end of the poloxamer chain. This setup allowed the acceptor dye to have a certain degree of

mobility. Based on the changes in the photo-luminescence spectra and applying the FRET theory distance between the dyes was correlated to the temperature of the environment. A possible mechanism of the surface configuration changes with temperature was suggested based on the obtained results.

The ability of propargyl acrylate - poloxamer complex to capture, retain and release when triggered small molecules is investigated. Often there is a need to protect or deactivate an active molecule before it reaches its target organ or tissue to prevent development of side-effects during treatment. Additionally, such a system can be used for waste water treatment applications to remove toxic organic contamination. The ability of the particles to trap and then release upon heating is advantageous compared to the systems that are capable of only trapping because it can be reused and serve the purpose of waste concentration to promote recycling of otherwise wasted materials.

Proposed is a scheme of synthesis and characterization of the carrier based on the propargyl acrylate nanoparticles coated with poloxamer copolymer. Carrier stability is greatly enhanced, compared to similar systems found in the literature. Advantage comes from the formation of a covalent bond between the core and the shell, ensuring that no changes of the nano-carrier composition can happen during its lifespan. This study shows the importance of the precise control over the grafting density of the poloxamer on the surface of propargyl acrylate nanoparticle. The ability to select various sizes of the nanoparticles and the selection of commercially available poloxamer copolymers provide the possibility to fine tune properties of the final carrier for the required task. The retention and release effectiveness was correlated to the nano-carriers composition and was shown on the example of Rhodamine B dye. The discovered principle of surface configuration changes during FRET section of this study helped with determination of the release mechanism.

Dedication

To my loving wife, Oksana Klep, whose unconditional love, support and encouragement provided me the strength and patience to pursue my dreams. To my parents, Viktor and Svitlana Klep, whose support and kind advice helped me through challenging times.

Acknowledgments

The research included in this dissertation could not be completed without all the help and support from many people. Foremost, I would like to express my thank you to my advisor Dr. Stephen H. Foulger for mentoring me over the course of my program, for teaching me how to use and more importantly how to trouble shoot various analytical instruments, for possibility to play with and learn how to operate an exceptional array of scientific tools. This work would not be possible without all the support and guidance from my academic advisor. Besides my advisor, I would like to thank the rest of my thesis committee members: Dr. Konstantin G. Kornev, Dr. Igor A. Luzinov and Dr. O. Thompson Mefford for their time and attention to the details that I have overlooked and for all the guidance through the challenging parts of my thesis. It is because of their knowledge and suggestions that this work was brought up to the high standard of PhD degree. Their experience in multitude of materials science aspects made it possible to fill my thesis with crucial details that made the work complete.

I would like to acknowledge the Department of Materials Science and Engineering, Department of Bioengineering and Center for Optical Materials Science and Engineering Technologies, for allowing me to conduct this research and providing assistance. I am thankful to the faculty and staff of these departments, particularly, Dr. Gary Lickfield, Ms. Tonya Bledsoe, Ms. Sam Bradberry, Ms. Sheryl

Gonzales and Ms. Wendy Baldwin for all their help with document processing, adaptation to new country and their time spend helping me to maintain my legal status in the country and keeping me on track with my PhD program requirements through constant reminders and follow-ups on all the document processing phases.

Also I want to say thank you to Ms. Kimberley Ivey for the countless hours she spend showing me the fine art of analysis using non trivial approaches, for all the support from her during hard times and for all her guidance through multiple instrument repairs and upgrades.

I would like to thank all my colleagues over the past years who have been with me during my journey to the PhD degree. I thank Dr. Yuriy Bandera for all the synthesis help and guidance. Dr. Bogdan Zdyrko, Ms. Katie Burdette, Mr. Tucker McFarlane, Dr. Ragini Jetty, Dr. Vladimyr Reukov, Ms. Olga Reukova, Mr. Myhaylo Savchak for their advices, support and camaraderie through all my years in Clemson.

I want to thank the Gregg-Graniteville Foundation and the National Science Foundation (DMR-1507266) for financial support of this project. It would be impossible for me to come to United States and complete this research without the financial support form these organization.

Table of Contents

List of Tables

List of Figures

Chapter 1

Introduction

Poloxamer block copolymer offers a unique set of properties that make it a potent candidate for the responsive component in drug delivery applications. Temperature responsive behavior combined with the ability of the poloxamer to encapsulate various organic molecules creates the possibility to design new devices that will have superior capabilities as compared to modern ones. One of the draw backs of the poloxamers is the fact that the micelles that they form are dynamic and sensitive to a wide range of environmental factors ranging from concentration dependence to solution ion strength. One of the possible solutions of this draw back is to immobilize poloxamer chains on the surface of the nanoparticle. Propargyl acrylate with its alkyne groups on the surface offers a versatile platform to build from. Poloxamer chains can be modified to include azide groups through which a strong and permanent bond between a propargyl acrylate nanoparticle and a poloxamer can be created. Immobilization of the poloxamer on the surface solves the micelle's instability issue since there is no possibility for the poloxamer to change its positioning with regards to its neighboring chains, thus any structure that can be adopted by the chains for a specific temperature condition will be independent of any con-

centration factors. Additionally propargyl acrylate core can be modified with other active moieties like dyes, for enhanced imaging applications; drugs, for extended drug delivery; targeting ligands, for targeted drug delivery creating a multifunctional carrier that can serve multiple functions at once.

A propargyl acrylate poloxamer nanocomposite (PAPN) production is simpler from the chemistry point of view but require more attention from the researcher on the characterization end of the device production when compared to other core shell systems. Most of the classical nanocomposite characterization techniques fall short when attempting to characterize polymer on polymer systems requiring some modifications to the technique or even a complete redesign of the method to adapt it for the proposed device. In this work a quick and reliable technique for PAPN characterization was developed and tested. Fourier transform infrared spectroscopy was used to determine the grafting density of the poloxamer chains on the propargyl acrylate surface with sufficient resolution and excellent reproducibility of the results. Through the use of the designed method differences between PAPNs with regard to the amount of the poloxamer on the surface were determined. It was found that control over grafting density of the poloxamer allows us to control how much of the drug can be released from the device. The ability to change the rate of drug release is essential when designing new drug delivery vesicles and offers the possibility to utilize the same strategy for a multitude of therapeutic applications.

Basic cartoon of the PAPN assembly and principal of operation is shown on Figure 1.1. First propargyl acrylate nanoparticles are assembled using emulsion polymerization. The next step involves the precise decoration of the nanoparticle with the exact amount of poloxamer chains to create PAPN. Then this nanocomposite is ready to encapsulate drugs or dyes with the possibility to release encapsulated molecules upon heating.

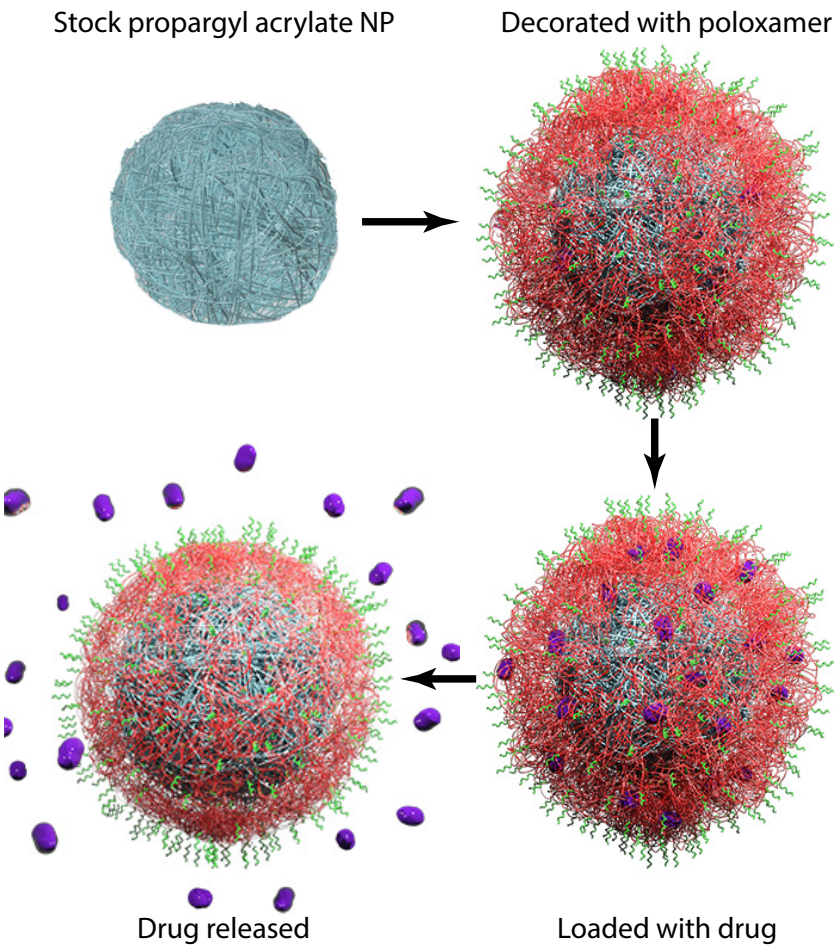

Figure 1.1: Principal scheme of propargyl acrylate poloxamer nanocomposite mechanism of action. Particles are synthesized, modified, loaded with drugs and then drug release is triggered with temperature. Image created by Olga Reukova using Autodesk 3DS Max software package.

Overview

A multitasking vesicle based on the propargyl acrylate nanoparticle is described and characterized in this work. Control over the poloxamer grafting density proved to be a useful tool to program the release rate of the active molecules from the nanocomposite. FRET theory helped with the determination of the release mechanism and allowed us to design a nanoscale temperature sensor.

The chapters of this thesis are structured as follows:

Chapter 2 offers an introduction to drug delivery with current challenges and state of the art techniques. A brief discussion about the importance of the nanoparticles as a base for the drug delivery vesicles is also presented. Temperature responsive polymers and their applications for medical devices are discussed with special focus on the poloxamer family of copolymers highlighting their advantages over the other temperature-responsive polymers. Common techniques of the nanoparticle size determination and their limitations are also discussed. FRET theory and equations used in this study are presented.

Chapter 3 describes the nanoscale temperature sensor build from the propargyl acrylate, poloxamer, naphthalimide and oxadiazole derivatives. Control over the positioning of the components allowed us to create a nanosized temperature sensor that utilizes the temperature dependence of the poloxamer coil dimensions to control the distance between a pair of dyes and thus influences the photo-luminescence properties of the device. Changes in the photo-luminescence are correlated to the changes in the environment temperature, allowing contact-free temperature measurement. Changes in the photo-luminescence were found to be reversible and in good agreement with FRET theory. Based on the observed results and previous knowledge about the immobilized copolymer behavior, a mechanism of response is discussed.

Chapter 4 shows the details about the synthetic procedures used during the preparation of the propargyl acrylate - poloxamer nanocomposite. We used FTIR based methods to determine the final grafting density of the poloxamer on the propargyl acrylate core. Equations to calculate the final grafting density are derived and the method's precision is verified. Developed methods allowed us to characterize the kinetics of the Click reaction, optimize the cleaning protocols for the removal of any unattached poloxamer, and helped with the evaluation of the

stability of the vesicles at the elevated temperatures.

Chapter 5 focuses on the encapsulation and release profiles of the system built and is characterized according to the methods described in Chapter 3. Rhodamine B dye was used as a model drug to evaluate device efficiency and to compare release rates of samples with various grafting densities. Knowledge about the mechanism of the poloxamer conformation changes due to temperature were used to describe the mechanism of the burst release and helped to explain why there is a need to closely monitor the grafting density on the final device.

Chapter 6 demonstrates the possibility of real world applications to enhance drug delivery. The vancomycin, an antibacterial drug, and Escherichia coli, as test subjects, were used to test the efficiency of the proposed nanocomposite. Efficiency of drug encapsulation and release was compared to the unmodified nanoparticles and pure drugs. Modified nanoparticles were proved to be capable of both encapsulation and triggered release, thus showing a significant increase in bacteria death rate above LCST of the poloxamer used.

Chapter 2

Literature review

Drug delivery using encapsulation of the active components in the composite vesicles offers a range of advantages [1, 2, 3, 4, 5, 6]. Ranging from the simple idea of an active molecule protection from the environment [7, 8] to creation of complex multitasking devices capable of identifying, targeting and treating cancer cells [9, 10, 11, 12]. Good examples of the multitasking nanoparticle idea were proposed by Veiseh[1], as shown on Figure 2.1. The ability to modify the surface of nanoparticles with various active components allows a researcher to program the behavior of the final nanocomposite. Covering the surface with temperature responsive polymers allows us to use the temperature to trigger the property changes, while causing the release of the active molecules or activating/deactivating dyes for imaging purposes. Typically this activation is achieved through the ability of some polymers to shrink the dimension of their coils, while expelling anything that was trapped inside into the solution [13, 14]

Cancer is characterized by uncontrollable growth of the abnormal cells that cause normal tissues to lose their functions and often leads to death of the patient if not treated in time [15], so devices that can specifically find, expose, and/or influ-

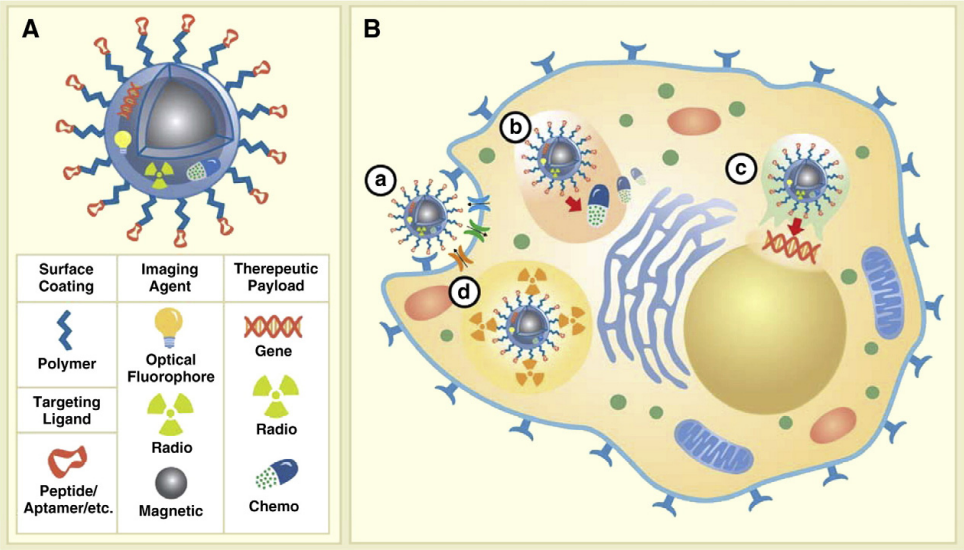

Figure 2.1: Illustration of the multifunctional imaging/therapeutic nanoparticle anatomy and potential mechanisms of action at the cellular level. (**A**) A multifunctional nanoparticle modified with targeting ligands extended from the nanoparticle surface with polymeric extenders, imaging reporters (optical, radio, magnetic), and potential therapeutic payloads (gene, radio, chemo). (**B**) Four possible modes of action for various therapeutic agents; a) Specific nanoparticle binding to the cell surface receptors (i.e. enzymes/proteins) facilitate their internalization and/or inactivation, b) controlled intercellular release of chemotherapeutics; c) release of gene therapeutic materials post endosomal escape and subsequent targeting of nucleus; and d) intracellular decay of radioactive materials. Reprinted by permission from Elsiver publisher: [1] Advanced Drug Delivery Reviews Copyright 2010.

ence the cancer tissue in the body are of high demand. Nanoparticle - based imaging and cancer treatment have gained significant attention in recent years [16, 17, 18] but there is still a vast field for improvement since none of the proposed methods are 100% effective or selective. Most chemotherapy drugs that are highly potent against cancer will also impact healthy tissues, so ability to spot the cancer at early stages means that it can be treated using smaller quantities of the drugs, decreasing the side effects of the treatment. The cancer's slightly higher temperature compared to normal tissues can be used as a targeting mechanism to activate the system [19]. To use this window of opportunity a device should have a temperature responsive component with the appropriate activation temperature, thus even in the absence

of active targeting ligands only the devices that reached the cancer tissue would be activated, thus minimizing the side effects from the treatment. To summarize, there is a clear need in the device that can be programmed to multitask to achieve effective treatment of cancer, or for that matter most any cell disorders through precises delivery of the active molecules to the inflammation site.

One of the routes considered is to encapsulate the active drugs in drug delivery vesicles [20, 3] that have a temperature activated shell, and the best way to do this is through the use of temperature responsive polymers. Because of this there has been a constant increase in the interest in the responsive polymer field over the last few decades. This interest has arisen due to the ability of temperature responsive polymers to undergo conformational changes as a function of the external temperature.

2.1 Temperature responsive polymers

Temperature responsive polymers exhibit changes in their conformation in an aqueous solutions at or around a specific temperature [21]. These changes are characterized by either a lower critical solution temperature (LCST) or an upper critical solution temperature (UCST); some polymers can have a combination of both [22]. These temperatures represent the borders above or below which the polymer and medium are no longer miscible. The width of the temperature range where this change is happening is highly dependent on the purity of the polymer and its polydispersity [23]. The lower the polydispersity of the polymer is, the narrower the temperature range of the response; therefore, the release of the active molecules will be happening over the narrower temperature range while decreasing the requirement for the difference in the temperature for the activation of the device

created from these polymers.

The most common types of such polymers are N-alkylacrylamides (Poly(N-isopropyl acrylamide) - PNIPAM, most common), vinyl ethers, alkylaminoalkyl-(meth)-acrylates, vinylcaprolactam, and poloxamer copolymers [24]. Two of the most used types are PNIPAM and alkylene oxide polymers or poloxamers [25]. The main disadvantage of the PNIPAM is its relatively hard synthesis, and the even more difficult modification of the end groups [26, 27]. It is hard to change the LCST temperature of PNIPAM, as it does not have any dependence on the molecular weight of the polymer [28]. The only way to change PNIPAM LCST is to copolymerize NIPAM with other monomers, which further complicates the synthesis [29]. Poloxamer polymers are much easier to synthesize at various sizes and copolymer compositions [30]; the end groups are hydroxyl groups, so they can be changed into other functional groups by using conventional methods. And more importantly poloxamers LCST temperature is dependent on the size and the composition of the copolymer, which is easy to control during synthesis [31]; thus, the LCST can be easily tuned to be in the desired temperature region. Poloxamer copolymers are commercially available with LCST ranging from 15 °C up to 100 °C and are produced in millions of tons per year. The list of some of the commercially available poloxamers are shown in Table 2.1 along with their main properties.

Besides being readily available in a wide range of LCST temperatures poloxamer family of copolymers offers a set of important properties that are desired in drug delivery applications. The first advantage comes from the structure of the copolymer: the outer ethylene oxide blocks act as a protective layer between the vesicle and the human body environment[32]. Immune system function is to destroy any foreign object that it can find inside of the human body. The particulates that are covered with ethylene oxide are processed by the immune system as the na-

Name	*Mn*	*LCST*	*%PO*	*%EO*	*Name*	*Mn*	*LCST*	*%PO*	*%EO*
L122	5000	19	80	20	**P75**	4200	82	50	50
L72	2750	25	80	20	**P85**	4600	85	50	50
F62	2500	32	80	20	**P103**	4950	86	70	30
L63	2650	34	70	30	**P123**	5750	90	70	30
L42	1550	37	80	20	**P105**	6500	91	50	50
L43	1850	42	70	30	**F38**	4700	100	20	80
L64	2950	58	60	40	**F68**	8350	100	20	80
L44	2200	65	60	40	**F77**	6700	100	30	70
L35	1900	73	50	50	**F87**	7700	100	30	70
P84	4200	74	60	40	**F88**	10800	100	20	80
P104	5850	81	60	40	**F98**	13000	100	20	80
P65	3600	82	50	50	**F108**	14000	100	20	20

Table 2.1: Commercially available poloxamer and their respective basic properties.

tive components and as such are not destroyed by the immune system [33]. Ability of a device to remain intact while circulating through the human body environment is crucial, as it allows enough time for the device to spread through the body, find its target organ, and complete the designed mission.

A second advantage of the poloxamers comes from their ability to influence the cell wall penetration characteristics while allowing the drugs to penetrate inside of the cell [34]. Cell wall permeability is often responsible for drug resistance and the ability to increase this permeability means that less drugs can be used to achieve the same therapeutic effect. This, in turn, leads to a decrease in the side effect probabilities.

A third and final advantage of the poloxamers is the availability of the relatively active hydroxyl groups on the copolymer ends. Plenty of chemistry has been developed that allows a researcher to substitute the hydroxyl groups with other functional groups that are needed during the final assembly of the drug delivery device, all while allowing the creation of a stable and well-established surface

chemistry.

Poloxamers can form micelles under certain conditions [30], but these micelles are susceptible to self destruction if the conditions change. A common solution to this problem is the immobilization of the polymer on the surface of the stable nanoparticle. The best way to successfully immobilize the polymer on the surface is to chemically bind it. The possibility to replace one of the hydroxyl groups on the poloxamer chain with the azide group allows us to use Azide-alkyne Huisgen cycloaddition reaction to permanently attach the copolymer to the surface under mild conditions, while reaching high yields during this process [35].

2.2 Nanoparticles as a base for the drug delivery devices

Nanoparticles appear in a growing number of the research articles when it comes to drug delivery field. This is happening because through the use of the nanoparticles it is possible to achieve multiple goals at once and, thus, to solve multiple problems associated with drug delivery. The first advantage of the nanoparticle as a base for drug delivery devices comes from the possibility to control the size of the final device [36]. This allows for a design vesicle with required penetration capabilities and utilizes the differences of the cell/tissue penetration properties for the targeted drug delivery applications [37, 38, 39].

The second advantage of the nanoparticles involves the ability to control the surface chemistry and, as a result, the morphology. Propargyl acrylate nanoparticles are one of the examples of a bio-compatible carrier with easy-to-control surface chemistry [40]. Through the strategic positioning of the active components on the

surface it is possible to design a multitasking device [40, 41, 42]. Various small molecule targeting ligands can be attached to enhance the targeting capabilities of the device while enhancing the treatment efficiency and decreasing the side effects from the treatment. One such example is the gefitinib ligand [43]. Gefitinb specifically binds to the epidermal growth factor receptor, also known as EGFR, on the surface of the cells. Expression of the EGFR on the cancer cells is typically two to three orders of magnitude higher than on the healthy cells [44], EGFR is thought to be responsible for the increased cancer cell viability and the ability of cancer cells to grow much faster than normal cells. The device that can recognize and specifically bind to the EGFR will lead to a two to three orders of magnitude higher device concentration near the cancer cells as compared to the healthy cells, and this fact combined with a triggered release can create a higher concentration of the drug around the cancer cells, all while maintaining low drug concentration near the healthy cells.

The possibility to build a specific structure on the surface of the nanoparticle allows us to create sensors that can detect changes of the environment on a micro scale without the need for wires or other invasive measuring devices [45, 46]. Most of the time the analysis of the environmental change is correlated to the changes in the luminescence of the nanoparticle [47]. Several approaches are used to create a device that can change the photo-luminescence profile when exposed to different conditions. Some of the approaches rely on the turn on or turn off of the dye when the dye is located in the vicinity of the core [48], while the others use the energy transfer dependence on the distance, also known as F*ö*rster or fluorescence resonance energy transfer (FRET)[49, 50]. When two dyes are located close enough and their spectral properties overlap, part of the energy from the donor dye can be transferred to the acceptor dye and the amount of the energy transferred is propor-

tional to the distance between the dyes and can be found using FRET theory [51].

Use of the nanoparticles as a base for the medical device fabrication is advantageous in many aspects. It allows for a creation of programmable vesicles that can encapsulate, protect, deliver and then release the active molecules into the site of interest. Additionally when the dyes are strategically positioned on the surface, and when the distance between these dyes is dependent on the environment parameters, a sensor to monitor these parameters can be created. So acquiring new knowledge about the synthesis and the characterization methods for the nanocomposites is essential for the future advances in the nanoparticle-based drug delivery systems and their imaging applications.

2.3 FRET as a mechanism of temperature sensor

F*ö*rster or fluorescence resonance energy transfer (FRET) is a process of energy transfer between two light-sensitive molecules called chromophores. A donor dye absorbs the photon, which promotes the electron from its highest occupied molecular orbital (HOMO) to become excited and to jump to a higher energy level. Then the electron loses part of this excess energy through one of the possible mechanisms: photon emission, heat, or transfer of energy through dipole-dipole coupling to the acceptor molecule, exciting acceptor electron from HOMO to a higher energy level. Then the electron on the acceptor relaxes back to its ground state through one of the above mechanisms, and if it emits the photon, that can be measured, a significant red shift of the emission observed [52]. This principle, including the typical time scales for each of the proces's, is shown on Figure 2.2.

To achieve any significant FRET, the pair of dyes has to satisfy all of the FRET criteria: including significant spectral overlap of the donor emission spectrum with

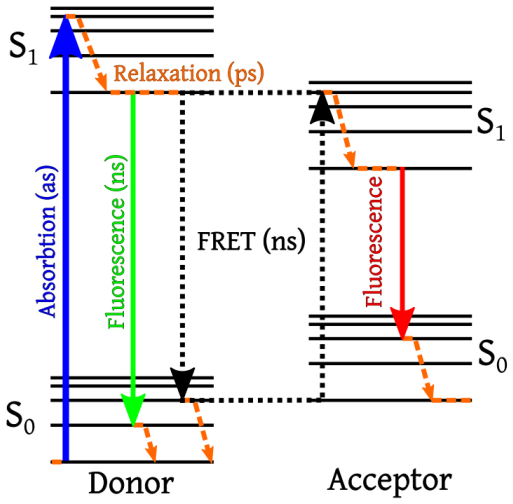

Figure 2.2: FRET Jablonski diagram with typical timescales. Absorption of the energy by the donor causes one of the electrons to be promoted to a higher energy orbital. When electron falls back to its lower energy state the energy is transferred to the acceptor promoting one of the acceptor electrons to a higher energy orbital. When this electron drops to the lower energy orbital the photon is emitted. Image created by Alex M Mooney, licensed under the Creative Commons Attribution-Share Alike 3.0 Unported license

the absorption spectrum of the acceptor; quantum yield of the donor has to be high; donor and acceptor transition dipoles must be in the same orientation plane; and the distance between the donor and the acceptor has to be less than twice the F*ö*rster distance. F*ö*rster distance is a distance at which FRET is 50% efficient often referred to as a characteristic distance, and is typically ranges from 2 to 6 nm.

FRET is characterized using the rate of energy transfer k_τ, and the rate of the energy transfer can be estimated from the following equation:

$$k_\tau = \frac{1}{\tau_D}(\frac{R_0}{r})^6$$

where k_τ is the rate of the energy transfer from the donor to the acceptor; τ_D is the decay time of the donor in the absence of the acceptor; R_0 is the F*ö*rster distance; r is the real distance between the donor and the acceptor at a given condi-

tion. As the above equation demonstrates, FRET is highly dependent on the distance between dyes - to the sixth power. Even small changes in the distance between the dyes can yield big differences in FRET. This is why controlling the distance between the dyes is so important and can be used as a tool to modify the emission spectra of the system. Energy transfer requires for the donor and the acceptor to be within a characteristic distance and to have suitable spectral overlap. The value of R_0 can be reliably predicted from the spectral characteristics of the donor and the acceptor using following equation:

$$R_0 = 0.211(\kappa^2 n^{-4} Q_D J(\lambda))^{\frac{1}{6}}$$

where Q_D is the quantum yield of the donor; κ^2 is the factor describing the relative orientation in space of the transition dipoles of the donor and the acceptor and is usually assumed to be equal to $\frac{2}{3}$, which is appropriate for the dynamic random averaging of the donor and acceptor orientations; n is the refractive index of the medium; the overlap integral $J(\lambda)$ represents the extent of the spectral overlap between the emission of the donor and the absorption of the acceptor at the wavelength range λ to $\lambda + \delta\lambda$ and can be estimated from the following equation:

$$J(\lambda) = \int F_D(\lambda)\varepsilon_A(\lambda)\lambda^4 d\lambda$$

where $F_D(\lambda)$ is the corrected fluorescence intensity of the donor in the wavelength range λ to $\lambda + \delta\lambda$, with the total intensity normalized to unity; $\varepsilon_A(\lambda)$ is the molar extinction coefficient of the acceptor at λ.

Knowledge of the rate of energy transfer allows us to estimate the efficiency of the energy transfer E. E is the fraction of the photons absorbed by the donor that are transmitted to the acceptor. E can be found from the ratio of the total decay

rate of the donor to the total transfer rate between the dyes through equation:

$$E = \frac{k_\tau}{\tau_D^{-1} + k_\tau}$$

Substituting the k_τ in the above equation with k_τ equation the efficiency of the energy transfer can be found through the lifetime differences of the donor dye in the presence and absence of the acceptor using following equation:

$$E = 1 - \frac{\tau_{DA}}{\tau_D}$$

Calculated this way values for the efficiency of the energy transfer allow to estimate the distance between the dyes using the following equation:

$$r = (\frac{R_0^6}{E} - R_0^6)^{\frac{1}{6}}$$

Knowing the surface chemistry and positioning of the dyes on the surface of the nanocomposite allows us to use the distance between the dyes as an indication of the surface morphology changes and, as such, to make a prediction of the device's behavior at a given condition.

2.4 Size determination

Precise surface chemistry characterization, specifically the grafting density determination, depends on the ability to measure the sizes of the cores accurately. Dynamic light scattering (DLS) and Scanning Electron microscopy (SEM) are among the most common techniques used to determine the size of spherical vesicles[53, 54, 55]. DLS gives an intensity-weighted mean value of the hydrodynamic radius

of the vesicle and is often the first tool of choice in the nanoparticle characterization. To convert hydrodynamic radius value to a number or volume-weighted mean value that can be used in the grafting density determination one needs to know the complex refractive index of the material. This requirement is the main reason why often obtaining real information about the dimensions of the vesicle is impossible. Though still the DLS allows us to reliably compare the different samples among themselves, as long as the material is the same and the only difference is in the size. SEM, on the other hand, provides the information about the size and the shape of the dried vesicles, so if the vesicle swells in the environment SEM will show a smaller size compared to real dimensions in solution[56], this is why DLS is a more preferred way of the nanoparticle size determination in most cases. Combination of the two techniques allows us to make a much more accurate prediction about the real solution size of the studied object as compared to data from just one technique.

In the DLS measurements particle size is determined through the monitoring of the rate of the particle's diffusion in the fluid. This rate depends on the fluid temperature, viscosity of the solvent and the nanoparticle size. The first two components are easy to control and can be precisely measured, and this allows for the determination of the third component - particle size.

Principle of the DLS instrument operations are as follows: instrument illuminates the particles with a laser and measures the scattered light with a photomultiplier tube (PMT). Intensity of the light detected by PMT depends on the pattern of the particles in the laser beam. As particles move through the laser beam, intensity of the scattered light changes and by monitoring the speed of the intensity change it becomes possible to make a decision about the particle size. Bigger particles move slower and, thus, the intensity changes are slower when compared to the smaller

nanoparticles.

In order to obtain information about the particle size from the intensity changes, the instrument uses a mathematical transformation which is called auto-correlation function. Basic algorithms behind the auto-correlation function are the comparison of a scattering intensity at time t to intensity at time $t+\tau$. If the correlation of the two intensities is high, the intensity has not changed much, this means that the particles have not changed their relative position much, and this is the direct indication of a big size of the particles, big things move slower than smaller ones. Instrument monitors this auto-correlation over a defined period of time and for various values of τ , then compares the obtained values to build a decay time graph. Time differential when auto-correlation curve changes from 1 (high correlation) to 0 (no correlation) is indicative of the particle size and when information about particle's refractive index is available the hydrodynamic radius (*Rg*) of the particles can be calculated[57, 58]. Precise determination of a complex refractive index (RI) of a nanoparticle is required to obtain a real value of *Rg*, and because often it is impossible to get an accurate measurement of RI, size of the nanoparticle determined using DLS is only an approximation, and thus there is a need for the additional size measurements to confirm the real size of the nanoparticle.

Often during synthesis the same processes that hold nanoparticles intact can lead to the attachment of two or more nanoparticles together. Alternatively, particles can stick together during storage after they have been synthesized. This combination of nanoparticles leads to a formation of aggregates and leads to increased polydispersity readings during DLS measurements. To determine the presence of the aggregates, nanoparticles can be separated according to their size using column chromatography. Depending on the size of the nanoparticle, the time required to pass through the column will be different thus making it possible to separate the

different fractions and analyze the average size of the nanoparticles in each fraction separately. If the sample has a mix of the single nanoparticles and aggregates after column chromatography these sets will be isolated. Running DLS measurements on each of the fractions allows us to determine the extent of aggregation and thus to make a better prediction about the final composition of the sample.

Chapter 3

Micro-scale temperature sensor based on FRET effect

An effective strategy to control the F*ö*rster resonance energy transfer (FRET) of a donor/acceptor emitter pair that were attached to a 60 nm poly(propargyl acrylate)(PA) nanoparticle using temperature variations was developed. The size dependent properties of a poly-(ethylene oxide)-poly-(propylene oxide)-poly-(ethylene oxide) (PEO-PPO-PEO) block copolymer (poloxamer) was exploited to vary the spatial separation of the emitters and vary the FRET efficiency. Specifically, a 2% change in FRET efficiency between the donor/acceptor pair was achieved per 1 °C change in temperature from 49 °C to 60 °C when using a poloxamer of 2950 g/mole molecular weight, with sections of PPO consisting of 32 repeat units, PEO sections consisting of 12 repeat units and a lower critical solution temperature (LCST) of 58 °C. The methodology presented in this effort is easily extended to other temperature regimes through a judicious choice in poloxamer and corresponding LCST.

.

3.1 Introduction

A particularly interesting and well-known optical emitter-emitter interaction is F*ö*rster resonance energy transfer (FRET) and has been widely utilized as a tool for signaling[59, 60] and measuring[61] molecular associations in biomedical and clinical applications, although many applications exploit FRET, including, photovoltaics[62], lighting & displays[63], and sensors[49]. FRET is a near-field nonradiative energy transfer between pairs of dipoles where the excitation energy is transferred from one emitter, referred to as the "donor", to a second emitter, referred to as the "acceptor"[64, 65].

Extensive research has been done on utilizing organic dyes in FRET assays with much success[50]. These small molecule systems have the advantage of simple preparation and low cost, resulting in a large variety of these dyes being commercially available for diverse applications. Nonetheless, these systems can suffer from poor photo-bleaching resistance[66], short fluorescence life time, low fluorescence quantum yield[67], non-specific quenching[68, 69], low chemical stability and intracellular toxicity. In addition, small molecule dyes often will bind to proteins[70], which leads to aggregation and subsequent elimination from the body. In response to the limitations, fluorescent proteins are being used increasingly in FRET systems. In these systems, a fluorophore is genetically appended onto the gene coding for a protein of interest so that a fluorophore and protein can then be co-expressed intracellularly and, when imaged, reveal the location and relative expression level[71, 72]. Since the initial development of green fluorescent protein (GFP), efforts on extending the color regime of the protein have resulted in a range of available colors for the fluorescent proteins[73]. Though these systems continue to develop and offer exciting new applications, there are challenges to coupling

them to targeting, diagnostic, and therapeutic payloads.

One approach to remedy these shortcomings is the inclusion of the chromophores on the surface of colloidal particles[74, 75, 76]. This attachment of the dye to a particle results in an extension of circulation half-life and enhanced *in vivo* stability relative to the free fluoroprobe[75]. The surface attachment of the dyes allows them to participate in advantageous host/guest assemblies that can alter their emission and FRET efficiency. This response can be utilized as a biologically-based sensor or switch due to the noticeable variations in the emission spectra when they form supra-molecular host/guest assemblies or complex with biomacromolecules[77, 78, 79]. The environmental sensitivity in the emission properties of the chromophores can also be exploited to assist in refining the proposed parameters that govern molecular recognition[80, 81, 82]. Photo-stable fluorescence nanoparticles which can be good candidates as donors in FRET that have received recent attention include semiconductor quantum dots (QDs)[83], graphene quantum dots (GQDs)[84, 85] and upconversion nanoparticles (UCNPs)[86, 87].

In the current effort, colloidal particles are developed that exhibit a significant change in FRET efficiency within a specified temperature regime. The methodology utilized is relatively general, and the system can be easily extended to operate in a wide range of temperature zones. Specifically, sub-100 nm particles are surface modified with two dyes that form a FRET pair. One of the dyes is attached to the particle through a copolymer that exhibits significant changes in its dimensions with temperature variations, and this temperature sensitivity is exploited to alter the spatial proximity of the donor and acceptor dyes, which alters the dyes' FRET efficiency and thus reporting on the temperature alteration. The class of polymer used is a poly(ethylene glycol)-*block*-poly(propylene glycol)-*block*-poly(ethylene glycol) (PEO-PPO-PEO) difunctional block copolymer often re-

ferred to as a “poloxamer”. Poloxamer copolymers can change their excluded volume (“size”) depending on the surrounding temperature and can form hydrophobic pockets that attract hydrophobic molecules, especially aromatic molecules, and stabilize them in aqueous environments[88, 31, 89]. This property is utilized in medical applications to promote the activity of hydrophobic dyes and drugs, that are otherwise ineffective in the aqueous environment of live cells[90, 91]. Another advantage of using poloxamers comes from their tri-block copolymer structure. The outer blocks are composed of ethylene oxide (EO) which is known to form vesicles that can engulf a payload rendering it invisible to the reticulo-endothelial system and macrophages, and therefore significantly increasing the lifetime of the payload in the body[92, 93, 94, 95]. In addition, poloxamer surfactants have been reported to increase the sensitization of tumors with respect to various anticancer agents [96, 97, 98], making anticancer drugs more effective.

Unfortunately, free poloxamers cannot create stable polymersomes below critical micellization concentration or temperature and they require additives to make stable vesicles[99] or the attachment to a nanoparticle to create a stable platform[93, 95]. Free floating poloxamers are very sensitive to the load that they carry and to the surrounding conditions[31], increasing the likelihood that the formed micelles will be damaged, which results in the loss of content effectively rendering them useless or, worse, triggering an unwanted side effects, such as general system toxicity. Immobilization of the poloxamer on the surface of nanoparticles eliminates these issues allowing the system to maintain its functionality[90]. Based on these characteristics, a poloxamer was chosen as the responsive component of the proposed colloidal device. In addition, the use of a particle as the platform on which various other “loads” can be attached[100, 41] is advantageous as it allows for further modifications with targeting ligands and therapeutic drugs[101, 102].

3.2 Results and Discussion

Figure 3.1A presents the system utilized in this study, which was composed of a propargyl acrylate (PA) nanoparticle, which had two complementary FRET dyes attached to its surface, with the acceptor dye being attached to the particle through a modified poloxamer. The donor dye was an oxadiazole derivative (azOx, cf. Figure 3.1B) that was attached directly to the surface of the PA nanoparticle through an azide-alkyne Huisgen cycloaddition resulting in a 1,2,3-triazole ("Click" transformation)[100], while the acceptor dye, a naphthalimide derivative (azPlurNaph, cf. Figure 3.1C), was attached to the same nanoparticle through a poloxamer chain. The poloxamer (Pluronic-L64) was a poly(ethylene glycol)-*block*-poly(propylene glycol)-*block*-poly(ethylene glycol) (PEO-PPO-PEO) difunctional block copolymer that initially terminated in primary hydroxyl groups but was modified so that one end contained a naphthalimide dye and the other an azide group so that it could also be "clicked" to the particle (cf. Experimental methods). The unmodified PEO-PPO-PEO triblock copolymer had a molecular weight of 2950 g/mole, with the sections of PPO consisting of 32 repeat units, while the PEO section consisted of 12 repeat units. The poloxamer exhibits a lower critical solution temperature (LCST) of 58 °C.

Free poloxamers typically form polymersomes of several hundred nanometers [31]; however, immobilizing them on nanoparticles of a fixed size limits the maximum size of the system to the sum of the size of the nanoparticle used plus twice the length of the fully extended poloxamer chain. Vesicle size is very important in therapeutic applications due to cell wall permeability limitations. In general anything greater than 200 nm will not be able to enter the cell through a simple diffusion process and anything smaller than 30 nm will be evacuated prematurely

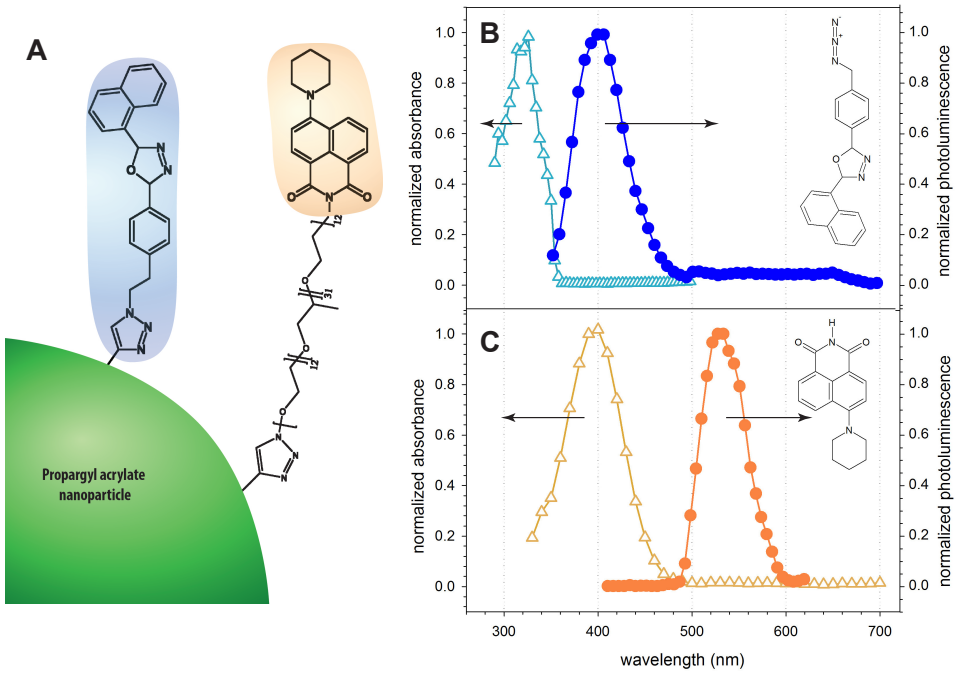

Figure 3.1: (**A**) Schematic representation of the built system, showing positioning of the dyes on the surface of the nanoparticle. (**B**) Emission and absorption patterns of donor dye (oxadiazole derivative - azOx) measured in tetrahydrofuran; excitation at 335 nm. (**C**) Emission and absorption patterns of acceptor dye (naphthalimide - Naph) measured in tetrahydrofuran; excitation at 400 nm.

through the urinary system[100, 103, 104]. In this study we used nanoparticles with an average size of 60 nm, and a poloxamer with a theoretical fully extended length of almost 15 nm, which yields a total theoretical maximum size of approximately 90 nm, which is within the desired size range for medical applications.

Figure 3.2 presents the photoluminescence (PL) at 20 °C in water of the particles with the dual dye-modification (PA/azOx/azPlurNaph) at a grafting density around 0.5 dye molecules per nm^2, as well as two additional sets of nanoparticles with similar grafting densities of dyes. One set of the nanoparticles was prepared with azOx and a poloxamer that had not been modified with the naphthalimide dye (PA/azOx/azPlur), while the other set of particles had been modified with only the azPlurNaph dye (PA/azPlurNaph). The poloxamer was attached to the

first set of particles to ensure a similar environment for the azOx dye. For the PA/azOx/azPlur, the excitation energy at 335 nm is within the absorbance window of the azOx dye and the particles exhibit an oxadiazole-based emission (cf. Figure 3.1B) at 400 nm. The excitation wavelength is outside the absorbance window of the naphthalimide dye (cf. Figure 3.1C), and the PA/azPlurNaph did not exhibit any appreciable emission, though exciting the particles at 400 nm did result in an naphthalimide-based emission (spectra not presented). When excited at 335 nm, the PA/azOx/azPlurNaph particles did exhibit emission characteristics of both the oxadiazole and naphthalimide dyes, indicating that energy transfer is taking place from the azOx to the azPlurNaph dyes, though there is an incomplete transfer since the emission of the oxadiazole-based dye is still present in the spectra.

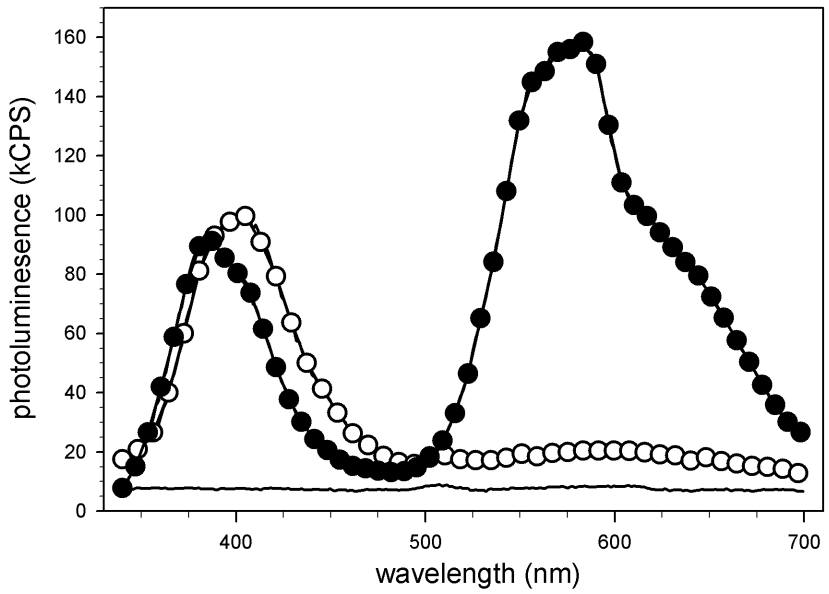

Figure 3.2: Photoluminescence of particles: (1) modified with oxadiazole dye (azOx) and poloxamer (○); modified with poloxamer terminated with naphthalimide dye (azPlurNaph) (—); (3) modified with both dyes azOx and azPlurNaph (●). All particles excited at 335 nm. Chromophores density for all samples is similar. Emission for azOx modified nanoparticles at 400 nm was matched to the emission of dual modified nanoparticles for better energy loss representation. azPlurNaph particle density was matched to azOx particle density. Measurements taken at room temperature.

Utilizing FRET theory[64] and the photoluminescence (PL) response of the PA/azOx/azPlurNaph particles (cf. Figure 3.2-3), the distance and energy transfer efficiency between the dyes were calculated. The FRET efficiency for the system was calculated using the half-lifetimes of the two sets of the nanoparticles. The first set contained the donor dye (azOx) and the poloxamer, the second set contained both the donor dye (azOx) and the acceptor dye (azPlurNaph). By comparing the ratio of the half-lifetime of the donor alone and the half-lifetime of the donor in the presence of the acceptor, the FRET efficiency was calculated[64, 65]. Based on the emission and absorption spectra of azOx and azPlurNaph, the F*ö*rster distance was found to be 3.54 nm with a transfer efficiency of ca. 70 % at 20 °C for the given pair of dyes.

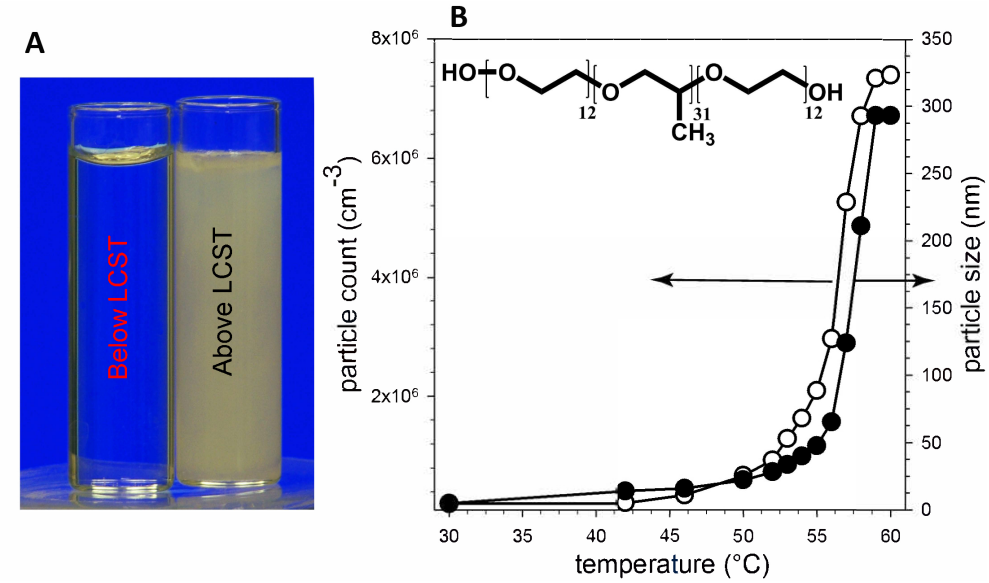

Figure 3.3: **(A)** Optical image of neat Pluronic-L64 (poloxamer/water) solution at room temperature (left vial) and at 60 °C (right vial) (LCST is 58 °C). **(B)** Dependence of micelles size and number of micelles formed by Pluronic-L64 in water with solution temperature (measured through dynamic light scattering).

The component selection of the particles was designed to maximize the FRET efficiency between the fluorophores. To achieve a high level of energy transfer

between a pair of dyes, emission of the donor has to have a significant spectral overlap with the absorption of the acceptor[64]. The naphthalimide (azPlurNaph) and oxadiazole (azOx) dyes employed in this effort satisfy this requirement; there is almost 100 % overlap of the donor emission with the absorption of the acceptor (cf. Figures 3.1B,C). The grafting density was determined to be ca. 0.54 molecules per nm^2 for the donor dye (azOx) and 0.39 molecules per nm^2 for the acceptor dye (azPlurNaph). Since FRET is very sensitive to the distance between dyes, it is expected that by controlling this distance one can achieve control over the extent of FRET[64].

Poloxamer copolymers are known to change their coil dimensions as a function of temperature, and these changes are reversible and predictable for a given composition of the copolymer[31]. The Pluronic-L64 poloxamer exhibits significant changes in its end-to-end distance with temperature variations and was employed as a means for modulating the distance (and FRET) between the donor/acceptor dyes. In Figure 3.3A, a neat Pluronic-L64/water solution goes from a transparent solution to a turbid one as the temperature passes through its LCST, while Figure 3.3B presents the micelles dimensions of the neat Pluronic-L64 poloxamer with temperature variations as analyzed through dynamic light scattering (DLS) procedures[105]. The size of the neat poloxamer appears to exhibit a dramatic increase between 50 °C and 60 °C, going from ca. 50 nm to 300 nm, which coincides with the lower critical solution temperature (LCST) temperature of the polymer (58 °C). In this temperature range, one can expect to see the largest changes in the FRET efficiency of the PA/azOx/azPlurNaph particles to occur. The DLS results are not indicative of the size of the copolymer coils, but are essentially measuring the scattering of the polymer coils as they go from a miscible state (low scattering entity) to a highly scattering dispersion with the increase in temperature.

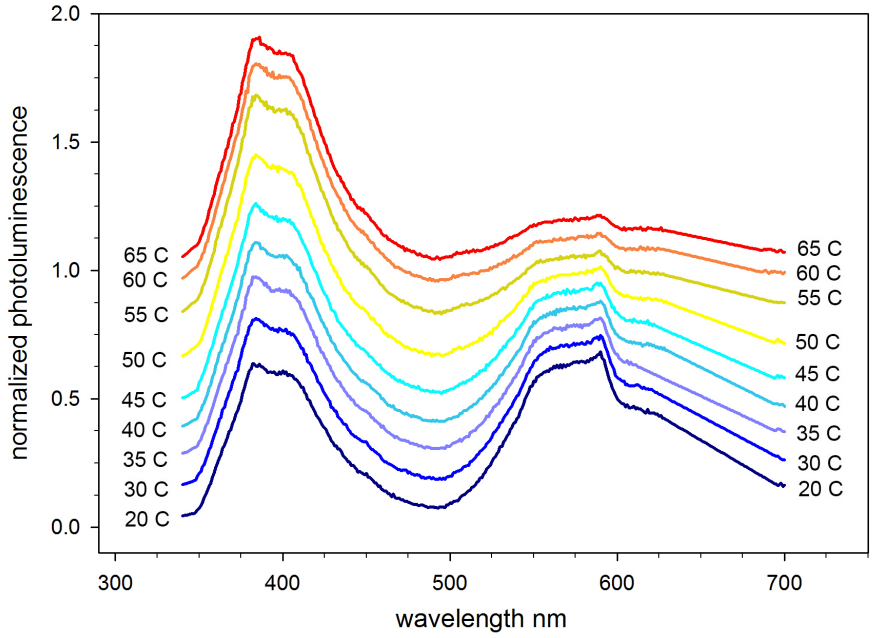

Figure 3.4: Photoluminescence spectra of PA/azOx/azPlurNaph particles at various temperatures. The donor dye is azOx with a peak emission ca. 400 nm, while the acceptor dye is azPlurNaph with a peak emission ca. 550 nm. The LCST of the poloxamer, on which the acceptor dye is attached at the end, is 58 °C. Particles dispersed in deionized water and graphs are shifted for clarity. Excitation energy at a wavelength of 335 nm.

The photoluminescence dependence on temperature of the PA/ azOx/ azPlurNaph particles is presented in Figure 3.4. At 20 °C, the PL response of the particles indicates that both dyes are emitting when excited by a 335 nm excitation, as is expected from the previously presented PL study at 20 °C (cf. Figure 3.2). This excitation wavelength is within and outside the absorption regime of the azOx dye and azPlurNaph dye, respectively, and should only result in emission from the donor dye. Nonetheless, the emission profile of the particle clearly has the signature of the azPlurNaph dye, suggesting that there is energy transfer taking place from the donor to acceptor dye. Subsequent scans at higher temperatures indicate a diminishing energy transfer until ca. 60 °C where minimal energy transfer is discernible in the spectral response of the particles. The increase in the emission at

ca. 400 nm (azOx) and the decrease in the emission at 580 nm (azPlurNaph) is indicative of a reduction in energy transfer from the oxadiazole to the naphthalimide dye. This change is most pronounced within the 50 - 60 °C range and suggests that the separation distance of the two dyes is becoming larger, thereby frustrating FRET[64]. This temperature range is also within the LCST range for the poloxamer. Surprisingly, according to previous studies on poloxamer behavior, it was expected that as the temperature increased, the poloxamer end-to-end distance would decrease, giving rise to a more compact coil packing[31]. This decrease in the size of the copolymer was expected to bring the two dyes closer together, resulting in an increase in the FRET efficiency, which was not observed.

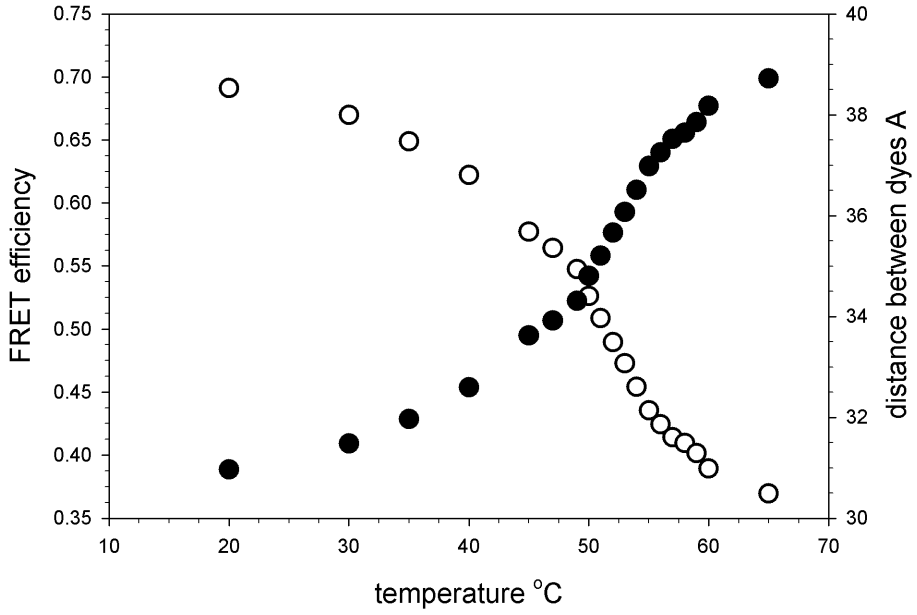

Figure 3.5: FRET efficiency (○) and calculated distance between the azOx and azPlurNaph dyes (●) for the PA/azOx/azPlurNaph particles system (in water) presented in Figure 3.1.

Dye's quantum yield can change at different temperatures, thus influencing the intensity of the emission peak at elevated temperatures. To check whether this

change was not a main factor behind observed results, quantum yield dependence on the temperature for both dyes was measured and was found to be much smaller than the observed changes, further suggesting that the main mechanism behind the observed emission change is FRET.

To check quantum yield dependence on the temperature, dyes were dissolved in a good solvent with high enough boiling temperature to measure the change of quantum yield over the widest possible temperature range. Based on the available literature data and properties of Ethanol, this solvent was chosen as a reference solvent. Ideally quantum yield dependence on the temperature should be measured from the same solvent as the device, but because both dyes are insoluble in water alternative solvent had to be chosen. Measurement of the quantum yield requires a reference dye, so anthracene was selected. According to the standard procedure to measure quantum yield emission and absorption spectra of the dye of interest should be compared to the emission and absorption spectra of the reference dye, which absorbs in the similar range as the investigated dye[106]. Anthracene has good solubility in ethanol, and its quantum yield is well established for this solvent. Additionally, absorbance and emission of anthracene are similar to the two dyes used in this chapter, thus making anthracene a good candidate for a reference dye role.

Procedure for quantum yield determination was as follows: first UV/Vis absorbance spectrum of ethanol was recorded. This spectra was used to correct the rest of the samples for any background absorbance effects from the solvent, the cuvette, or the instrument. Then for each dye five concentrations were prepared ensuring that absorbance maximum for all samples was below 0.2 and the increment in the absorbance between each concentration was 0.04. After the absorbance for all 5 concentrations and for all dyes were recorded, the fluorescence of each solu-

tion was recorded. For each dye based on the recorded data a graph of fluorescence intensity versus absorbance was plotted. If the obtained graph was close to the straight line then the data was considered to be reliable and slope of the line was calculated. Obtained lines for two temperature are presented on Figure 3.6

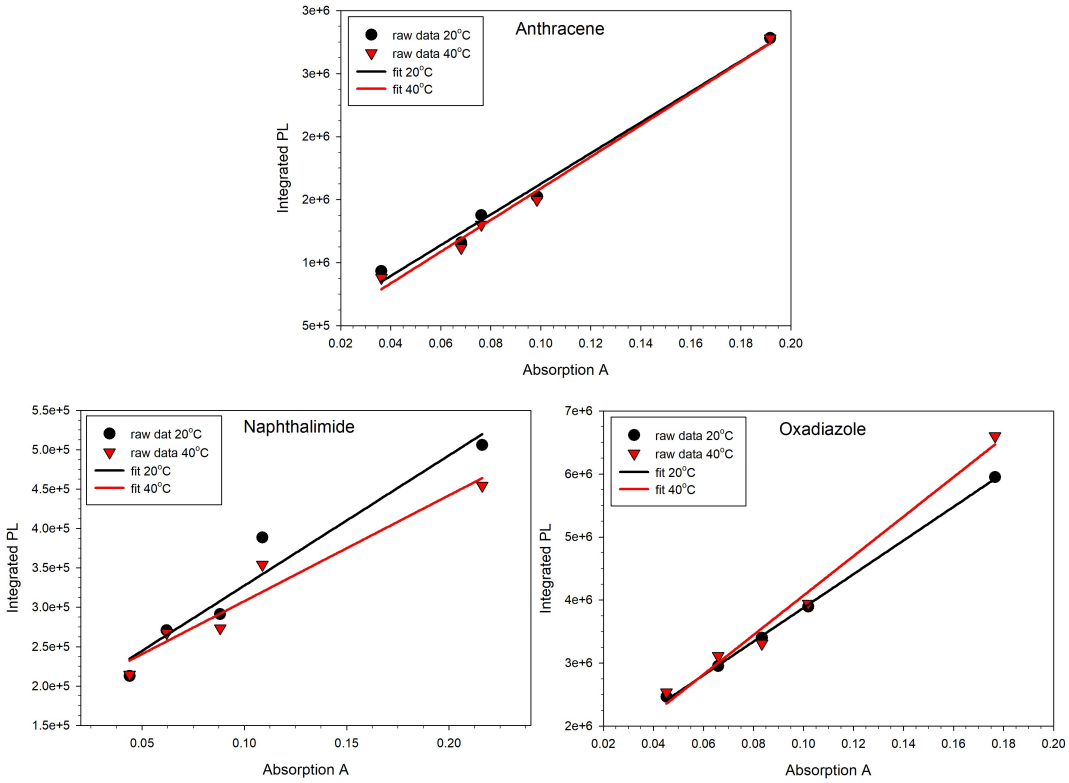

Figure 3.6: Dependence of fluorescence emission on the absorbance for Anthracene, Naphthalimide and Oxadiazole. Based on these graphs, quantum yield dependence on the temperature for Naphthalimide and Oxadiazole dyes was determined.

Slope of the lines for each dye is proportional to the quantum yield of the dye. To determine the absolute value of the quantum yield for each dye ratio of the slope gradients of the unknown sample to the anthracene were multiplied by the literature value of anthracene quantum yield. Because all measurements were done from the same solvent, there was no need to account for the refractive index difference between the runs. As can be seen on the Figure 3.6, there is almost no

change in the slope for the anthracene dye indicating that quantum yield for this dye has not changed much in the investigated temperature window and thus can be used as a reference dye for both temperatures.

Both of the dyes used in this study showed slight deviations in the slopes when temperature was changed from 20 °C to 40°C . According to the literature[106] quantum yield of anthracene at 20°C is 0.27, calculated slopes for anthracene were 12.1E6 at 20°C with correlation coefficient R=0.9944 and 12.5E6 at 40°C with correlation coefficient R=0.9953, calculated slopes for oxadiazole were 26.7E6 at 20°C with correlation coefficient R=0.9996 and 31.3E6 at 40°C with correlation coefficient R=0.9922, calculated slopes for naphthalimide were 1.65E6 at 20°C with correlation coefficient R=0.9698 and 1.34E6 at 40°C with correlation coefficient R=0.9704. Based on these numbers a 20°C change in temperature causes 6 and 5 percent change in the quantum yield of oxadiazole and naphthalimide respectively, or less than 0.3 percent per degree. This change is much smaller than the observed 2 percent change seen for the device, thus supporting the idea that FRET is the main mechanism that is causing observed emission changes. To calculate quantum yield (QY) the following equation was used[106]:

$$QY_{unknown} = QY_{reference} * \frac{slope_{unknown}}{slope_{reference}} * \frac{\eta^2_{unknown}}{\eta^2_{reference}}$$

where QY is quantum yield of either reference dye or dye of interest, *slope* values are found based on the graphs described above, η is refractive index of the solvent from which emission and absorbance for the dye were collected. Since all three dyes were recorded from Ethanol, the last fraction in the formula was equal to 1.

Using the ratio of peak areas for azOx and azPluroNaph dyes for dual dye

modified nanoparticles at various temperatures referenced to the FRET efficiency at 20°C as calculated based on the lifetime measurements for the system, the FRET efficiency and corresponding distances between the dyes over a range of temperatures were calculated[64] results are presented in Figure 3.5. The distance was found to change from 3.1 nm to 3.9 nm in the 20°C - 65°C temperature range, which translates into a change of the FRET efficiency between 70% - 36%. The highest rate of change in the inter-dye distance and corresponding FRET efficiency was observed at temperatures near the LCST temperature of the poloxamer (i.e. 58 °C).

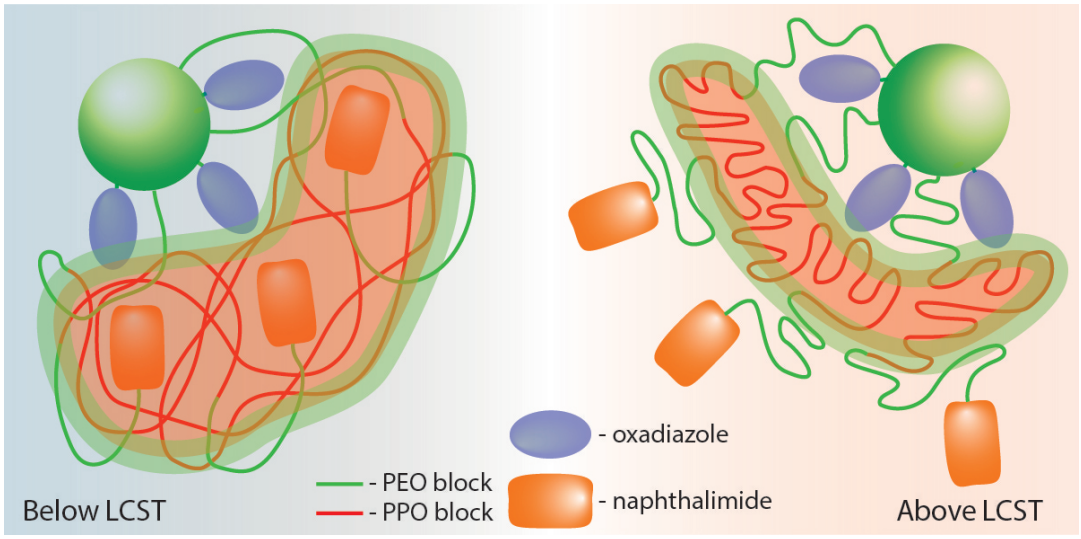

Figure 3.7: Proposed mechanism of the variation in photoluminescence response with temperature of PA/azOx/azPlurNaph particles (cf. Figure 3.1A). At temperatures below LCST, the PPO block forms a hydrophobic domain with loose packing which allows the naphthalimide dye to sequester into its domain, but with a temperature rise above LCST, the PPO domain packs more densely forcing the naphthalimide dye from the domain, resulting in an increase of the distance between donor and acceptor dyes.

We speculate that the simple end-to-end distance argument of the poloxamer to account for FRET efficiency does not account for the poloxamer's unique environment created when it transitions from a coil to an extended structure[30, 88]. Previ-

ous studies on block copolymer behavior have found that these copolymers can fold their free ends back into the polymer matrix under specific conditions[107]. This fact combined with the hydrophobicity of the naphthalimide dye suggests that in the proposed system poloxamer end with naphthalimide will be flipped back inside of the poloxamer matrix positioning the dye in the propylene oxide block volume.

Propylene oxide block creates a hydrophobic environment and thus forms preferred conditions for free end flipping while bringing two dyes closer together. We speculate that at lower temperatures, the free end of the poloxamer, which contains the hydrophobic naphthalimide dye, folds itself back into the polymer matrix, schematically presented in Figure 3.7. This folding of the poloxamer brings the two dyes closer together (since the mobility of the oxadiazole dyes is limited), resulting in an enhanced FRET efficiency. As the temperature approaches the LCST of the poloxamer used, packing of the PPO block becomes too dense[31, 108, 109] and, as a result, the naphthalimide can not fit inside the polymer matrix and is pushed to the outer edge, increasing the distance between the dye and the surface of nanoparticle along with oxadiazole dye, which results in the observed reduced FRET efficiency.

Using the characteristic ratios of ethylene oxide (EO) and propylene oxide (PO) segments of the poloxamer copolymer, the theoretically calculated end-to-end distance of the chain in a theta solvent was calculated to be ca. 4.9 nm[61]. The theta condition is defined as the state when a polymer can not distinguish between itself and its surrounding solvent molecules and adopts relatively “compact” conformations that are defined by local interactions. This calculated value was 58 % to 25 % greater than the shortest and longest, respectively, distance between the dyes obtained from the FRET calculations and supports the concept that the naphthalimide end of the copolymer is folded back into the polymer matrix.

Previous studies have shown that hydrophobic drugs have a tendency to concentrate in the core of a poloxamer PPO block[93, 99, 110, 111]. Additionally, previous reports indicate that hydrophobic drugs sequestered in the PPO domain of a poloxamer can be ejected as the temperature is raised above the LCST of the copolymer[93]. As indicated previously, we speculate for the PA/azOx/azPlurNaph particles at temperatures below the LCST, the PPO block of the poloxamer forms a hydrophobic pocket around the PA particles, which attracts the naphthalimide dye[31], since this layer provides a more favorable condition relative to the aqueous environment outside of these PPO layers (schematically presented on Figure 3.7). At temperatures higher than the LCST, the packing of the PPO block becomes too dense[95, 91, 13] to accommodate the naphthalimide dye inside of the layer and the dye is forced out to the outer edge of the polymer matrix, away from the donor dye. This increase in the distance between azOx and azPlurNaph dyes leads to a decrease in the FRET efficiency.

The role of the poloxamer was investigated by modifying a set of particles with a azide fictionalized naphthalimide dye (azNaph) instead of azPlurNaph. These PA/azOx/azNaph particles did not exhibit any emission when dispersed in water and excited at a 335 nm or 400 nm excitation wavelength, indicating that there is fluorescence quenching when the particles do not have the poloxamer on the particles. Dispersing the particles in tetrahydrofuran (THF), a solvent in which both dyes are miscible, resulted in the reappearance of the typical spectra of the dyes. This observation further suggests that changes in the poloxamer state is the main mechanism responsible for the changes in emission patterns for the PA/azOx/azPlurNaph particles when in an aqueous state.

To test the proposed mechanism, a small molecule study was performed with just the azOx, azPlurNaph, and the unmodified poloxamer. In this system, the

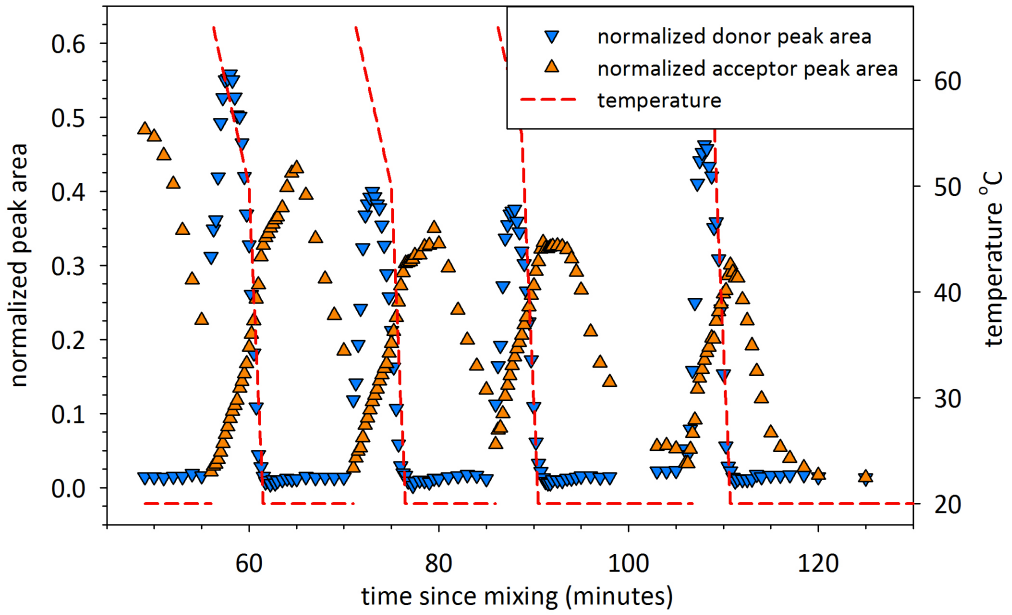

Figure 3.8: Normalized integrated emission attributed to azOx (▽) and azPlurNaph (△) dyes in small molecule study performed with azOx, azPlurNaph, and the unmodified poloxamer in deionized water. Sample was repeatedly heated to 65°C (LCST of poloxamer was 58°C) and then allowed to cool down. For the donor dye (azOx), the emission was integrated between 340 nm and 480 nm while for the acceptor dye (azPlurNaph) the emission was integrated between 510 nm and 590 nm. The sample was excited at a wavelength of 335 nm.

three components were placed in deionized water and excited at a wavelength of 335 nm while the temperature was cycled between 20 °C and 65 °C, all the while observing the emission of the system. The ratio of the dyes was 1 to 1 and total concentration of poloxamer copolymer was 15 mg/mL. The results of the study are depicted in Figure 3.8, where the integrated emission attributed to the azOx and azPlurNaph dyes is presented relative to time and temperature. Initially at temperatures around 20 °C, there is only an emission from the azPlurNaph dyes (acceptor) that is replaced by an emission from the azOx dye (donor) when the system is heated to 65 °C. We attribute this to the fact that the system initially exhibits FRET between the dyes, at room temperature, and then the energy transfer is disturbed when the system is heated to 65 °C, above LCST of the poloxamer. This

emission switching from the azPlurNaph dye to the azOx dye as the temperature is cycled back and forth was repeated multiple times with four cycles being presented in Figure 3.8.

There is a clear emission switching from the donor dye to the acceptor dye with the temperature cycling. The small molecule model system exhibited the same patterns of emission as the PA/azOx/azPlurNaph particles, but there are two differences. First, the emission of the small molecule system is time dependent (decreases with time) due to the precipitation of the dyes from solution, supporting the need for the particles acting as a stabilizing carrier. Second, the FRET efficiency variation of the small molecule system is much more prominent as compared to the particles. It is hypothesized that almost complete 0 % to 100 % FRET efficiency change exhibited by the small molecule system is due to the much higher mobility of both dyes as compared to the system where the dyes are attached to the nanoparticles. Performing the same study without the poloxamer resulted in no emission since the dyes are hydrophobic and presumably precipitate from solution quickly. Clearly, the poloxamer plays an important role in sequestering the dyes in an aqueous environment, and this role is highly temperature dependent.

3.3 Conclusion.

In the present work, we achieved control over the changes in FRET efficiency of an emissive colloidal system through the attachment of a donor dye (azOx) directly to the particle surface, while an acceptor dye (azPlurNaph) was attached to the surface of particles through a poloxamer copolymer. The poloxamer (Pluronic-L64) was utilized as the temperature responsive component to regulate the distance between the dyes. The current system achieved its maximum variation in FRET ef-

ficiency ($\Delta\varepsilon_{FRET} \approx$20 %) in the temperature range of 49 °C to 60 °C, which is in the region of the cloud point of the poloxamer (LCST) used in this study, though other poloxamers with differing LCST temperatures could be utilized to tune the temperature range of the colloidal device.

3.4 Experimental methods

3.4.1 Materials and Reagents

All reagents were purchased from Sigma-Aldrich with at least 97% purity level. Deionized water was obtain from Barnstead Nanopure Diamond water system and had 18.2 MOhm resistance. Spectroscopic grade of tetrahydrofuran was used to measure absorbance and emission of the dyes.

3.4.2 Characterization

^{1}H spectra were recorded on JEOL ECX-300 spectrometers (300MHz for proton). Chemical shifts for protons are reported in parts per million downfield from tetramethylsilane and are referenced to the carbon resonances of the solvent ($CDCl_3$: δ 7.26), 2 mg/mL solutions were used to record ^{1}H spectra. Photoluminescence (PL) spectra were collected using Photon Technology International (PTI) spectrometer equipped with Hamamatsu C9940-01 detector and Jobin-Yvon Fluorolog 3-222 Tau spectrometer. Lifetime measurements were collected using a Jobin-Yvon Fluorolog 3-222 Tau spectrometer. Photoluminescence dependence on temperature was measured using PTI spectrometer equipped with Quantum Northwest TC125 temperature control unit using 10 mm quartz cuvette. Nanoparticle size was checked using Coulter N4Plus dynamic light scattering (DLS) instrument using 10

mm plastic cuvette. UV/Vis spectra was obtained using Perkin Elmer Lambda 850 spectrometer using 10 mm quartz cuvette.

3.4.3 Nanoparticle preparation

Emulsion polymerization was performed in a single necked round bottom flask (100 mL) with magnetic stirring. Potassium persulfate (70 mg) was dissolved in water (29 mL) and nitrogen was purged through the solution for 15 minutes. Sodium dodecyl sulfate solution (29% in H_2O, 0.4 mL) was added to the flask under nitrogen. The resulting solution was stirred and placed in a preheated bath at 70 °C for 2 minutes, then a degassed solution of propargyl acrylate (2 mL) and divinylbenzene (0.1 mL) were added to the main reaction. The mixture was stirred at 70 °C under nitrogen for 90 minutes. Magnetic stirrer was used to mix the reaction, speed of steering was set at 400 rpm. Size of the magnetic stirrer was selected such that ensured creation of a stable vortex that was not reaching bottom of the solution. If the conditions of stirring were not met resulting nanoparticles had very wide size distribution rendering them useless for the intended application. After 90 minutes at 70°C reaction was cooled, then filtered using paper filter; followed by purification by dialysis using Spectra/Por Dialysis membrane with MWCO 50000 for 3 days at 40 °C in a 20 liter dialysis bath filled with 18.2 MOhm resistance deionized water, with water being changed every 8 hours. Nanoparticles were characterized using DLS, median size was 60 nm with a standard deviation of 10 nm. The final emulsion contained 45 mg/mL of nanoparticles.

3.4.4 Oxadiazole-N3 preparation

Oxadiazole-N_3 was synthesized and purified prior to use according to literature procedure[41]. Synthesis consisted of three steps:

2-(4-Methylphenyl)-5-(1-naphthyl)-1,3,4-oxadiazole (Figure 3.9A). A mixture of 5-(4-methylphenyl)-2H-tetrazole (2.5 g, 15.6 mmol), 1-naphthoyl chloride (3.27 g, 17.2 mmol) and pyridine (30 mL) was stirred and refluxed for 5 h. After cooling to room temperature, the mixture was quenched with water to precipitate the product. White crystals were filtered and dried on air to give the titled compound. Yield: 4 g (90%). ^{1}H NMR ($(CD_3)_2SO_2$) 2.43 (s, 3H), 7.46 (d, 2H), 7.667.80 (m, 3H), 8.10 (m, 3H), 8.24 (d, 1H), 8.40 (d.d, 1H), 9.19 (d,).

2-[4-(Bromomethyl)phenyl]-5-(1-naphthyl)-1,3,4-oxadiazole (Figure 3.9B). A solution of 2-(4-methylphenyl)-5-(1-naphthyl)-1,3,4-oxadiazole (1 g, 3.39 mmol), N-bromosuccinimide (0.622 g, 3.49 mmol) and benzoyl peroxide (0.03g, 0.12 mmol) in chloroform (40 mL) was refluxed for 4 h to result in 50% conversion of the starting compound as determined by ^{1}H NMR. N-bromosuccinimide (0.622 g, 3.49 mmol) and benzoyl peroxide (0.02 g, 0.08 mmol) were added again and the solution was refluxed for 5 h. The solvent was evaporated and the residue was washed with water, filtered, dried on air and recrystallized from acetone to produce white crystals. Yield: 0.86 g (67%). ^{1}H NMR ($CDCl_3$) 4.55 (s, 2H), 7.567.65 (m, 4H), 7.72 (m, 1H), 7.95 (d, 1H), 8.06 (d, 1H), 8.19 (d, 2H), 8.28 (d.d), 9.28 (d, 1H).

2-[4-(Azidomethyl)phenyl]-5-(1-naphthyl)-1,3,4-oxadiazole (Figure 3.9azOx). A mixture of 2-[4-(bromomethyl)phenyl]-5-(1-naphthyl)-1,3,4-oxadiazole (0.8 g, 2.19 mmol) and sodium azide (0.17 g, 2.61 mmol) in dimethylformamide (10 mL) was heated and stirred at 80 °C for 8 h. After cooling to room temperature, the mixture was quenched with water and cooled to 5 °C . The solid was filtered, washed

with water and dried on air to give white crystals. Yield: 0.65 g (76%). ^{1}H NMR ($CDCl_3$) 4.47 (s, 2H), 7.53 (d, 2H), 7.62 (m, 2H), 7.72 (m, 1H), 7.95 (d, 1H), 8.06 (d, 1H), 8.23 (d, 2H), 8.28 (d.d, 1H), 9.29 (d, 1H).

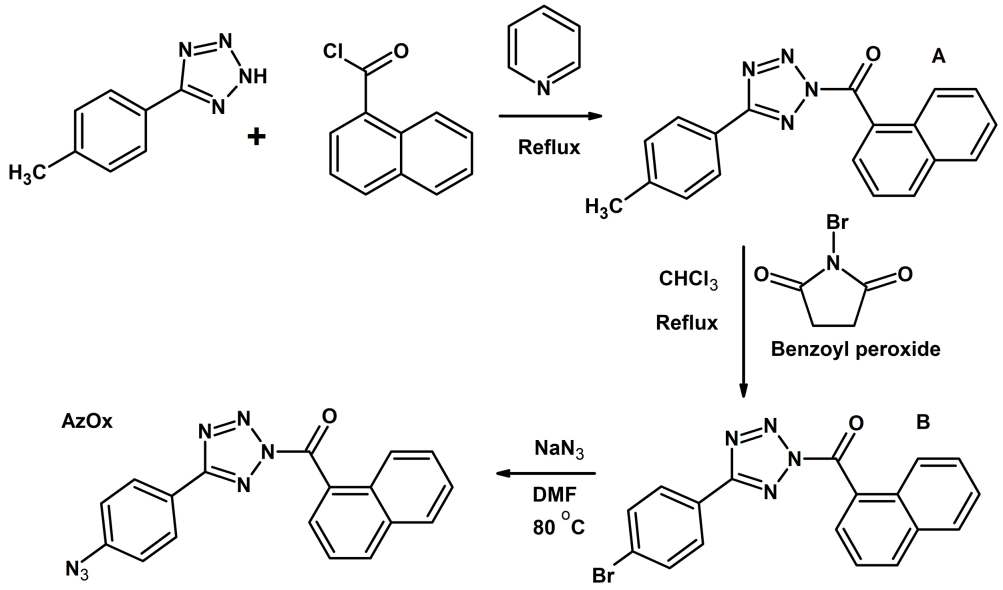

Figure 3.9: Scheme of AzOx dye synthesis.

3.4.5 Naphthalimide preparation

Naphthalimide was synthesized prior to use according to literature procedure [112]. 0.67 g of Naphthalic anhydride was mixed with 340 mg of formamid in 15 mL of methanol using 35 mL pressurized reaction vial. Vial was hermetically closed with Teflon screw and heated to 120°C for 40 hours. Solvent was evaporated under vacuum and resulting product was analyzed using ^{1}H nuclear magnetic resonance (NMR) technique. Obtained 0.65 g of brown powder. ^{1}H ($CDCl_3$) δ 7.93 (m, 1H), 8.19 (s, 1H), 8.22 (m, 1H), 8.47 (m, 2H).

Second step was addition of piperidine ring. Product from previous step

was mixed with piperidine in 8 mL of dimethyl sulfoxide (DMSO) in 25 mL round bottom flask equipped with condenser. Reaction was mixed at 85°C for 20 hours. 20 mL of deionized water was added to dissolve byproducts and DMSO, 10 mL of dichloromethane was added to dissolve product. Mixture was transferred into separation funnel and was vigorously shaked for 2 minutes. After mixture had phase separated, typically this process required 2 to 5 minutes, lower organic layer was collected into Erlenmeyer flask. 20 mL of deionized water were added to the separated organic layer and mixture was again transferred into clean separation funnel. Process of mixing and separation was repeated as described above. After last separation 5 g of sodium sulfate was added to organic layer to remove remaining water. Mixture was mixed for 3 minutes and filtered through paper filter. Organic layer was evaporated under reduced pressure and checked with ^1H ($(CDCl_3)$ δ 1.66 (m, 6H), 1.89 (m, 4H), 7.68 (m, 1H), 8.49 (m, 4H)), obtained 0.65 g of yellow powder. This powder was used in Poloxamer-N3 modification process as described below. Scheme of reaction is shown on Figure 3.10.

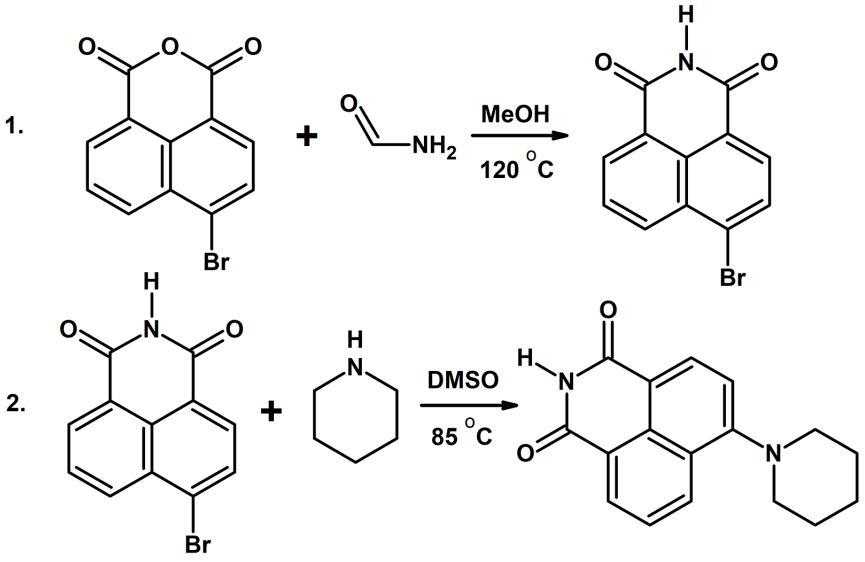

Figure 3.10: Scheme of naphthalimide dye synthesis.

3.4.6 Poloxamer modification

$MeSO_2$-pluronic-L64. Pluronic-L64 (3.14 g, 1.064 mmol) was dissolved in dry dichloromethane (DCM) (10 mL), triethylamine (0.132 g, 1.3 mmol) was added to the solution. The obtained solution was stirred at room temperature for 15 minutes to ensure good mixing of the components. Methanesulfonyl chloride (62 mg, 0.543 mmol) was dissolved in 2 mL of dry dichloromethane and added drop-wise to the reaction mixture over 3 minute period. Temperature of the reaction mixture was monitored while methanesulfonyl chloride was added, if the reaction started to warm up the rate at which methanesulfonyl chloride was slowed or even stopped completely until the reaction had cooled down to room temperature.

After all methanesulfonyl chloride was added reaction mixture was stirred for 6 hours at room temperature. After 6 hours 20 mL of water was added to the reaction mixture to remove triethylamine chloride and any other water soluble contaminants. Mixture was vigorously shaked for 2 minutes and then left for 20 minutes to allow phase separation process between water and DCM to complete. If after 20 minutes no clear phase boundary was observed 20 mg of sodium chloride was added to the mixture and again shaked vigorously for 2 minutes or until all sodium chloride was dissolved. After this mixture was again left to stand for 20 minutes to allow water and DCM to phase separate. Bottom layer was collected and 20 more mL of deionized water was added to it. Mixture again was vigorously shaked for 2 minutes followed with separation as discussed above. This process was repeated 3 times. After 3 time DCM layer was pored over 3 g of sodium sulfate salt. Obtained mixture was mixed for 2 minutes or until all cloudiness was cleared. After this mixture was filtered through paper filter to remove sodium sulfate salt and evaporated under reduced pressure. Yield 3.1 g (95%), clear oil. This product

was used in the next step without further purification. ^{1}H NMR ($CDCl_3$) δ 1.11 (m, 96H), 3.06 (s, 3H), 3.38 (m, 32H), 3.52 (m, 64H), 3.63 (m, 98H).

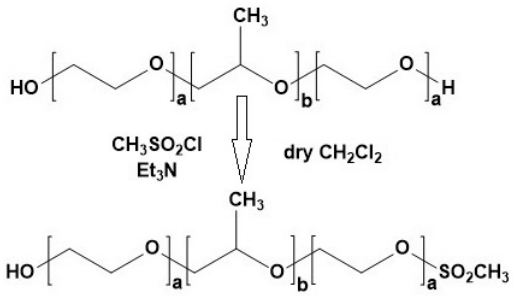

Pluronic-L64-N3. Sodium azide (195 mg, 3 mmol) was added into solution of $MeSO_2$-pluronic-L64 (3.1 g, 1.03 mmol) in dimethylformamide (DMF) (10 mL). The mixture was stirred and heated to 80 °C for 3 hours. After cooling the mixture was extracted with DCM and washed with water 2 times following the same procedure as for $MeSO_2$-pluronic-L64. The organic layer was separated, dried with Na_2SO_4, filtered and evaporated under reduced pressure. Yield 2.27 g (75%), clear oil. Pluronic-L64-N3 was used in the next step without further purification. ^{1}H NMR ($CDCl_3$) δ 1.07 (m, 96H), 3.34 (m, 32H), 3.48 (m, 64H), 3.59 (m, 98H).

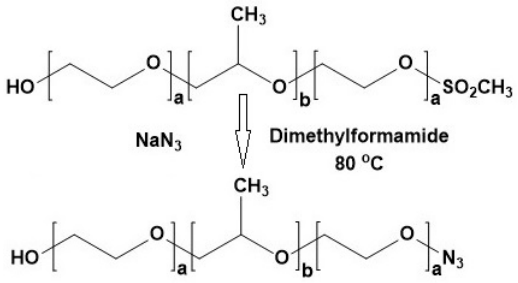

$MeSO_2$-pluronic-L64-N3. Pluronic-L64-N3 (1 g, 0.34 mmol) was dissolved in dry DCM (3 mL), then triethylamine (42 mg, 0.408 mmol) was added. The solution was stirred at room temperature and methanesulfonyl chloride (78 mg, 0.68

mmol) in 2 mL of dry DCM was added drop-wise following the same precautions as described above. The reaction was stirred at room temperature for 6 hours, followed by extraction with DCM and washed with water as described above. The organic layer was separated, dried with Na_2SO_4, filtered and evaporated under reduced pressure. Yield 0.7 g (65%), clear oil. This product was used in the next step without further purification. ^{1}H NMR ($CDCl_3$) δ 1.11 (m, 96H), 3.07 (m, 3H), 3.38 (m, 32H), 3.52 (m, 64H), 3.64 (m, 98H).

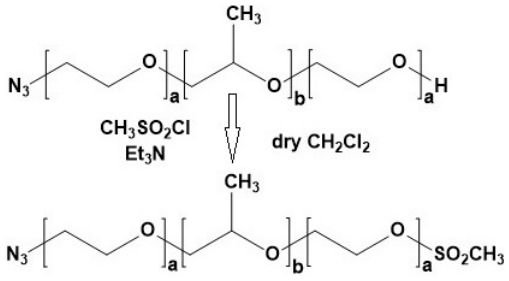

azPlurNaph. The mixture of $MeSO_2$-pluronic-L64-N3 (0.7 g, 0.22 mmol), naphthalimide (100 mg, 0.36 mmol) and potassium carbonate (80 mg, 0.58 mmol) in acetone (15 mL) was stirred and refluxed for 48 hours. The mixture was filtered, and the filtrate was evaporated under reduced pressure; the residue was extracted with DCM and washed with water using the same procedure as described above. The organic layer was separated, dried with Na_2SO_4, filtered and evaporated under reduced pressure. Yield 0.58 g (80%), yellow oil. ^{1}H NMR ($CDCl_3$) δ 1.11 (m, 96H), 1.70 (m, 6H), 1.86 (m, 10H), 3.38 (m, 32H), 3.52 (m, 64H), 3.62 (m, 98H), 7.14 (m, 2H), 7.65 (m, 2H), 8.31-8.54 (m, 8H).

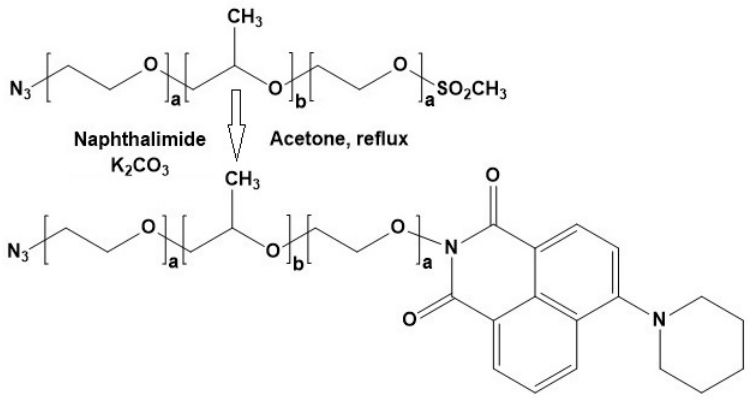

3.4.7 Nanoparticle modification

Nanoparticle modification was performed using the azide alkyne Huisgen cycloaddition reaction (Click chemistry). A typical procedure was used as described elsewhere[41]. In short, copper(II) sulfate ($CuSO_4$) (2 mg, 8 μmol) was dissolved in 2 mL of deionized water and added to the propargyl acrylate nanoparticles suspension in water (2 mL) that contained 45 mg of dry propargyl acrylate cores. The solution of azOx (2 mg, 7 μmol) in the mixture of tetrahydrofuran (THF) (2 mL) and methanol (4 mL) was added to the suspension of nanoparticles. Reaction vessel was purged with nitrogen for 5 minutes while stirring with magnetic stirrer, then sodium ascorbate (10 mg, 50.5 μmol) was added. The mixture was stirred at 28°C for 24 hours, nitrogen was purged at slow rate over the top of solution; then the solution of azPlurNaph (22 mg, 7 μmol) in THF (2 mL) was added. Then the solution of $CuSO_4$ (2 mg, 8 μmol) in water (2 mL) was added. The reaction was stirred and purged with nitrogen through solution for 5 minutes, then sodium ascorbate (10 mg, 50.5 μmol) was added. The reaction continued at 28 °C for 24 hours under nitrogen purge over the top of solution.

The reaction mixture was centrifuged at 10000G for 5 minutes. All solvent and dissolved reagents were decanted while leaving precipitated nanoparticles on

the bottom of the centrifuge tube. Dye content in the supernatant solution was measured based on the UV/Vis absorption utilizing Beer-Lambert Law: dependence of absorbance maximum on the dye concentration. The calculated amount of the dye was subtracted from the loaded amount of the dye to find the encapsulated quantity for both dyes.

Separated nanoparticles were redispersed in the mixture of THF:Methanol 1:1 (20 mL) using a vortex shaker set to maximum speed. If after 1 minute on the shaker big aggregates were still present, the centrifuge tube was placed in the sonication bath for 15 minutes. After sonication, suspension was again agitated using a vortex shaker for 15 seconds set to maximum speed. If aggregates still were visible, then sonication process was repeated. When all aggregates were dispersed, suspension was centrifuged at 7000G for 10 minutes. After centrifugation all solvent was again decanted, leaving nanoparticles in the centrifuge tube and then the dye content in supernatant was measured and added to the amount of the dye as was found after first centrifugation.

This purification process was repeated 5 times to remove all impurities. If after the 5th time the peak for any of the dyes was still detectable by UV/Vis, the cleaning process was repeated again until UV/Vis was no longer able to detect the dye in supernatant solution. The content of unreacted dyes in the supernatant solution was monitored by observation of UV/Vis absorption (for azOx peak at 330 nm was monitored, for azPlurNaph peak at 400 nm was monitored). When these peaks were impossible to identify the cleaning process was considered complete. In some cases, more than 5 repetitions of centrifugation were required. After the last centrifugation the nanoparticles were suspended in water (3 mL) and stored in the dark until further use.

3.4.8 Grafting density determination

To determine grafting density of the dyes all supernatant solutions from nanoparticle cleaning process were collected and the dye content in them was calculated using the Beer-Lambert law based on the specific absorption for each dye. The mass of both dyes in all supernatant solutions was calculated and summed. To determine the mass of the dye total volume of the collected supernatant after each step was multiplied by the concentration of the dye in this supernatant solution as found according to Beer-Lambert law. This sum was subtracted from the loading quantities of the dyes to calculate mass of the dyes that had reacted. Total surface area of the nanoparticles was calculated using the assumption that nanoparticles are perfect mono-disperse spheres with 60 nm diameter. Nanoparticles core size was determined prior the modification process using dynamic light scattering and was found to be be 60 nm. To find the final grafting density for each dye total number of molecules was calculated based on the calculated total mass of the dye that has reacted, was determined as described above, this total number of molecules was divided by the total surface area of the nanoparticles to yield grafting density in molecules per nm^2 of the core surface. The final grafting density for oxadiazole-N_3 was found to be 0.54 molecules per nm^2, naphthalimide-pluronic-L64-N3 complex 0.39 molecules per nm^2.

3.4.9 Fluorescence measurements

Sample preparation procedure for fluorescence measurements for dual dye modified nanoparticles were as follows: portion of the suspension obtained after cleaning was dispersed in water to achieve nanoparticle density of approximately 0.1 mg/mL, which translates to approximately $1*10^{-9}$ mole/mL of dye. All samples

were allowed 24 hours for equilibration at room temperature prior to any measurement. For each measurement, 3 mL of the nanoparticle suspension in water was transferred into 1 cm quartz cuvette equipped with stirrer. Prior to conducting a measurement at a given temperature, the sample was allowed to equilibrate at this temperature for 15 minutes to ensure that the system has reached equilibrium state. Experimentally, it was shown that for all temperature ranges, stable emission levels were reached within 3 to 6 minutes at a given temperature, so allowing an extra 10 minutes is expected to be sufficient for nanoparticles to reach stable equilibrium.

For a single dye modified nanoparticles, concentration of the nanoparticles was selected based on the emission maximum of azOx modified nanoparticles to match the emission maximum of oxadiazole peak of dual dye modified nanoparticles. PlurNaph modified nanoparticles concentration was matched to the azOx nanoparticles. During the preparation of single modified nanoparticles, loading amounts for both dyes were calculated to match the total number of chromophores on dual dye modified nanoparticles. This was done to ensure similar separation distance between dyes for all 3 samples. Matching of the emission maximum for azOx dye was done to better illustrate that the emission's peak shape for dual modified nanoparticles had changed.

Chapter 4

Control over poloxamer grafting density

Poloxamer copolymers have a unique set of the responsive and encapsulation properties that find implementation in the biomedical applications. Through the immobilization of the poloxamer on the surface of a bio-compatible polymeric nanoparticle, control of the nanocomposite properties was achieved. Precise control over the composition and, as a result, of the final properties of the nanocomposite allowed to fine tune the performance of the system build. In this study, an original nanocomposite of poly(propargyl acrylate) (PA) and poloxamer is synthesized using graft to approach. Azide-alkyne Huisgen cycloaddition reaction allowed the formation of a stable bond between the poloxamer and PA nanoparticle and eliminated the need of an aggressive solvent or toxic, hard to remove, catalyst in the preparation process. Quick and reliable method to monitor the nanocomposite composition based on the Fourier transform infrared (FTIR) spectroscopy is described. Additionally, the system is characterized by dynamic light scattering (DLS), scanning electron microscopy (SEM), Nuclear Magnetic Resonance (NMR) and BrunauerEm-

mettTeller (BET) techniques. The developed method allowed us to design a protocol for synthesis of a device that is free of any unattached poloxamer chains and has a well defined surface chemistry. FTIR allowed to reliably determine mass ratio of PA to poloxamer above 1 mass percent of poloxamer in the nanocomposite. Based on the observed results optimal synthesis and purification procedures are described.

4.1 Introduction

In the recent years, decease treatment using active molecules have seen an increase in the number of methods developed based on the polymer nanocomposites [20, 113, 114]. One of the investigated approaches is based on the devices built from the copolymers that tend to self assemble into micelles under certain conditions [115, 116]. Another important approach is based on the core-shell nanocarriers [117, 118]. Both of these approaches have their advantages and draw backs. Some of the challenges of the self assembly carriers is the lack of the control over the micelles size and the instability of the micelles under certain conditions. Two common challenges of the core-shell systems are complicated synthesis and lack of the control over the trigger mechanism. Often core-shell systems lack adjust ability and are locked for a certain temperature or pH range [119, 120]. As one of the approaches to achieve the adjust ability of the final properties of the drug carrier the control over the grafting density of the shell was proposed by Asai [121]. In this work a synthesis scheme for a nanocarrier that combines advantages of both approaches while eliminating their disadvantages is discussed.

An important step during the evaluation of any drug carrier is the complete and accurate characterization of the final assembly. Thus ability to quickly and reliably characterize the composition of the nanocarrier becomes an essential tool

when designing a drug delivery vesicle [122]. Fully polymeric systems often present a challenge in the precise determination of the composition of the nanocomposite after the final device was assembled and often require a non-standard analytical approach to determine the final composition of the nanocomposite. The knowledge about exact nanocomposite composition can provide a valuable incite about the influence of surface morphology on the final properties of the device and ability to differentiate between different grafting densities is essential tool in the final testing of active drug delivery vesicles.

Schematically the difference between various grafting density states is shown on Figure 4.1. As can be seen from the cartoon, Figure 4.1A, at low GD some of the core surface is still open, this creates a possibility of drug absorption by the surface rather than by the active shell layer thus upon trigger event these surface bound molecules will remain unaffected and even though the loading capacity of such devices can still be relatively high the release, and specifically triggered release efficiency will be small. At some intermediate grafting density, Figure 4.1B, all surface is covered with the active shell, all cargo will be encapsulated inside of the shell rather than being absorbed by the surface as in first case, and thus upon trigger event the probability of release is much higher since all cargo is contained within the active layer of the device.

Graft to method has an upper limit of the grafting density. Only limited number of the polymer chains can be attached to the surface since the chains that have been attached first will create a steric barrier for any additional chains. After reaching certain grafting density using graft to methods speed of reaction decreases and the dominant factor that determines this speed becomes the ability of the reactive end to penetrate through the brush formed from already attached to the surface chains. Combining high loading ratio with long reaction times it is possi-

ble to reach grafting densities at which polymer chains will start to influence their neighbors ability to undergo thermal transitions. At such conditions, as shown on Figure 4.1C, device can start loosing its ability to burst release cargo due to limited mobility of the polymer chains on the surface.

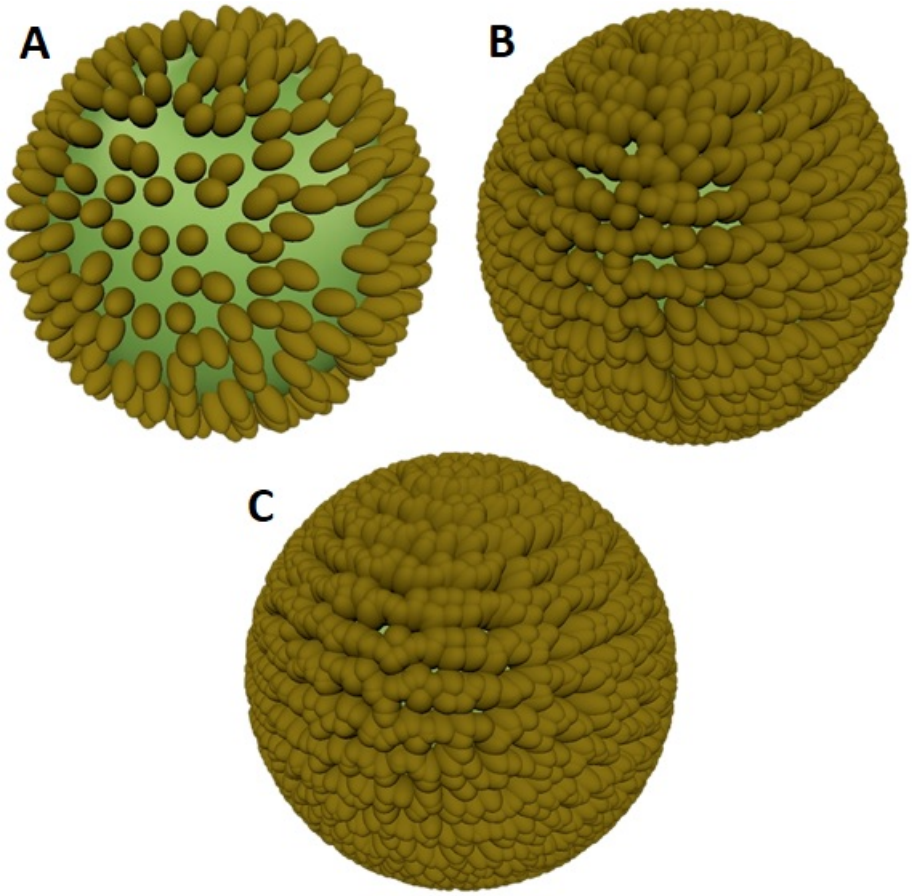

Figure 4.1: Cartoon illustrating the influence of grafting density on the surface morphology. **(A)**. Nanoparticle with low grafting density of the shell, lots of open core surface, limited temperature responsiveness. **(B)**. Nanoparticle with optimal grafting density, all surface is covered, maximum temperature responsiveness. **(C)**. Nanoparticles with too high grafting density, shell chains restrict each others movement ability decreasing temperature responsiveness. Cartoon is based on the theoretically calculated dimension of the core and poloxamer copolymer representing 0.15, 0.35 and 0.55 poloxamer chains per nm^2 grafting density equivalents. Surface decoration with poloxamer was done using Maya 2016 software package utilizing random surface population with X-gen function of the software utilizing Mental Ray package version 3.13.1.2.

Poloxamer family of copolymers originally was developed as an effective sur-

factant for both personal and commercial use [30, 31]. Later these copolymers were found to be useful in drug delivery application [123, 124]. Copolymer chains consists of a hydrophobic block positioned between two hydrophilic blocks. Such structure offers a favorable environment for drugs while protecting these drugs from the aqueous environments. Some of the benefits of poloxamer based systems for medical applications are: their ability to re-sensitize cancer tissue to the drug [98, 34], decreasing the required drug concentration and as a result decreasing the possibility of the side effects; the ability to prolong the circulation of the devices decorated with poloxamer in the human body [33], allowing ample time for the device to complete its designed drug delivery mission; the ability to program the temperature of response based on the selection of appropriate commercially available poloxamer [31] eliminating the need to modify the synthetic procedures every time a different temperature of response is needed.

Additionally, poloxamer solves the challenge of complex synthesis and allows the programming of the temperature of the response simply through the use of a correct copolymer version. Hydroxyl groups on the ends of the copolymer chain can be substituted with other functional groups making it possible to attach the poloxamer to the surfaces or to attach active molecules to the poloxamer.

Poloxamers can self-assemble into micelles, but stability of such micelles is dependent on both temperature and concentration, thus they can disassemble before reaching their target and the release of the active molecules can occur outside of the region of interest rendering the treatment ineffective. To solve this challenge a method is proposed to immobilize the poloxamer on the surface of the propargyl acrylate nanoparticle creating a designed formation, making the hydrophobic pockets formed by the propylene oxide block stable.

Propargyl acrylate nanoparticles (PAn) besides serving the purpose of the

inert bio-compatible core [41] helps to solve one more challenge: control over the size of the drug delivery vesicle. As was shown by Roeder [36] PAn can be readily synthesized in a wide range of sizes with a narrow size distribution. Control over the size of the drug delivery vesicle is important because it allows the researcher to use passive targeting as a mechanism of targeted drug delivery[103]. Cancer tissue is known to have a higher blood vessel porosity allowing the devices with size range 40-200 nm to concentrate inside of the tissue [125, 103, 104]. Another benefit of PAn is the ability to use Azide-alkyne Huisgen cycloaddition, also known as Click chemistry, to attach various molecules to the surface [41, 40]. Click chemistry is a highly selective and very efficient process with very low sensitivity to impurities and can be done from a variety of solvents, including water. Use of the Click chemistry eliminates the need for a complex purification steps before the final assembly of the device because even if the starting components have some contamination from the previous synthesis steps, only molecules bearing an azide and an alkyne groups will react under the reaction conditions. Since Click chemistry does not require complex hard to remove catalysts or aggressive solvents the post assembly purification can be done simply through the centrifugation or the dialysis solving the complex synthesis challenge of other core-shell based systems.

Lastly, the challenges related to nanoparticle characterization is quantification of surface chemistry on the final device. In the inorganic core/organic shell composite systems determination of the grafting density often is made using thermogravimetric analysis (TGA)[126, 127, 128]. TGA is a relatively quick and reliable way to determine the ratio of the core mass to the mass of the shell, making it possible to calculate the number of molecules per nm^2 of the surface. For the organic on organic nanocomposites TGA fails most of the time due to similarities of the decomposition temperatures of the core and the shell rendering it impossible to

differentiate between the two.

Various indirect techniques have been developed to estimate the shell density on the organic nanoparticles[129, 130], and among these methods FTIR offers the most value and precision[131, 132]. FTIR allows us to detect the functional groups and assuming that a correlation between the height of two peaks and the ratio of the groups that correspond to these peaks can be established a quantification can be achieved[133]. Quantification of the sample using FTIR is not always possible and some of the prerequisites of the successful quantification are: the ability to distinctively separate the signals from the bonds of interest; the strong absorption of the infrared light by these bonds; and the ability to create a model sample with a well defined ratio of the bonds of interest at a wide mass ratio range.

Quantification of the sample using FTIR is a labor intensive process. First a calibration curve has to be obtained against which the unknown samples will be compared. To build a calibration curve a set of the standard samples, at least 3, more is better, has to be created. These standards have to be chemically identical to the unknowns and only the ratio of the functional groups of interest should vary. In the case of the polymer composites, this means that a mix of all components has to be prepared and the ratio of the components has to be well defined in this mix. Next step is to record FTIR spectra of all the standards and to measure the absolute heights of all the peaks of interest. Then using the ratio of peaks a calibration curve can be built. This curve represents the dependence of the peak ratio to the component mass ratio. Comparing the unknown sample peak ratio to the calibration curve allows us to obtain the information about the mass ratio of the components in the sample. Combining the mass ratio data with the size of the cores data and the molar mass of the shell components allows us to calculate the true grafting density of the nanocomposite. In case of spherical cores simple geometry equations can

provide the required information about the total surface area (S) in a given mass of the sample, and in case of a mono-disperse coating knowledge of the molecular weight (MW_{shell}) of the coating combined with the mass ratio of the shell to the core yields a number of molecules per nm^2 of the surface. Number of the molecules in the coating can be determined from the following equation:

$$N = \frac{TM_{shell}}{MW_{shell}}$$

Total mass (TM_{shell}) of the shell is obtained based on the mass ratio information from the FTIR calibration curve. To convert the number of the shell molecules into the grafting density (GD) the following equation is used:

$$GD = \frac{N}{S}$$

4.2 Results and Discussion

4.2.1 Nanocomposite assembly

Propargyl acrylate nanoparticles (PAn) were prepared via emulsion polymerization and characterized using DLS and SEM according to previously reported methods [36], target size for the PAn was 30 nm to maintain high mass ratio between the core and the shell. In short, the emulsion polymerization was carried out under the following conditions: potassium per-sulfate was added as an initiator of the polymerization; 15% by mass of the divinil benzene was added to propargyl acrylate monomer as a cross-linking agent, to create highly rigid cores; temperature of the reaction was maintained at 75°C and the reaction was stopped after 90 minutes to prevent hydrolysis of the carbonyl group on the propargyl acrylate.

Emulsion was followed by a dialysis in 18.2 MOm deionized water to remove any unreacted monomers, excess of catalyst and surfactant. Emulsion performed under this conditions allowed to achieve the desired size with a narrow size distribution that was confirmed by DLS and SEM measurements. To check for aggregates, a column chromatography was used to separate the sample on fractions according to the nanoparticles sizes. Analysis of each fraction confirmed that in the analyzed sample only one nanoparticle size was present, so any aggregation observed on SEM imaging is, most likely, due to the sticking of nanoparticle together during the drying process, rather than the presence of actual aggregates in the sample.

Azide-alkyne Huisgen cycloaddition, also known as the Click chemistry, was used to attach the poloxamer chains to the surface of PAn. Control over the feed ratio and the reaction time allowed us to synthesize the nanocomposite of a desired composition, schematically the synthesis scheme is shown on the Figure 4.2.

Click chemistry requires that one of the reagents have alkyne group, and the other to have azide group. PAn has alkyne groups on its surface and does not require any additional modifications post the purification step. Poloxamer, on other hand, needs to be modified prior it can be grafted on to PAn. Poloxamer copolymer has two hydroxyl groups on its ends and at least one has to be replaced with the azide group. Modification of both ends with the azide group is the easiest synthetic task, but having two active ends on one polymer chain creates a possibility for double attachment of the poloxamer chain to the same core or even cross core attachment leading to a formation of cross-linked matrix with PAn imbedded in it. In order to prevent this, the feed ration of methanesulfonyl chloride during the first step of poloxamer modification was limited to 85% of the amount required to replace just one hydroxyl group. This starvation of the reaction was done to decrease the probability of the formation of poloxamer chains with azide groups at both ends. ^{1}H

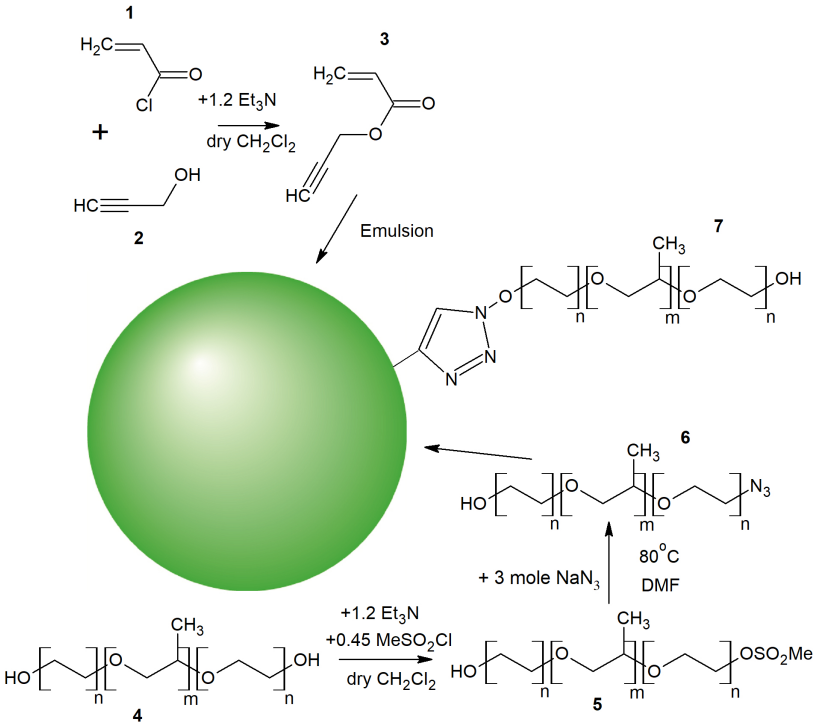

Figure 4.2: Scheme of nanocomposite assembly. 1 - acryloyl chloride, 2 - propargyl alcohol, 3 - propargyl acrylate (PA) monomer (distilled under vacuum before polymerization), 4 - Pluronic L-64, 5 - methyl sulfonyl mono-substituted poloxamer, 6 - azide mono-substituted poloxamer, 7 - final assemble of PA nanoparticle decorated with poloxamer chains.

NMR was used to monitor the reaction, peak from the methanesulfonyl appeared at 3.06 ppm and integrated at 2.42 to 96 total hydrogen atoms in CH_3 group of PPO block, comparison of ^{1}H NMR spectra of the stock poloxamer and the methanesulfonyl modified poloxamer is shown on Figure 4.3A. The ratio of the area of these peaks translates into 80% conversion of one end of the poloxamer. Total number of PPO groups in the chain is 32, number of methanesulfonyl groups according to ^{1}H NMR is 0.8 groups per one poloxamer chain. This means that there is still at least 20% of unmodified poloxamer left in the mix, but because it does not contain an azide group it can not participate in the Click reaction and thus can be removed after it. The total yield of the poloxamer modification reaction measured by the final

amount of the product obtained was 89%. The second step was the substitution of the methanesulfonyl group with the azide group. For this step, excess of the sodium azide was used, the reaction was considered complete when 3.06 peak in ^{1}H NMR was undetectable by the instrument, spectra is shown on Figure 4.3B.

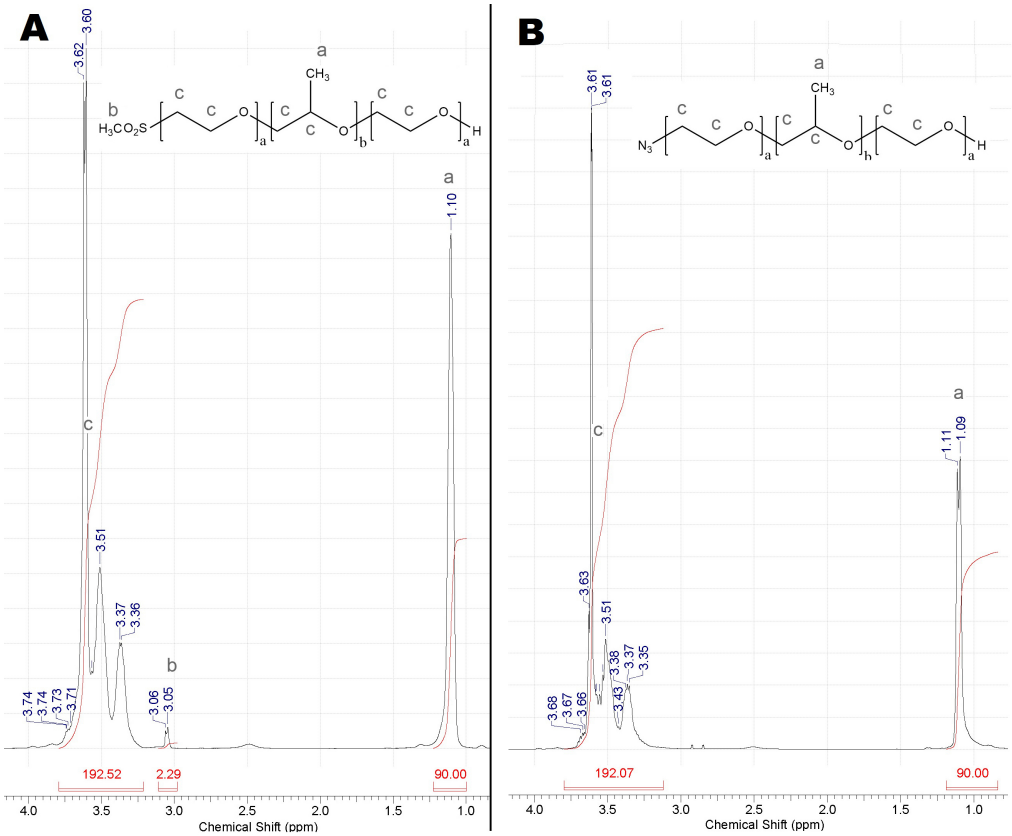

Figure 4.3: Poloxamer ^{1}H NMR. **A** Methyl sulfonyl modified poloxamer. **B** Azide modified poloxamer.

Combination of low feed ratio with dilute conditions creates a favorable thermodynamic conditions that resulted in the mix of unmodified and one end modified poloxamer. This step simplified the synthetic route through the elimination of any post synthesis separation steps. The strive to minimize the waste of the poloxamer will mean significant increase in the purification costs and since poloxamer copolymers are the cheapest component in the device it is economically not feasible to

attempt to reach 100% conversion on the first step.

4.2.2 Grafting density determination

Precise determination of the achieved shell density is a required step for any future investigations with the PAn - poloxamer nanocomposite. Thermogravimetric Analysis (TGA) is a typical method to determine grafting density of a polymer shell on the surface of the nanoparticle. For PAPN TGA method failed due to the similarities in the decomposition temperature of the components. For propargyl acrylate - poloxamer pair FTIR proved to be the best alternative method to determine mass ratio of the components. Propargyl acrylate has strong peaks at 1150 cm^{-1} and 1728 cm^{-1}, while poloxamer has a sharp and strong peak at 1100 cm^{-1}. The difference between the 1150 and 1100 peaks is big enough for the instrument to reliably distinguished the two. Experimentally it was determined that instrument is capable to reliably distinguish down to 1% of the poloxamer by mass in the mixture of poloxamer and PAn. FTIR spectra of PAn, poloxamer and the mix of the two is shown on Figure 4.4.

To be able to measure the mass ratio using FTIR a calibration based on the known mixture ratio of the poloxamer to PAn was developed. Standard mixtures with the mass ratios ranging from 1% to 40% of the poloxamer were prepared and their FTIR spectra were recorded. To prepare standard mixtures, 30 mL of nanoparticles after dialysis were dried under vacuum at 50°C . 1000 mg of dry cores was transferred into medium mortar (3 inch in diameter). 100 mg/mL solution of poloxamer in water was also prepared. To obtain 1 percent mass ratio of poloxamer to cores, 0.1 mL of poloxamer solution was added to mortar with nanoparticles and mixed using a pestle until a uniform paste-like material was formed. Mortar was

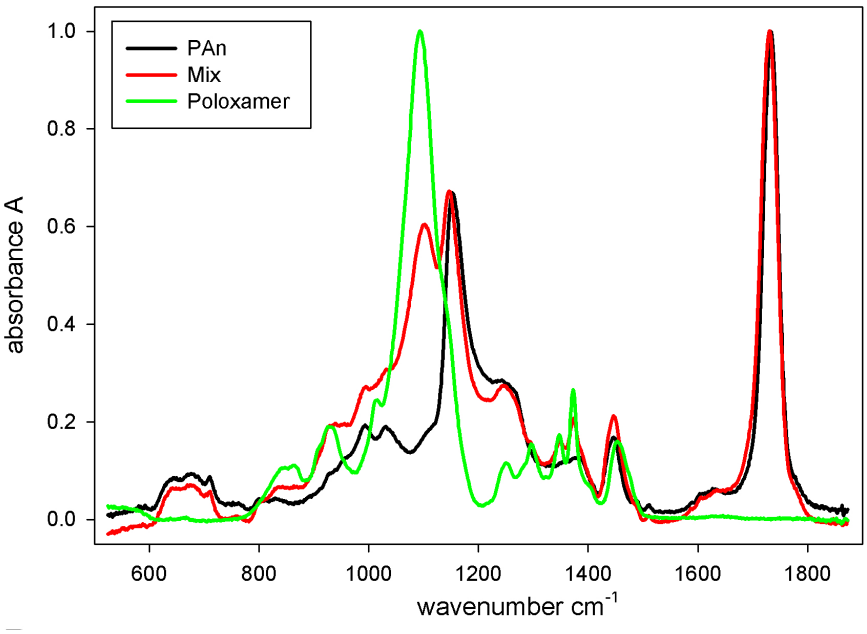

Figure 4.4: FTIR spectra of poloxamer (green line), PAn (black line) and mix of the two (red line) showing three peaks of interest. Based on the ratio of the 1100, 1150 and 1728 cm^{-1} peaks calibration curves were created.

placed in the vacuum oven at 50°C for 6 hours. After the mortar cooled to room temperature, the sample was mixed for an additional 5 minutes and at least 10 FTIR measurements were recorded.

Attenuated total reflectance (ATR) accessory with diamond crystal was used to simplify measurements and to ensure that there was minimal deviation from measurement to measurement. Using this technique, the depth of penetration, and thus, the thickness of the sample, is constant, depending only on the refractive index of the sample.

A measurement was considered satisfactory if absorbance of the highest peak was greater than 0.4 and there was minimal or no deviation of baseline in the water region (around 3500 $cm^{-}1$). If the maximum peak was less than 0.4, the sample was repositioned on the ATR crystal and measurements were retaken until

satisfactory condition was met. If there was evidence of water presence in the sample, mortar was placed in the vacuum oven for additional time until no water was detectable by the FTIR.

For each of the 10 measurements, a sample was taken from different location on the mortar. After the measurement was completed the maximum possible amount of the sample was collected from the ATR crystal and returned into the mortar, then mixed with the rest of the particles, and finaly 1-2 mg of the sample from a different location on the mortar were taken for measurement. A set of runs was considered successful if the deviation between the runs was less then 0.5 %. If the deviation was greater, nanoparticles were mixed in the mortar with pestle for additional 15 minutes and all 10 measurements were retaken until desired reproducibility was met. This step was done to ensure that the small sample that was taken to record spectra was representative of a bulk sample. After ensuring that collected data meets set requirements, more poloxamer solution was added to the mortar and the process was repeated until mixture ratio was 40 % poloxamer by mass.

Based on this data calibration curves for peak pairs 1150:1100 and 1728:1100 were build, calibration curves are shown on Figure 4.5. As can be seen from the Figure 4.5 the peak pair 1150:1100 has a greater range of peak ratio value change for the same mass ratio range, 0.8 change for 1150:1100 versus 0.45 change for 1728:1100, thus a better sensitivity for the mass ratio determination can be achieved when 1150:1100 peak ratio is used, all future calculations were done based on 1150:1100 pair of the peaks.

The procedure to analyze unknown samples was as follows: drop of the vesicle suspension was placed on the ATR crystal, all water was allowed to evaporate, then data was collected. This procedure requires that only one parameter is main-

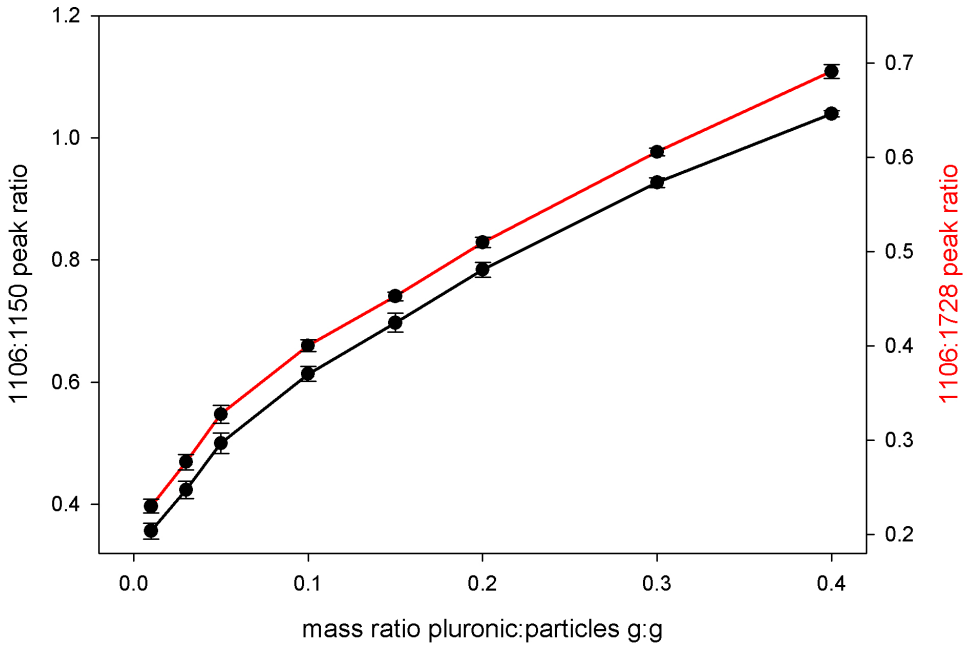

Figure 4.5: Calibration curves build based on the 1100:1150 and 1100:1728 peak ratios for poloxamer - PAn mix with mass ratio of the poloxamer ranging from 1% to 40%.

tained: good contact of sample to the ATR crystal. The quality of contact between sample and ATR crystal was monitored through the observation of the maximum peak height value. Good reproducibility of the results was achieved when the value for the highest peak was over 0.4. The resulted peak ratio proved to be independent of all parameters except the mass ratio of the components if the above condition was met and all water was removed from the sample. The peak ratio measured for the unknown samples was compared to the calibration curve values and from the value for the peak ratio mass ratio of the poloxamer to the PAn was determined. To convert the mass ratio into grafting density (GD) the following equation was derived:

$$GD = 200.7 * \upsilon * r * \rho \div MW$$

In this equation: GD - grafting density in poloxamer chains per nm^2; 200.7 - coefficient resulted from unit conversion; υ - mass ratio of poloxamer to PAn cores obtained from FTIR calibration curve; *r* - diameter of PAn cores in nm; ρ - density of PAn cores in g/mL; *MW* - molecular weight of poloxamer copolymer. Equation was derived using the assumption that PAn are perfect hard spheres that does not form any aggregates and poloxamer chains are spread evenly on the surface of PAn.

To achieve better mass ratio resolution the core size was targeted to be close to 30 nm, if the nanoparticles of a bigger size are used the mass of the core becomes predominant and 1% change in the mass of poloxamer in the mixture would result in a huge difference of GD, rendering the method ineffective. Prepared particles were assumed to have average size of 28 nm. An assumption was made based on the analysis of the results from three techniques: BET, SEM and DLS. According to BET analysis, particle size is almost 28 nm. SEM imaging showed 26.9 nm. And DLS showed 37nm average size. SEM and DLS techniques showed a relatively narrow size distribution.

A typical image observed during SEM imaging is shown on Figure 4.6. To calculate average size and standard deviation 200 separate, distinct cores were measured using Quartz PCI software package.

To calculate an average size of the nanoparticles based on the SEM imaging 200 distinct single nanoparticles were measured and averaged. Since besides single nanoparticles SEM also showed formation of double, triple, quadruple and higher aggregates fraction of each aggregate was measured. To do this, a number of every type of aggregate was counted in 6 different areas of the sample. Based on this, a size distribution chart was created as shown on Figure 4.7. As can be seen from the chart, there is strong evidence that aggregates can be present in the sample after nanoparticles were synthesized.

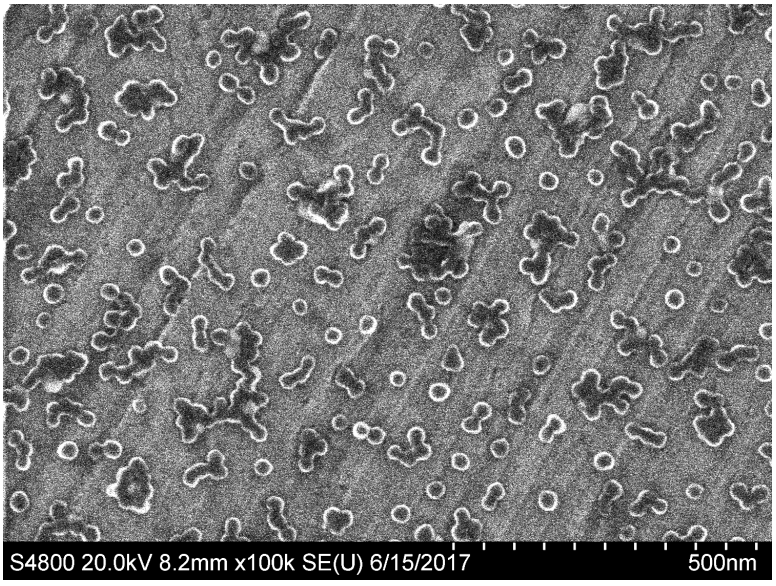

Figure 4.6: Typical image observed during SEM imaging. To calculate average size and standard deviation 200 separate distinct cores were measured.

Since preparation of the SEM sample requires the sample to be dried, there is a probability that the observed aggregates were formed during SEM sample preparation rather than during synthesis and as such are not representative of the actual nanoparticles that were modified. To clarify these observations, a size exclusion column chromatography was performed. Half inch wide column was filled to 4 inches height with Bio-Gel P-100 beads, with bead's size range 90-180 μm for wet beads. Nanoparticles were separated according to their size using this column.

According to the SEM there is almost 15% of aggregates that consist of two particles stuck together, and about 10% of triple and quad aggregates. If observed on the SEM images aggregates were formed during synthesis the resulting fractions from the separation column should have at least 4 different size fractions with bigger aggregates coming out from the column first. Nanoparticles were purified with 0.45 μm filter before loading them into the separation column. Based on the observed size for single, dual, triple and quad aggregates these fractions were ex-

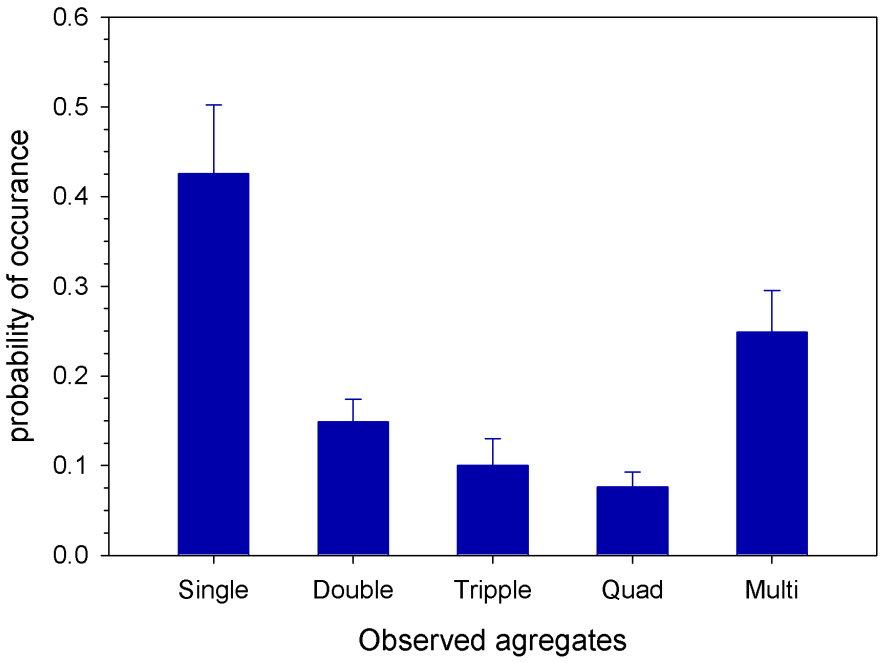

Figure 4.7: Distribution of aggregates as observed with SEM, number average was counted.

pected to pass through 0.45 μm filter, with the quad aggregate having a maximum size of about 100 nm. Based on the SEM observed ratio, all of these fractions should be easily detected. To test this hypothesis 1.5 mL of particles after dialysis were passed through the separation column. This amount is equivalent to 60 mg of dry cores, thus there was a probability that the sample will have 9 mg of double, 6 mg of triple and 5 mg of quad aggregates. These quantities are well above detection limit for the instrument. As can be seen from Figure 4.8 only one size was observed exiting the column, and the results were a close match to the DLS results of the unseparated sample.

Observed DLS results, Figure 4.8, indicate that the amount of aggregates in the sample is much lower than was predicted by SEM, and thus particles were assumed to consist of only separate single cores with an average diameter of 28 nm

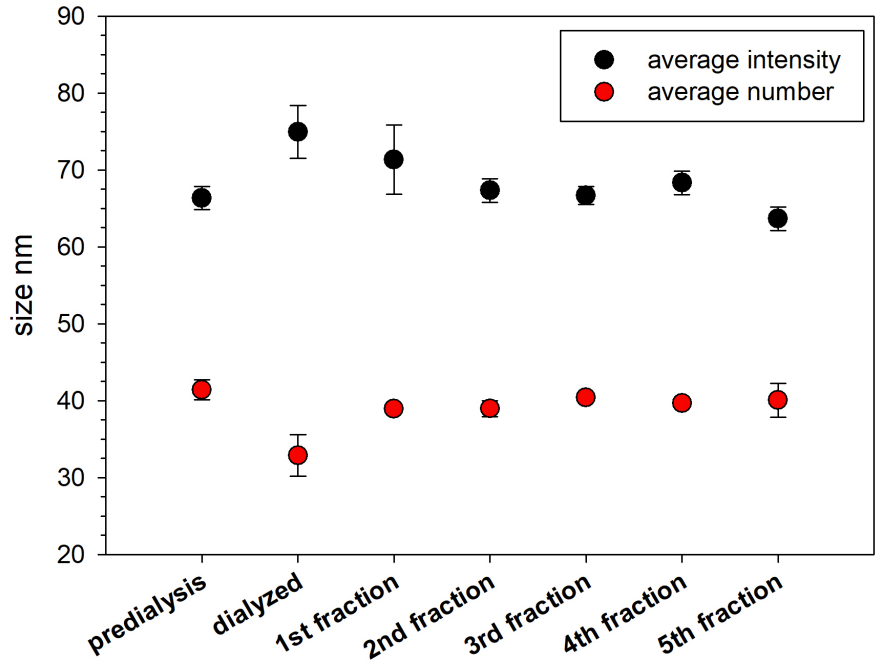

Figure 4.8: Number and intensity based average size distribution of the unmodified nanoparticles before and after dialysis, and from the different fractions after size exclusion chromatography.

for the purpose of simplifying grafting density calculations. Most probable causes for why such a high amount of aggregates were observed on the SEM images is the SEM sample preparation procedure. In order to take SEM images, the sample should be completely dry and since during drying process sample concentration increases as the water is evaporated and nanoparticles are not bonded to the surface of the SEM sample holder the probability of aggregate formation increases as the concentration is increasing. Thus observed images appear to have more aggregates than there are in the actual sample. Since after column chromatography only one average size was observed, the assumption that sample does not have any aggregates can be considered representative of a bulk sample.

The total surface area of the sample as measured using BrunauerEmmett-

Teller (BET) nitrogen absorption analysis on Quantachrome instrument using Quantachrome ASiQwin Automated Gas Sorption Data Acquisition and Reduction version 4.0 software package was found to be 185.7. To measure total surface area using BET 0.3 mL of propargyl acrylate nanoparticles after dialysis were loaded into BET tube, this volume contained 9 mg of dry cores. This tube was placed into a vacuum oven heated to 35°C , at a pressure of 45 mm Hg for 72 hours to remove all water. After this sample was degassed in the BET instrument for 10 hours at 70°C . Normally degassing is done at the highest safe temperature for the sample to ensure complete removal of all absorbed gasses. Glass transition temperature for some of the acrylate based polymer can be as low as 100°C ,thus to be below this temperature 70°C was chosen as a working temperature during degassing process. It was expected that due to high cross-linking density and relatively low degassing temperature, no changes of nanoparticle surface area will happen. Absorption of nitrogen was done at 77.35 K and total analysis time was 1 hour 52 minutes. Based on a multi-point BET analysis the surface area was found to be 185.7 m^2/g with correlation coefficient, R=0.999970. Report is included in the Appendix.

Since all of the three techniques used to determine real nanoparticle dimensions have their short comings and are not ideal when measuring polymeric samples, few assumptions were made to calculate the size of the cores that were prepared. Average size of nanoparticles as calculated based on the SEM images was 26.9 nm, DLS number average size for purified samples was 37 nm, BET based size was 28 nm. SEM imaging required the samples to be dried, potentially leading to some shrinkage and most certainly leading to significant aggregation of the particles. Additionally, the electron beam had enough power to melt propargyl acrylate polymer while making high magnification imaging impossible due to melting. Thus the size determined from SEM alone can not be considered to be a true size of the

nanoparticles.

In the case of DLS measurement, to determine the real size of the nanoparticles, a true refractive index for the sample has to be inputted into the instrument software. Refractive index of the particles was assumed to be equal to the refractive index of the propargyl acrylate polymer. Due to the presence of sodium dodecyl sulfate and potentially potassium per-sulfate ions that were left after emulsion polymerization process real refractive index of the particles can be slightly different from the pure polymer number that was used. Additionally, nanoparticles can have a layer of bound water molecules around their surface that can lead to a higher than actual reading by the instrument.

BET requires the sample to be completely degassed before it can be measured. This process involves high vacuum and elevated temperature that has the potential to alter the surface area of the nanoparticles. Also BET measurement is taken at 77 K and this can cause thermal shrinkage of the sample. Because BET results were between the SEM and DLS results and factoring in the possible influences from all three techniques, as discussed above, the average size for the nanoparticles was assumed to be 28 nm for the purposes of grafting density determination calculations.

Derived equation for grafting density calculation combined with the developed characterization technique allows us reliable determination of the achieved grafting density differences between various samples for the final devices using simple and fast measurement. This tool allowed us to complete the development of the synthesis and the purification methods required to build a nanocomposite that if free of unattached copolymer and has fully characterized surface chemistry.

4.2.3 Purification of the vesicles

According to Shubhra[134] findings poloxamer chains can be absorbed on the surface of polystyrene nanoparticles at an equivalent of up to 0.2 GD and even in a very dilute solutions number of poloxamer chains on the surface can still be relatively high, staying above 0.1 chains per nm^2 for poloxamer solutions of 0.05 mg/mL or above. Designed method of GD determination has a lower precision limit of 1% by mass of poloxamer. Based on this lower limit and assuming perfect sphere geometry for the PAn for 28 nm cores a lower precision limit for GD determination starts at 0.025 poloxamer chains per nm^2, equivalent of 1.2 mass percent of poloxamer. This allows to reliably differentiate between the mixes that have the difference of 0.025 GD or more of the poloxamer which is below the expected absorption range as reported by Shubhra.

Typical purification procedure to remove unreacted chemicals from nanoparticle mixes after modifications is done via centrifugation from a suitable for impurities solvent. Since equilibrium concentration of poloxamer on the surface and in the solution are very low, poloxamer tends to stay absorbed on the surface leading to the increase in the number of cleaning repetitions required, leading to accumulation of waste chemicals that need to be disposed off. So there is a clear need in the optimization of the cleaning procedure to remove the last few percents of the unreacted poloxamer. Some of the common approaches to remove the impurities from the nanoparticle suspensions include sonication followed by centrifugation, dialysis, use of the salts to shift equilibrium states, and centrifugation at the elevated temperature. All of these methods proved to be inefficient in the removal of the last 10% of poloxamer from the vesicles.

Testing of the cleaning methods was done on a mix of PAn with stock polox-

amer in 1 to 1 ratio. Upon first cycle of cleaning using the typical centrifugation routine it was found that almost 12% of the poloxamer, of original 50%, was still left in the mix. This observation matched good with what Shubhra reported before. Upon attempting to remove the remaining poloxamer it was found that all of the typical procedures had minimal or no effect and a 10 to 12% of poloxamer remained absorbed on the PAn. Results of the attempted cleanings are shown on Figure 4.9.

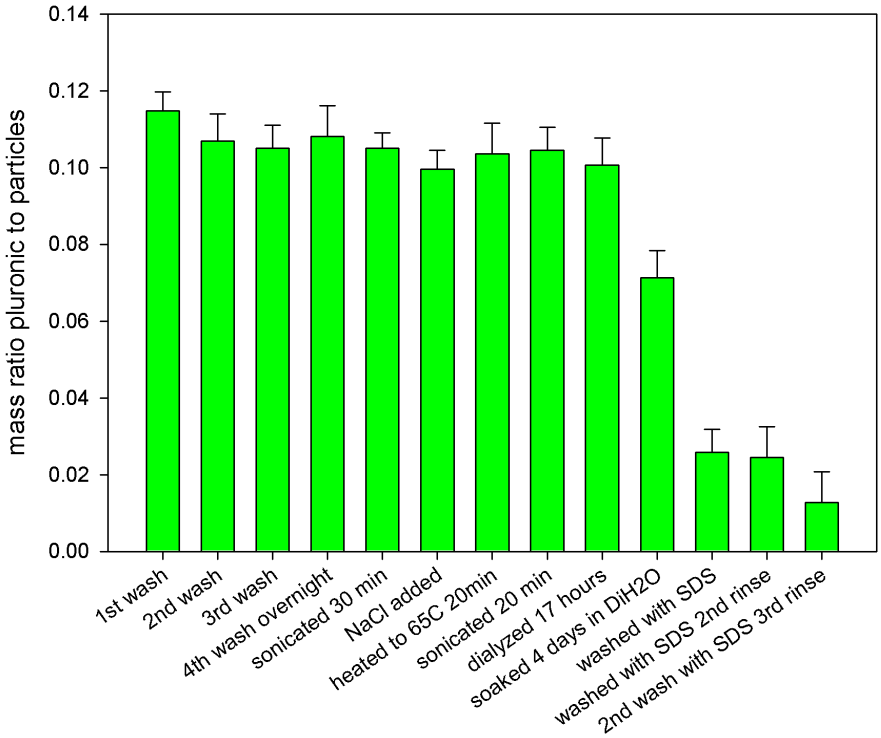

Figure 4.9: Amount of unmodified poloxamer left in the PAn poloxamer mixture after different cleaning routines were attempted. Ligand exchange proved to be the fastest and most efficient method for the removal of the unreacted poloxamer.

Repetition of the centrifugation for 4 times showed no effect on the amount of poloxamer left in the mixture. Sonication for 30 minutes also did not have the

desired efficiency. Addition of a sodium chloride salt as well as heating proved to have minimal effect on the equilibrium concentration and were not effective in the removal of the last 10% of the poloxamer. Dialysis at room temperature for 17 hours also had minimal effect and only after 4 days of dialysis a decrease in the amount of the poloxamer chains absorbed by the PAn was observed, but this generate liters of waste, aside of taking 4 days of time. To remove the remaining poloxamer using dialysis the time requirement would be in weeks rendering this method economically unfeasible.

Ligand exchange procedure proved to be the most successful, and the fastest in the removal of these last few percents of the poloxamer. As a ligand of choice, sodium dodecyl sulfate (SDS) was used. SDS was used during the preparation of the nanoparticles and as such it is already present at an equilibrium amounts and addition of more SDS would just restore the original PAn surface equilibrium that was disrupted during Click reaction.

This cleaning study allowed us to optimize the cleaning procedures after the assembly of the nanocomposite. This knowledge proved to be of the most importance for the samples with very low GD. Poloxamer modification reaction, as described above, yields a mix of azide modified poloxamer and unmodified poloxamer and if the unreacted poloxmaer is not removed after the Click reaction is complete the presence of these free floating chains will result in a false GD reading.

4.2.4 Stability of the nanocomposite

Propargyl acrylate has a carbonyl bond which is susceptible to the hydrolysis under certain conditions. Additionally, there is over 100 bonds between the surface of the nanoparticle and end of the poloxamer that can be effected when exposed

to higher temperatures for prolonged periods of time. To check the stability of the proposed device PAPN was heated close to the transition temperature and changes in the grafting density were monitored over the period of one week. Activation of the poloxamer requires the device to be heated to relatively high temperature for short periods of time thus knowledge about the stability of the device at temperatures close to the transition temperature gives an insight on the probability of the device destruction under normal operational conditions.

To determine the percent of the poloxamer chains that have been detached a small portion of the sample was removed at certain time intervals and cleaned using designed cleaning procedure (Chapter 3). Change in the poloxamer to core ratio was monitored, the results are shown on Figure 4.10. It was found that less than 1% of the poloxamer chains was lost per day of hydrolysis. Since for the most treatment procedures the time needed for the vesicles to spread through the body is just few hours the amount of the active molecules that can be lost due to high poloxamer detachment from the vesicle is negligible and even after few days the composition of the device is expected to be close to the original design.

4.2.5 Kinetics of Click reaction

There are two concurrent approaches to regulate the final ratio of the components in a composite. First is to dose the feeding ratio for the chemical reaction and let the reaction run to a completion. Second option is to add the excess of one of the components, typically molecule that is used to create the shell, in this work azide modified poloxamer, and to stop the reaction after some distinct period of time, usually minutes to hours. In the first case there is no waste of the components and typically the cleaning of the final composite is not required, but the time

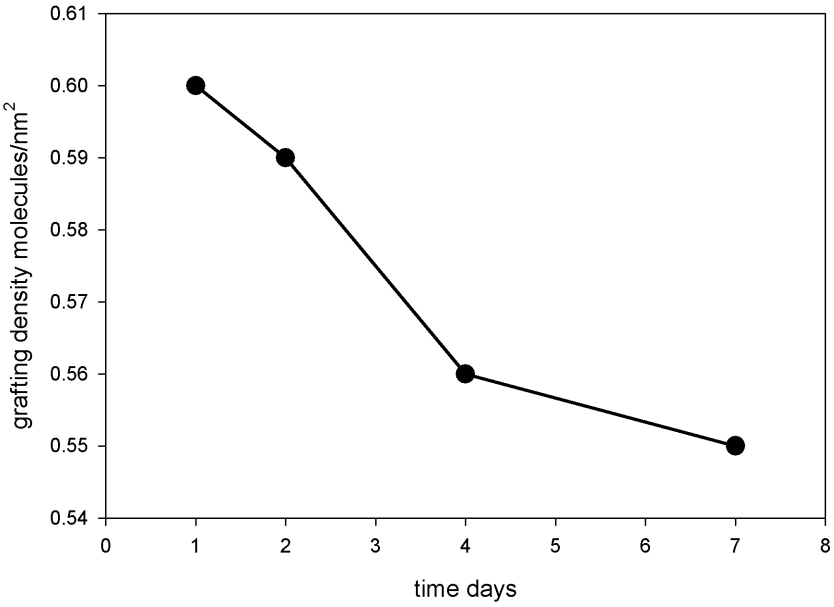

Figure 4.10: Change in poloxamer grafting density of the PAPN after being exposed to 50 °C temperature for one week.

required for the reaction to complete can be days if not weeks, so this approach is more suitable for expensive components and when post reaction purification is complicated. Second approach allows to speed up the process, but requires an additional step to remove the excess of the reactants. This is more suitable for the processes where post purification is simple and efficient, and starting compounds that are used in excess are cheap. Also second approach requires a knowledge about the kinetics of the reaction to determine when to stop the reaction.

To measure the rate of poloxamer attachment reaction was loaded with 5 times excess of the poloxamer and samples were taken at 1, 3, 6, 24, 48, 96 and 168 hour after the start of the reaction, results are shown on Figure 4.11. A clear surface saturation around 0.55 poloxamer chains per nm^2 of the surface after 96 hours of reaction is observed. Based on this data an estimation of the required time to achieve the desired grafting density level can be made.

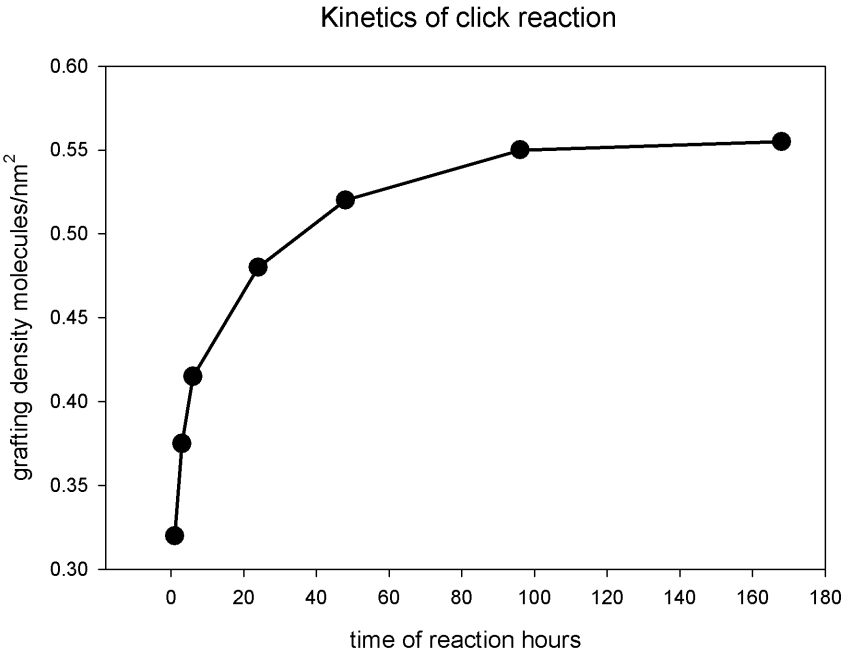

Figure 4.11: Dependence of the achieved GD of the poloxamer on the time of the reaction. 5 times excess of azide modified poloxamer was added into the reaction and samples were taken, cleaned and analyzed at 1, 3, 6, 24, 48, 96 and 168 hour.

4.2.6 Numerical estimation of grafting density influence

Numerical estimation of grafting density influence on the shell properties were made to check if the shell that is created by the poloxamer has enough volume to accommodate encapsulation of the dyes or drugs at a level that can have a practical application. Theoretical dimensions of the modified nanoparticles were calculated based on available literature data. Length and dimension of ethylene oxide (EO) and propylene oxide (PO) blocks were calculated based on the literature values for characteristic values of polyethylene oxide (C_N 4.1) and polypropylene oxide (C_N 4.85) polymers[135]. Following assumptions were made: expansion factor for polymer chains is equal to 1; poloxamer copolymer is a perfect monodisperse polymer with each ethylene oxide block consisting of 12 repeat units and propylene oxide block consisting of 32 repeat units. Average bond length for the

repeat unit was found as a mathematical average between typical theoretical O-C, C-C and C-O bond lengths (0.143, 0.154 and 0.143 respectively, average 0.1466 nm was used). End to end distance for EO block at theta conditions was calculated to be 1.78 nm, calculated using the following equation[135]:

$$\langle r^2 \rangle^{\frac{1}{2}} = \alpha (nC_N)^{\frac{1}{2}} l$$

PO block was assumed to be in a blob conformation and as such radius of gyration (R_g) at theta conditions was calculated to be 1.25 nm, calculated using the following equation[135]:

$$R_g = \frac{\langle r^2 \rangle^{\frac{1}{2}}}{\sqrt{6}}$$

Theta conditions are characterized by a more compact conformation for polymer chains than in the good solvent. Based on this fact calculated dimensions for EO and PO as described above were assumed to be equal to the height of the shell when heated above LCST. As was shown in Chapter 3 the distance between two dyes changes by almost 1 nm when described device is heated from room temperature to above LCST. Based on this data the assumption that poloxamer shell height increases by 1 nm when heated above LCST was made as compared to the theta conditions state.

Using basic geometrical calculations for the volume of a sphere ($V = \frac{4}{3}\pi r^3$) the total volume for two states was found: collapsed shell - $V = 140800 nm^3$, expanded shell - $V = 154300 nm^3$. As a radius for the collapsed state of the shell sum of core radius, the end to end distance for EO block and the diameter (twice the radius of gyration) of the PO block was found (28 + 1.78 + 2 * 1.25 = 32.28 nm), for expanded state 1 nm was added based on the results obtained in Chapter 3. The dif-

ference between these two volume is the expansion of the shell thus change in shell volume due to the temperature triggered collapse is estimated to be 13500 nm^3 for the 2400 nm^2 of the single nanoparticle surface. Calculated volume is sufficient to accommodate hundreds or even thousands of molecules, since molar volume for most of the dyes and small molecule drugs is less than 1 nm^3, as predicted by the ACD/Labs 12.0 ChemSketch software package, thus the proposed system has the potential to be used as a drug delivery device.

When making the calculations of the total radius of the device conformation of the poloxamer on the surface was assumed to be as shown on Figure 4.12, second, upper layer of EO was not included in the total length calculations because based on the literature review it is expected that dyes or drugs would be encapsulated in the PO block leaving the EO block the function of protection layer rather than active layer.

4.2.7 Numerical prediction of optimal grafting density

Polymer chains that form brushes on the surface of the nanoparticle will form various structures based on the grafting density and at certain conditions it is predicted that chains will be restricted in their ability to change conformation when going through phase transition processes[136]. To find if the poloxamer chains have the optimal grafting density that will results in the maximum volume change for the shell, the length of tethered chains for good solvent and theta solvent conditions were calculated. Calculations were based on the Van Der Waals volume for repeating unit and the dependence of the flexible polymer chain length on the solvent[137].

Van Der Waals volume for repeating units were found on polymerdatabase.com

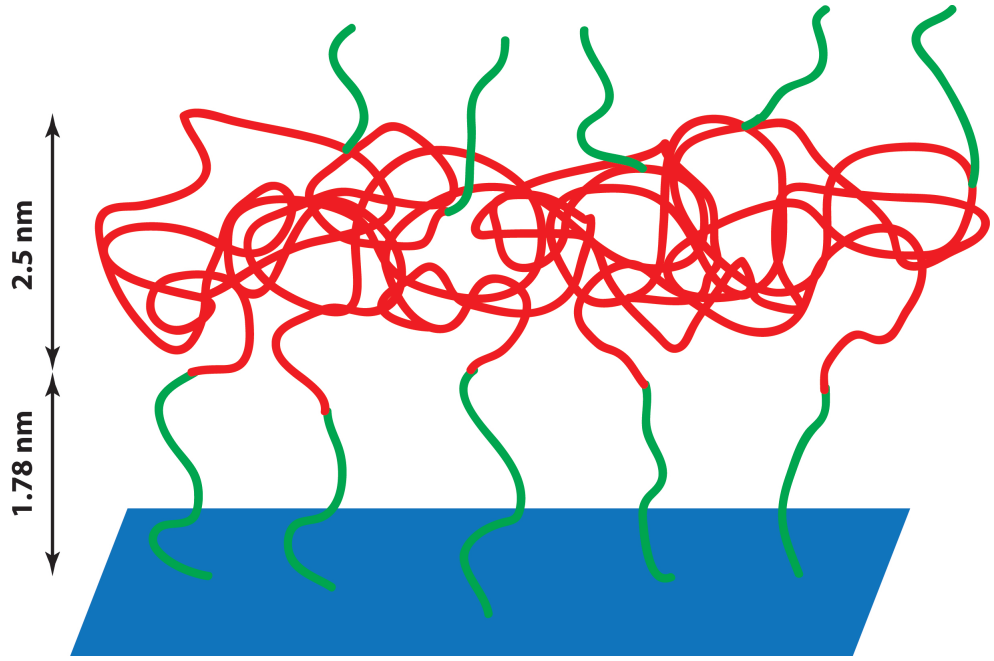

Figure 4.12: Cartoon showing assumed conformation of the poloxamer covered nanoparticles with calculated dimensions of the blocks. Ethylene oxide block is shown in green, propylene oxide block is shown in red.

website: Poly(ethylene glycol) has volume of 26.4 cm^3/mol, Poly(propylene glycol) has volume of 36.4 cm^3/mol. This website provides Van der Waals volumes that have been calculated from the bond lengths and the atomic radii of the elements. This approximation is expected to be good enough to demonstrate the expected behavior as the grafting density of the poloxamer approaches critical density and steric effects start to govern the conformation of the chains.

The average molar volume of the repeat unit for poloxamer was found according to the molar fractions of EO and PO blocks in the copolymer. Molar fraction of EO block equals to (12 + 12) / (12 + 32 + 12) = 0.42857, molar fraction of PO block equals to 1 - 0.42857 = 0.57143. Based on this average repeat unit volume is 26.4 * 0.42857 + 36.4 * 0.57143 = 32.1143 cm^3/mol or 0.0533 nm^3/unit. To simplify the calculations brush thickness was considered to be equal to the length of

the polymer chain in good solvent for temperature below LCST and to the length of polymer chain in theta solvent for condition when the temperature is above LCST.

The relationships between dimensions of polymer chain and grafting density were calculated using equations for good solvent and theta solvent as reported by Flory[137]. Equation for good solvent[137]:

$$L = N(a/d)^{\frac{2}{3}}a$$

where L is the length of the polymer chain, thickness of the brush was assumed to be equal to this length; N is number of repeat units in the polymer chain, number of repeat units was added for all three blocks (56 total for Pluronic-L64); a is volume of one repeat unit, found as described above; d is the distance between poloxamer chains on the surface, this was the parameter that was varied to build the graph (x-axle on Figure 4.13. To calculate brush thickness at theta conditions the following equation was used[137]:

$$L = N(a/d)a$$

Difference between theta and good solvent (y-axle) was plotted to demonstrate the maximum volume change when triggered with temperature for poloxamer copolymers, shown on Figure 4.13.

Using calculated shell thicknesses as predicted by the theory on the conformation of the flexible polymer chains in solution[138, 136] a maximum for the volume change between the theta and good solvent conditions was found, shown on Figure 4.13. Based on this prediction it is expected that for proposed system an optimal grafting density exists that will lead to the maximum release rate due to maximum volume change of the shell that will be triggered by the maximum

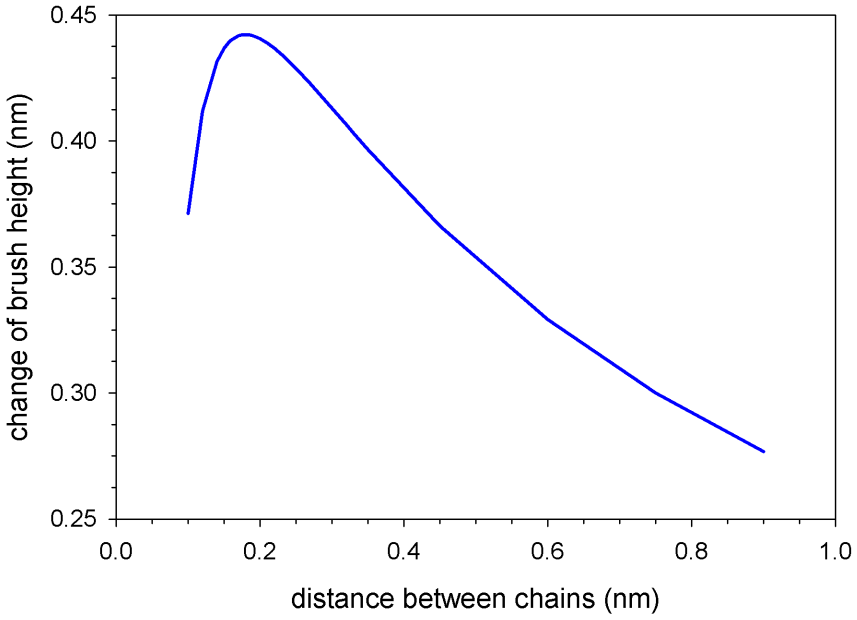

Figure 4.13: Dependence of poloxamer brush thickness on grafting density.

change in the brush height.

Obtained numbers are only approximation since a lot of assumptions and approximations had to be made during calculations and that is probably why the observed calculated maximum is at the chains separation distance of just 0.2 nm, making grafting density much higher than the possible maximum grafting density as found during kinetics of click reaction study section.

4.3 Conclusion.

Proposed is a method of synthesis and characterization of a well defined nanocomposite from propargyl acrylate and poloxamer. The proposed nanocomposite has a better stability compared to the self assembled devices and a wider range of temperature tuning compared to the PNIPAM based core shell systems. A quantita-

tive method based on FTIR was designed to simplify the process of nanocomposite characterization. This method allowed us to quickly and reliably determine the composition of the nanocomposite. The ability to choose from a wide range of the commercially available poloxamers and the ability to synthesize PAn with a wide range of the core sizes allowed us to create a device with a desired shell density. Poloxamer copolymer, the temperature responsive component, allows us to tune the response of the device to the desired temperature range simply through the selection of a correct copolymer version. Stability of the nanocomposite was tested and determined to be sufficient for medical applications conditions. Based on the properties of the components optimal method for purification of the final nanocomposite was described. This method allowed us to remove all of the unattached poloxamer from the device in a few easy steps.

4.4 Experimental methods

4.4.1 Materials and Reagents

All reagents were purchased from Sigma-Aldrich with at least 97% purity level, solvents were purified using standard procedures. Deionized water was obtain from Barnstead Nanopure Diamond water system and had 18.2 MOhm resistance.

4.4.2 Characterization

^{1}H spectra were recorded on JEOL ECX-300 spectrometers (300MHz for proton). Chemical shifts for protons are reported in parts per million downfield from tetramethylsilane and are referenced to the carbon resonances of the solvent

($CDCl_3$: δ 7.26 or DMSO-d_6: δ 2.50). Nanoparticle size was checked using Malvern Instruments Zetasizer nano series Nano-ZS using 10 mm plastic cuvette. Additionally, average size was confirmed using scanning electron microscope Hitachi S4800 FESEM at maximum accelerating voltage of 20.0 kV, images were analyzed using Quartz PCI v.8.5 software package. BET analysis was done on Quantachrome Instrument and analyzed using Quantachrome ASiQwin- Automated Gas Sorption Data Acquisition and Reduction software package version 4.0. FTIR was done on a Nickolet Magna IR 6700 spectrometer equipped with a diamond attenuated total reflectance (ATR) accessory.

4.4.3 Nanoparticle preparation

Emulsion polymerization was performed in a single necked round bottom flask (250 mL) equipped with the magnetic stirrer. Potassium persulfate (110 mg) was dissolved in water (80 mL) and nitrogen was purged through the solution for 15 minutes. Sodium dodecyl sulfate (90 mg) was added to the flask under nitrogen purge. Obtained solution was stirred and placed in the preheated bath at 75 °C for 3 minutes, then degassed solution of propargyl acrylate (4 mL) and divinylbenzene (0.65 mL) were added to the main reaction flask. The mixture was stirred at 75 °C under nitrogen purge for 90 minutes. The emulsion was allowed to cool on air. Then mixture was filtered through paper filter. After filtering samples were purified by dialysis using Spectra/Por Dialysis membrane with MWCO 50000. Dialysis was performed for 3 days at 40 °C in 18.2 Megaohms water with regular water changes, typically every 8 hours. Nanoparticles were characterized using DLS,SEM and BET analysis to determine average size and aggregation. Average size of the nanoparticles, based on the analysis from all three techniques, was assumed

to be 28 nm. Obtained emulsion contained 45 mg/mL of nanoparticles.

4.4.4 Poloxamer modification

$MeSO_2$-pluronic-L64. Pluronic-L64 (3.14 g, 1.064 mmol) was dissolved in dry dichloromethane (DCM) (10 mL), then triethylamine (0.132 g, 1.3 mmol) was added to the solution. The obtained solution was stirred at room temperature. Methanesulfonyl chloride (48 mg, 0.42 mmol) was dissolved in 0.5 mL of dry DCM and obtained solution was added drop-wise to the poloxamer solution over 1 minute period of time. The mixture was stirred for 6 hours at room temperature. 20 mL of deionized water was added to remove any unreacted methanesulfonyl chloride. Mixture was transferred to separation funnel and mixed for 2 minutes. Then separation funnel was positioned vertically and mixture was allowed to phase separate. If phase separation was not observed for more than 5 minutes 10 mg of sodium chloride was added, mixture was shaked again for 3 minutes and again allowed to phase separate. Bottom, organic, layer was collected and transferred in clean separation funnel. 20 mL of deionized water were added and mixture was shaked for 3 minutes again. After shaking mixture was allowed to phase separate and organic layer was collected from the bottom of the separation funnel. 5 g of sodium sulfate was added to remove remaining water from the mixture. After 5 minutes the mixture was filtered and evaporated under reduced pressure. Yield 3.1 g (95%), clear oil. This product was used in the next step without further purification. ^{1}H NMR ($CDCl_3$) δ 1.11 (m, 96H), 3.06 (s, 3H), 3.38 (m, 32H), 3.52 (m, 64H), 3.63 (m, 98H).

Reduced amount of methanesulfonyl loading was chosen to decrease the probability of dual end azide modified poloxamer formation at the end of the mod-

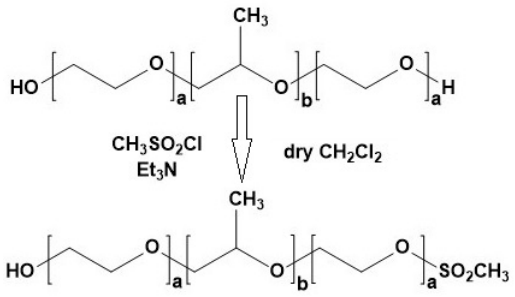

ification process. Separation of the single and dual end azide modified poloxamers would be a very challenging task and because the price for the poloxamer is relatively low it is more rational to starve the reaction and have some umodified poloxamer left at the end of the modification process, rather than spending time and reagents in an attempt to separate the single and dual end modified poloxamers. Unmodified poloxamer can be easily removed after Click reaction because it does not have azide group, thus it cannot react with the alkyne group on the surface.

Assuming equal rate of reactions for umodified poloxamer and single end modified poloxamer the probability of formation of dual end modified poloxamer at the proposed loading is close to 3.5 % according to statistical probability calculations, while probability of single end modified poloxamer is 33 %.

Probability of dual end modified poloxamer was calculated using the following assumption: there is no difference between end hydroxyl groups on either of the versions of poloxamer and the probability of any of the hydroxyl group reacting with methanesulfonyl chloride is equal. The initial state of the system was calculated based on the loading ratios, following numbers were used: there was a total of 100 unmodified poloxamer chains available, that have a total of 200 end hydroxyl groups; there was a total of 40 methanesulfonyl chloride molecules. This ratio was calculated based on the molar loading ratio that was used during first step

of poloxamer modification.

Each reaction step one methanesulfonyl group was reacting with any of the available hydroxyl groups. The total number of possible events was found as 200 * 40 for the initial state of the system. After consuming the first methanesulfonyl group only possible product was first single end modified poloxamer chain, making new state of the system with the following parameters: 99 unmodified poloxamer chains bearing 198 end hydroxyl groups available for reaction, 1 single end modified poloxamer with 1 group available for reaction and 39 remaining methanesulfonyl chloride molecules. New total number of possible reactions: 198 * 39 + 1 * 39 after first step.

Probability of single end modified chain reacting during next step was found as the number of possible events for single end modified chains participating in the reaction divided by the total possible number of hydroxyl group reacting with any of methanesulfonyl group: 1 * 39 / (198 * 39 + 1 * 39). Probability of unmodified chains participating in the reaction was found based on the number of available end hydroxyl groups left after first step: 198 * 39 * /(198 * 39 + 1 * 39). This process was repeated until all 40 methanesulfonyl chloride molecules were consumed. Based on these calculations the resulting number of chains in the mix, after all methanesulfonyl chloride was consumed, was: 63.49% of unreacted, 33.02% single end modified and 3.49 of dual end modified chains. Table with calculations is included in the Appendix section.

Pluronic-L64-N3. Sodium azide (195 mg, 3 mmol) was added into solution of $MeSO_2$-pluronic-L64 (3.1 g, 1.03 mmol) in dimethylformamide (DMF) (10 mL). The mixture was stirred and heated to 80 °C for 3 hours. After cooling the mixture was extracted with DCM and washed with water 2 times as described in the first step of the poloxamer modification. The organic layer was separated, dried with

Na_2SO_4, filtered and evaporated under reduced pressure. Yield 2.27 g (75%), clear oil. Pluronic-L64-N3 was used in the next step without further purification. ^{1}H NMR ($CDCl_3$) δ 1.07 (m, 96H), 3.34 (m, 32H), 3.48 (m, 64H), 3.59 (m, 98H).

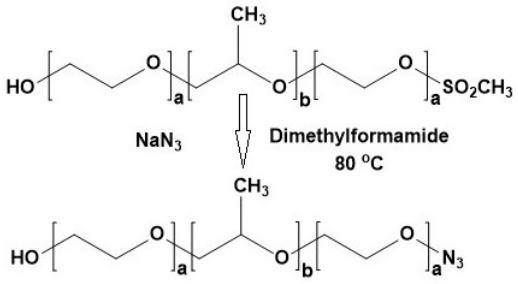

4.4.5 Nanoparticle modification

Nanoparticle modification was performed using the azide alkyne Huisgen cycloaddition reaction also known as Click chemistry. Typical procedure was used as described elsewhere [41]. Copper(II) sulfate ($CuSO_4$) (2 mg, 8 μmol) was added to the propargyl acrylate nanoparticles suspension in water (2 mL) and stirred until completely dissolved. Then solution of pluronic-L64-N3 (6) (22 mg, 7 μmol) in water (2 mL) was added. Next the solution of $CuSO_4$ (2 mg, 8 μmol) in water (2 mL) was added. The reaction was stirred and purged with nitrogen for 5 minutes, then sodium ascorbate (10 mg, 50.5 μmol) was added. The reaction continued at 28°C for 24 hours under nitrogen purge. Reaction mixture was centrifuged at 10000G for 10 minutes. Separated nanoparticles were washed with the mixture of water:Methanol 1:1 (20 mL). Then 1 mL of 0.1 M ethylenediaminetetraacetic acid (EDTA) solution was added to remove copper catalyst. Nanoparticles were re-dispersed in 40 mL of 18.2 Megaohms water and sonicated for 3 minutes. After sonication suspension was centrifuged at 10000G for 10 minutes. This step was

repeated 2 times. Next 0.1 mL of 20% sodium dodecyl sulfate (SDS) solution was added to remove any unreacted poloxamer. Nanoparticles were re-dispersed in 40 mL of 18.2 Megaohms water and sonicated for 3 minutes. After sonication suspension was centrifuged at 10000G for 10 minutes. This step was also repeated twice. Lastly nanoparticles were re-dispersed in 40 mL of 18.2 Megaohms water and sonicated for 3 minutes. After sonication suspension was centrifuged at 10000G for 10 minutes. This step was repeated 5 times to ensure that all impurities were removed. After last centrifugation nanoparticles were redispersed in 10 mL of 18.2 Megaohms water and stored in the refrigerator.

Chapter 5

Dependence of encapsulation and release efficiency of propargyl acrylate poloxamer nanocomposite on the grafting density of poloxamer

Recently developed drug delivery vesicles act as promising next generation disease treatment devices. However, the majority of these vesicles are synthesized using complex synthesis routes, or in the case of self-assembly vesicles, lack stability in the human body environment. Here, an original propargyl acrylate (PA) - poloxamer composite vesicle capable of encapsulating and releasing active molecules in a controlled way is described. This is the first demonstration of the poloxamer grafting density (GD) influence on the release efficiency from the PA - poloxamer nanoparticle composite. Control over the poloxamer grafting density on the PA surface allows us to program the drug release speed of the vesicles. Optimization of GD allowed us to increase the release rate of active molecules by up to 63 times

when compared to the unmodified PA nanoparticles. This burst release is temperature sensitive, and through the combination of various versions of the poloxamer copolymer, it is expected that the temperature of the fastest release can be tuned to the desired temperature region allowing programing of the treatment plan based on the specific needs.

5.1 Introduction

With the current advances in disease treatment technologies, there is a push towards a targeted drug delivery [113, 139]. A lot of current research efforts are aimed at creating a system that is capable of multitasking: specifically bind to a target cells; enhance visibility of the target cells through the use of a photo- or radio-luminescent markers; and deliver active drugs while minimizing damage to the healthy cells [140]. One of the approaches to achieve the above goals is to encapsulate the active molecules in a vesicle that can be activated by an external or internal trigger when the device reaches its target [141]. A system that can be used for a multitude of active molecules must meet the following criteria: should be bio-compatible; capable of encapsulating a wide range of active molecules; provide adequate protection for these molecules from the human body environment; prevent activation of the active molecules before they reach the target cell; have a targeting route to ensure the accumulation at the cite of interest; and have a reliable activation mechanism.

Core-shell structured vesicles that use graft to method to attach an active corona to the core are among the most promising systems currently being developed [142]. The main benefit of such systems is the stability of the formed vesicle due to the formation of a chemical bond between the core and the corona. Most

of the time, as a temperature responsive component, poly(N-isopropylacrylamide) (PNIPAM) derivatives are used [143, 144]. A major challenge of such systems is the complex synthesis routes and more importantly PNIPAM temperature of response is locked at 32°C. To change this temperature PNIPAM, has to be co-polymerized with other polymers increasing the complexity of the synthesis [145]. An alternative approach is based on the use of the self-assembly of temperature responsive polymers [146]. Such systems benefit from much simpler synthesis and the possibility to control the temperature of response [31]. One of the challenges of the self-assembled systems is their instability due to the nature of the bond between components and most of the self-assembly systems lack the control over the size of the final device, limiting their application range [147, 19]. Ability to control the size of the drug delivery vesicle for cancer therapy is crucial because it allows the use of a passive targeting to achieve the accumulation of the vesicles in the cancer tissues. Cancer tissue is known to have a higher porosity of the blood vessels compared to a normal tissue and vesicles within the 40 to 200 nm size range were shown to specifically accumulate in the cancer tissue just due to the higher penetration capability of the blood vessels [125, 103, 104].

To address the issue of the complex synthesis and to retain ability of the precise control over the size of the final device while maintaining high stability of this device in different environments, a system build around propargyl acrylate (PA) nanoparticle core decorated with the poloxamer corona is proposed. PA nanoparticles have been proven to be bio-compatible and effective when used for medical applications [40]. The PA surface can be modified through Click chemistry [148] eliminating the need for expensive or aggressive solvents or catalysts and can be done in a one pot, one step reaction. PA nanoparticles can also be prepared in a wide range of sizes.

Temperature control is achieved through the use of the poloxamer family of copolymers. A corona composed of the poloxamer offers the possibility to control the temperature of response simply through the change in the poloxamer composition [31]. Additional benefits of the poloxamers include: improved stability of the active molecules trapped inside of the poloxamer matrix [88, 96]; ability to re-sensitize the cancer cells to the drugs [98]; hydroxyl groups on the ends of the copolymer can be substituted with the azide group to simplify the assembly of the device through the use of Click chemistry; and the poloxamer has been shown to prolong the lifetime of the vesicles surrounded by it in the blood stream environment [149, 32], increasing the time requirement until the next drug administration event.

A multitude of properties of the drug delivery vesicles are important when designing an optimal treatment plan. For situations where there is a need to maintain a certain level of the active molecules in the blood stream for extended periods of time, there is a need for a system that is capable of slowly releasing the encapsulated molecules over long periods of time. When there is a need to locally increase the concentration of the drug at the site of interest, there is a need for a system that can burst release high concentrations of the active molecules when triggered. In this work, we demonstrate that grafting density (GD) can be used to program the release efficiency of the device. This allows the design of a drug delivery device with the highest possible effectiveness for the intended application.

5.2 Results and Discussions

5.2.1 Nanocomposite preparation

To build a programmable drug delivery vesicle, a versatile emulsion polymerization of PA was used. This allowed us to synthesize a nanoparticle with a 28 nm core size, as measured with the BET analysis. PA core was covered with a temperature sensitive poloxamer copolymer with a 2950 molecular weight that consisted of 32 propylene oxide units in the center block and 12 ethylene oxide units in each end block. To attach the poloxamer to the surface of the nanoparticle, one of the hydroxyl groups on the end of the copolymer was substituted with the azide group and then a set of devices with a wide range of poloxamer grafting densities was prepared and characterized using Fourier Transform Infrared (FTIR) spectroscopy and Scanning Electron Microscopy (SEM) techniques as described in previous chapter. To test the encapsulation and release efficiency, Rhodamine B dye was used as a model drug. General scheme of the device and suggested positioning of the dye is shown on Figure 5.1A.

To estimate the range of the grafting densities for the samples that have to be prepared, a theoretically fully covered with poloxamer PA core was calculated. Calculations were based on the characteristic ratios of ethylene oxide and propylene oxide polymer, based on literature values as described in Chapter 4. Radius of the propylene oxide block was assumed to be equal to the radius of gyration (Rg) of the propylene oxide (PPO) polymer of the same length and was calculated using the following equation, an assumption that PPO is in the blob conformation was made and all calculations were done for Theta conditions[105]:

$$Rg = 0.41 * \alpha * (nb * C_n)^{0.5} * l$$

In this equation α is the chain expansion factor (for theta conditions α is equal to 1); n is number of bonds (for PPO block in the poloxamer used this number is 96, PPO block contains 32 propylene oxide repeat units); C_n is characteristic ratio (tabulated value was found in literature[105]); l is bond length (tabulated value was found in literature[105]).

To determine the length of the ethylene oxide (PEO) block the end to end distance ($< r^2 >^{0.5}$) was estimated using the following equation[105]:

$$< r^2 >^{0.5} = \alpha * (n * C_n)^{0.5} * l$$

In this equation n is number of bonds (for PEO block in the poloxamer used this number is 36, it consists of 12 ethylene oxide repeat units on each end).

The following assumptions were made during the calculations of the theoretical fully covered with poloxamer PA nanoparticle: perfectly spherical shapes for the nanoparticles and PPO blobs; no overlapping of the poloxamer chains, and square positioning of the PPO blobs in the space around the nanoparticle surface. Based on the calculated values for Rg, $< r^2 >^{0.5}$ and the assumptions made the fully covered GD was calculated to be 0.25 poloxamer molecules per nm^2. This value is in agreement with the results obtained in Chapter 4 and is roughly half of the maximum GD that was achieved experimentally.

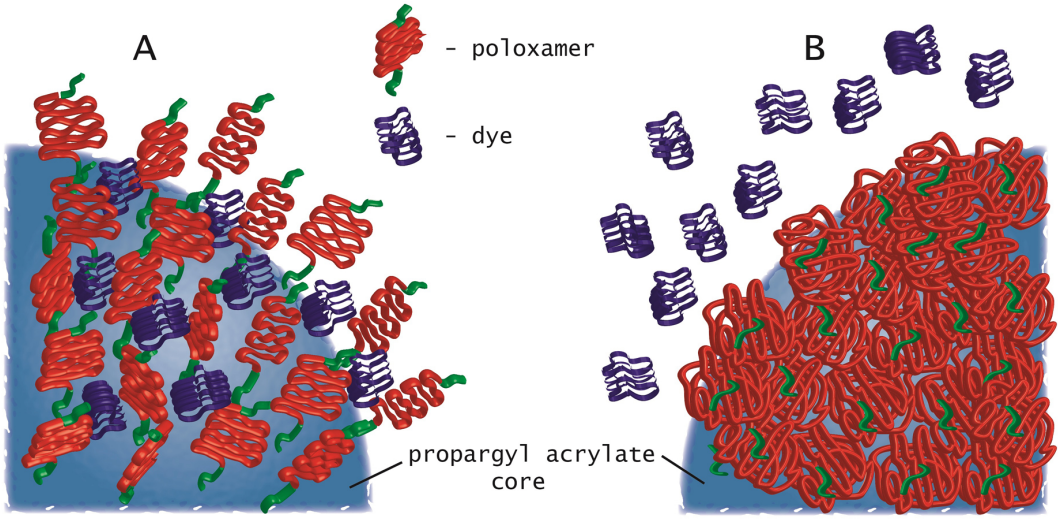

Figure 5.1: Scheme of the grab and release mechanism for the proposed system. **A** Device is below LCST of the poloxamer. Poloxamer chains are in their expanded state. This creates ample space for the dye to fit in. **B** Device is heated above LCST of the poloxamer. Poloxamer chains are in their collapsed state. Free volume inside of the shell is not sufficient enough to hold the dye any longer, the dye is released into solution.

5.2.2 Temperature triggered burst release

As a possible mechanism of the burst release, the following process is suggested. When vesicles were heated above the lower critical solution temperature (LCST) of the poloxamer used, the corona collapsed, triggering the release of the dye. Schematically this state is shown on Figure 5.1B. Poloxamer chains form hydrophobic pockets [31] that form the corona around the PA core. This corona acts like a ”sponge” with internal spring mechanism that can be activated at a specific temperature. At temperatures below LCST, poloxamer chains are in their relaxed state, the spring is expanded, and offer ample volume for the dye to fit in. Below LCST the ”sponge” is in its swelled state. When the vesicle is heated above LCST, the packing of the poloxamer chains densifies [31], the springs contracts, decreasing the free volume, while squeezing the ”sponge”, forcing the dye in to the solution.

To achieve the ability to program the release rate of the device GD influence on the release dynamics at various temperatures was investigated. As was shown in Chapter 4, theory predicts that there should exist a grafting density that will result in the maximum volume change of the shell. Thus it was expected that a maximum burst release rate can be observed. Rhodamine B was used as a model drug due to its well defined absorption characteristics and the ease of its concentration determination. The dependence of the release rate of Rhodamine B on the temperature and GD is shown on Figure 5.2. As can be seen on Figure 5.2, the increase in the dye release rate with the temperature is dependent on the GD of the poloxamer and demonstrates a clear optimal GD when the maximum release rate is reached, confirming theory based calculations. This knowledge allows us to design a device with a defined release efficiency to optimize the treatment plan for each individual case and to achieve the fastest remission while decreasing the side effects from the treatment.

Unmodified PA cores have no temperature responsive components and, as such, have a very limited increase in the release rate with the increase in the temperature. This can be mostly attributed to the increased mobility of the dye at a higher temperatures, resulting in the shift of the equilibrium states between the absorbed and free dye, represented by a zero grafting density data point on Figure 5.2. With the introduction of the poloxamer, a temperature responsive component is included in to the system, making burst release a possibility due to the changes in the poloxamer chain conformation. Rearrangement of the poloxamer chains when heated above LCST of the poloxamer causes the reduction of the shell's free volume pushing anything trapped inside of the shell to the outside edge of the vesicle, and eventually leading to a complete release of the dye from the device volume and in to the solution.

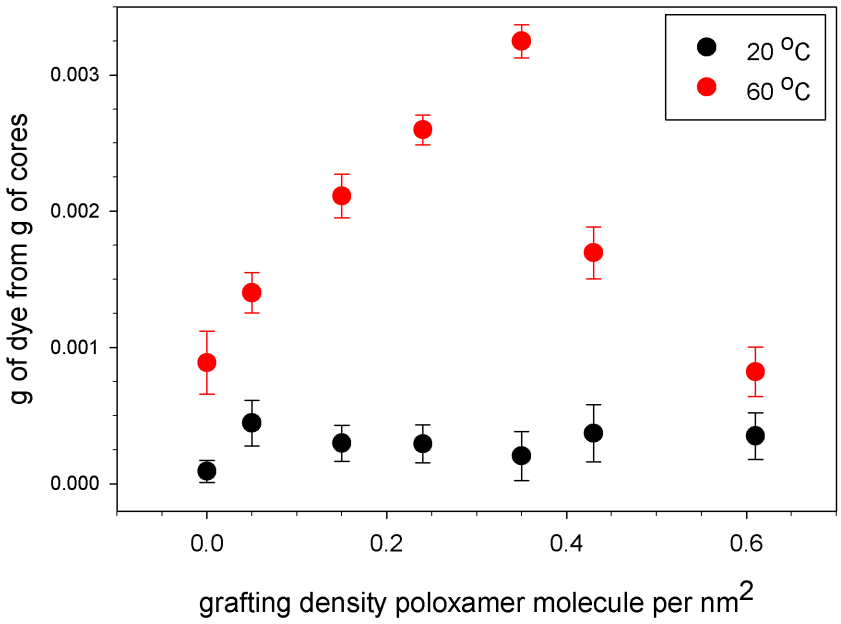

Figure 5.2: Rate of Rhodamine B release from vesicles with different GDs below and above LCST of the poloxamer used. Unmodified nanoparticles showed the best retention and almost no release. Vesicles with poloxamer shell showed initial increase in release capabilities with increase in GD, but after reaching GD of 0.35, poloxamer chains per nm^2 release effectiveness started to decrease until it almost completely lost the temperature triggering capability.

Observed differences in the dye release are most likely the result of a combination of two factors: positioning of the dye in the vesicle, governed by the ability of poloxamer to form hydrophobic pockets [31] (schematically positioning of the dye in the vesicle is shown on Figure 5.1A); and the change in the dimensions of these pockets with the temperature, governed by the changes of the poloxamer coil packing (the two states are schematically shown on the Figure 5.1A and B).

Using F*ö*rster Resonance Energy Transfer theory, as described in Chapter 3, and based on the calculations in Chapter 4, the extent of the poloxamer corona dimensions change was found to be on the order of 1 nm when the device is heated from 20°C to 60°C. This change of the dimensions of the corona is proposed as the

main mechanism behind the release mechanics of the device. The change of the poloxamer coil dimension causes the release of the dye: poloxamer goes from the expanded sponge like state to a squeezed sponge state, releasing its cargo.

At a very low grafting density, Figure 5.3A, the percent of the dye that is located inside of the poloxamer pocket is small. Thus, upon temperature triggering, only the part of the dye that is encapsulated in the poloxamer pockets is burst released, as shown by the first three data points on Figure 5.2, and the rest of the dye is released through the same mechanisms as in the case of the unmodified nanoparticles which is much slower and depends only on the concentration gradient.

At the optimal GD, Figure 5.3B, all of the surface of the PA core is covered with the poloxamer, preventing the dye from sticking to the surface. At this GD, there is plenty of volume for the poloxamer chains to accept any conformation. This allows the chains to arrange themselves according to the lowest energy state configuration. Upon heating above LCST, a complete rearrangement of the poloxamer chains is happening. This rearrangement causes the release of the dye at a much higher rate than the rate of any other samples, as shown by the peak on Figure 5.2. There is almost a 16 times increase in the release rate for the same GD sample when heated from room temperature to above LCST (poloxamer used in this study has LCST of 58°C) and 63 times increase in the release rate when compared to the unmodified nanoparticles at room temperature.

It is possible to increase the grafting density past this optimal value through the increase in the reaction feed ratio and the reaction times [150]. Increasing the GD past the optimal point causes the decrease of the free volume in the corona and, thus, limits the ability of the chains to alter their coil dimensions with temperature due to steric effects. This leads to a decrease in the burst release efficiency. Schematically, this packing state is shown on Figure 5.3**C**. At this packing state, coils

are packed too densely and their ability to change the coil dimensions is partially restricted by the steric hindrance, decreasing the rate of the dye release. Volume around the PA core is limited by the dimensions of the core and length of the copolymer. Thus, at high GD, the majority of this volume is occupied by the poloxamer coils instead of being available for the dye.

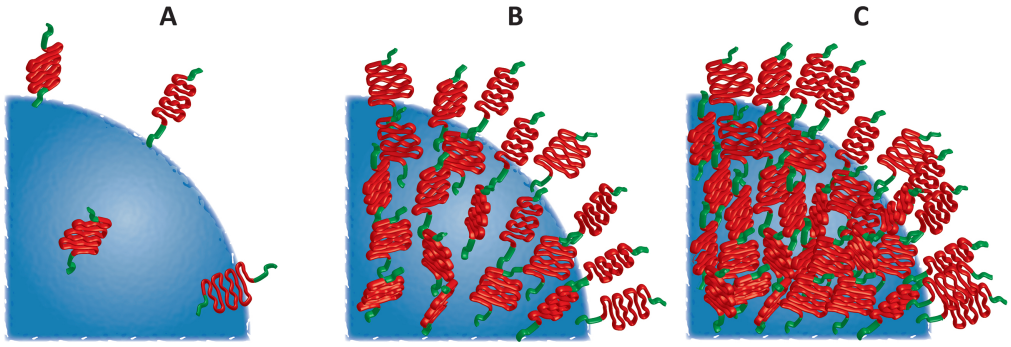

Figure 5.3: Schematic representation of the surface morphology based on the grafting density. **A**. GD is low and a significant surface area is open, allowing the load to stick to the surface rather than being trapped inside of the poloxamer pockets. **B**. GD is optimal, all surface is covered with poloxamer chains, all load is encapsulated inside of the poloxamer pockets. **C**. GD is too high, chain movement is restricted by the neighboring chains, release rate is decreased compared to optimal GD.

The ability to design a system with the capability to burst release large quantities of active molecules when triggered with temperature can facilitate the creation of a smart drug delivery vesicle for the cancer treatment application. Poloxamers are commercially available in the wide range of the response temperatures, allowing us to match the temperature to the required application. As one of the examples of such temperature ranges, cancer tissue elevated temperature can be targeted. Cancer tissue was shown to have a higher temperature [19] compared to the rest of the body and this difference can be used to trigger the burst release of the anticancer drugs in the cancer tissue while maintaining a safe concentration of the drug in the rest of the body.

5.2.3 Encapsulation efficiency

To compare encapsulation efficiency of PAPN with different grafting densities an equivalent of 20 mg of dry cores was loaded into the dialysis bag with a 12000 Dalton molecular weight cutoff. Float-A-Lyzer G2 dialysis membranes were used for this study, since they offer an easy to load solution with the screw on cap and come assembled and ready to use, pre-cut to the same dimensions. Each sample was brought to a total volume of 5.5 mL and 2 mg of Rhodamine B dye was added (equivalent of 0.675 Rhodamine B molecule per nm^2 of the surface). This amount of the dye was experimentally determined to be just over the limit of the encapsulation capacity for the unmodified nanoparticles. Then each dialysis bag was loaded in to a 50 mL centrifuge tube and 37 mL of deionized water was added to the tube.

Two centrifuge tube holders were glued together to allow loading of 8 centrifuge tubes at the same time. This assembly of two holders was attached to the horizontal shaft of the electric motor with rotation speed control. Centrifuge tubes were fixed inside of the holders, ensuring that they will not fall out when the holder is rotated upside down. Speed of rotation was set to approximately 1 revolution every 5 seconds. This speed was found to be efficient enough to ensure good mixing of the sample while remaining slow enough to prevent the possibility of the dialysis membrane rupturing. Whole assembly was placed in the cardboard box lined with aluminum foil on both sides, leaving the electrical motor outside of the box. Box dimensions were selected to allow free rotation of the holder inside of it, leaving ample space for the heating plate at the bottom. The heating plate was positioned at the bottom of the box centered under the samples and a temperature sensor was attached to the top of the box hanging down 2 inches, touching the top of the centrifuge tubes. The box was sealed with aluminum foil to create an oven like

environment.

For the room temperature encapsulation or release measurements, no heat was used, just rotation. For the burst release above LCST of the poloxamer, box temperature was set to 65°C . The 7 degree increase over LCST of poloxamer was chosen to ensure that the samples will be heated over LCST. Positioning of the sensor was at the top of the box, creating a possibility that the actual sample temperature can be slightly different from the sensor readouts. Thus this extra 7 degrees were added to compensate for the setup deficiencies.

Figure 5.4 shows the dependence of the encapsulation capacity on the grafting density. Unmodified nanoparticles, the sample with GD of 0, showed the best encapsulation capability and their effectiveness was used as a normalization reference for the rest of the samples. Measurements of encapsulation efficiency were done based on the difference between the loaded amount of the Rhodamine B and the amount of Rhodamine B dye that was detected in the supernatant solution after 2 hours of dialysis. Water in the centrifuge tubes was changed every two hours and the content of Rhodamine B dye in the supernatant was measured. To measure the dye content in the supernatant solution the UV/Vis spectra was recorded and absorbance of each sample was compared to the previously recorded calibration curve for the known Rhodamine B concentrations. To obtain total mass of the Rhodamine B dye that was released, measured concentration was multiplied by the total volume of the supernatant solution (37 mL). This total mass was subtracted from the 2 mg that were initially loaded, to obtain the encapsulation efficiency number.

It was established, that at a very low GD, there was only a slight change in the encapsulation efficiency of the vesicles compared to the unmodified cores, as shown by the second data point on Figure 5.4. As the grafting density was increased, encapsulation efficiency quickly dropped to about 80% of the unmodified

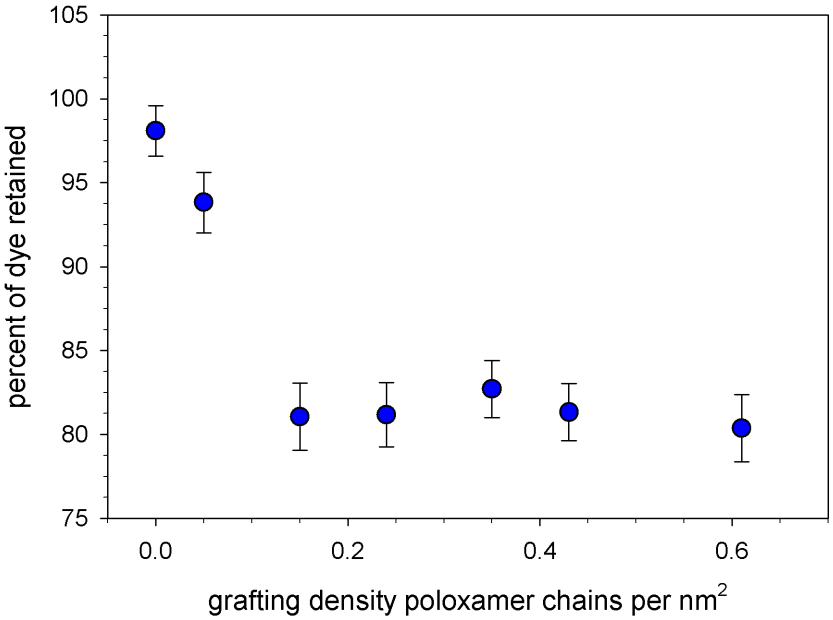

Figure 5.4: Encapsulation effectiveness of vesicles with various GDs in the first 2 hours. Unmodified nanoparticles were capable of holding close to 1 Rhodamine B molecule per 3 nm^2 of the surface, while modified nanoparticles were able to retain about 80% of this efficiency.

nanoparticles and remained mostly independent of the grafting density there after, as shown by the 3rd data point and to the end of the graph on Figure 5.4. We suggest that this is caused by the balancing of the two volumes that are available for the dye to go in to: first is the volume formed by the propargyl groups on the surface of the cores and the second volume is formed by the hydrophobic pockets of the poloxamer chains. Even though the total volume that is formed by the poloxamer chains is greater than the volume formed by a single layer of propargyl groups on the surface, majority of this poloxamer formed volume (the shell around the PA core) is filled by the co-polymer itself, and only the voids between copolymer chains are accessible for the dye. This finding shows that there is no significant dependence in the encapsulation ability of the vesicles based on the grafting density, and from the retention point of view, there is no significant difference between different grafting

density samples. This finding suggests why in all the literature that was reviewed, no studies related to the grafting density influence on the encapsulation capacity was reported.

5.2.4 Extended release

High encapsulation efficiency alone is not enough to make an effective extended release delivery vesicle. Second and more important property needed, is a well defined release profile over the extended periods of time. All 7 samples were loaded in the dialysis bags and were placed in a 50 mL centrifuge tubes, then 37 mL of deionized water was added to each tube. Next samples were placed on a rotating mixer to provide sufficient mixing to simulate the dilute environment of a human body. The change in the release rate was determined based on the increase of the Rhodamine B content in the dialysate water as measured by UV/Vis and calculated using Beer-Lambert law, results are shown on Figure 5.5.

The observed initial big decrease in the release rate was due to intentional overloading of the vesicles with the dye to ensure that the maximum possible encapsulation was reached. The limited penetration speed of the dialysis membrane was most likely the reason why few hours were needed to remove the free floating dye from the solution.

To test the dialysis membrane's penetration ability, dialysis bag was filled with deionized water and 2 mg of Rhodamine B was loaded in to it. Only trace amount of the dye were left in this sample after just 2 water changes (4 hours of dialysis). Based on this result the observed release rate of the poloxamer modified nanoparticles after 8 hours of the dialysis was considered to be true release rate from the nanoparticles, rather than a combination of the last with the free dye

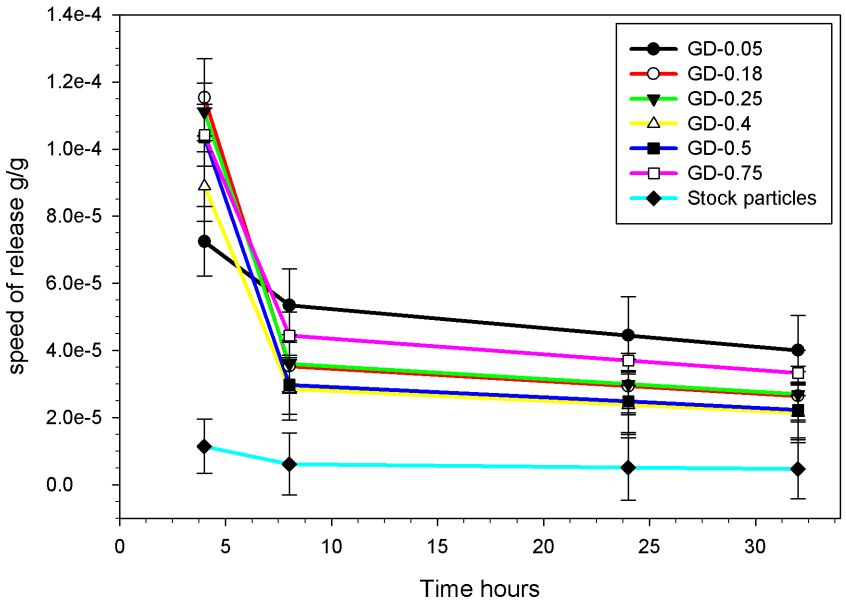

Figure 5.5: Release rate, measured in grams of dye from gram of the cores, of the Rhodamine B. Majority of the vesicles with poloxamer shell showed very similar release patterns at room temperature which was relatively high at the beginning and leveled out after 8 hours. The lowest GD sample showed a slower initial release but at the same time it did not loose as much of the release rate with time and maintained relatively linear release from the beginning. Unmodified particles worked mostly as a grab and hold vesicle showing very limited release with time.

leakage from the membrane. The rate of the release before the 8th hour is most likely a combination of the two. The burst release test was done on the same samples at the 10th hours of the experiment eliminate the possibility of the sample preparation procedure influencing the observed results. After heating for 2 hours samples were again cooled to room temperature, supernatant was removed and fresh water was added to the samples. The rest of the room temperature release rate measurements were done on the same samples at the indicated time intervals.

To check the influence of the equilibrium states on the release efficiency of the different grafting densities samples were left in the same dialysate water for 17 hours. As expected the release rate has dropped to almost zero due to small

dye concentration gradient between the dialysate water and the sample. After the dialysate water was replaced with fresh deionized water the release efficiency was restored and remained fairly constant for the next 10 hours. This results suggest that the device will maintain its performance upon storage. Equilibrium concentration of the dye will be reached within the first few hours after the dilution and the majority of the dye (or drug) content will still be encapsulated in the shell of the nanoparticles until the injection or replacement of the storage water.

5.3 Conclusion.

Core shell system capable to retain and release upon request small molecules was developed. Proposed system combines simple synthesis with high stability of the device, while maintaining its bio-compatibility. The ability to choose multiple commercially available poloxamers is expected to allow us the possibility to program the temperature of the burst release of the drug. Described here in is a technique that allows to prepare a well defined device with the desired properties simply through the control over the grafting density of the poloxamer on the propargyl acrylate core. Device can be programmed to serve either an extended release purpose or to be used as a targeted drug delivery with a burst release of the drug at the point of interest using temperature as a trigger. Possibility to create a device with a well defined drug release profile opens a window of opportunity to increase the treatment efficiency and decrease the number of side effect occurrences along with their severity. The ability to program the device to burst release upon temperature trigger combined with the possibility to manufacture cores in a wide range of core sizes allows usto use this system as a targeted and temperature activated cancer drug delivery device.

5.4 Experimental methods

5.4.1 Materials and Reagents

All reagents were purchased from Sigma-Aldrich with at least 97% purity level, solvents were purified using standard procedures.

5.4.2 Characterization

^{1}H spectra were recorded on JEOL ECX-300 spectrometers (300MHz for proton). Chemical shifts for protons are reported in parts per million downfield from tetramethylsilane and are referenced to the carbon resonances of the solvent ($CDCl_3$: δ 7.26 or DMSO-d_6: δ 2.50). Nanoparticles size was checked using Coulter N4Plus DLS using 10 mm plastic cuvette. FTIR was done on a Nickolet Magna IR 6700 spectrometer equipped with diamond attenuated total reflectance accessory.

5.4.3 Nanoparticle preparation

Emulsion polymerization was performed in a single necked round bottom flask (250 mL) equipped with the magnetic stirrer. Potassium persulfate (110 mg) was dissolved in water (80 mL) and nitrogen was purged through the solution for 15 minutes. Sodium dodecyl sulfate (90 mg) was added to the flask under nitrogen purge. Obtained solution was stirred and placed in the preheated bath at 75 °C for 3 minutes, then degassed solution of propargyl acrylate (4 mL) and divinylbenzene (0.65 mL) were added to the main reaction flask. The mixture was stirred at 75 °C under nitrogen purge for 90 minutes. The emulsion was allowed to cool on air. Then mixture was filtered through paper filter. After filtering samples were purified by dialysis using Spectra/Por Dialysis membrane with MWCO 50000.

Dialysis was performed for 3 days at 40 °C in 18.2 Megaohms water with regular water changes, typically every 8 hours. Nanoparticles were characterized using DLS,SEM and BET analysis to determine average size and aggregation. Average size of the nanoparticles, based on the analysis from all three techniques, was assumed to be 28 nm. Obtained emulsion contained 45 mg/mL of nanoparticles.

5.4.4 Poloxamer modification

$MeSO_2$-pluronic-L64. Pluronic-L64 (3.14 g, 1.064 mmol) was dissolved in dry dichloromethane (DCM) (10 mL), triethylamine (0.132 g, 1.3 mmol) was added to the solution. The obtained solution was stirred at room temperature, and methanesulfonyl chloride (48 mg, 0.42 mmol) was added drop-wise. The mixture was stirred for 6 hours at room temperature; then was washed with water. The organic layer was separated, dried with Na_2SO_4, filtered and evaporated under reduced pressure. Yield 3.1 g (95%), clear oil. This product was used in the next step without further purification. ^{1}H NMR ($CDCl_3$) δ 1.11 (m, 96H), 3.06 (s, 3H), 3.38 (m, 32H), 3.52 (m, 64H), 3.63 (m, 98H).

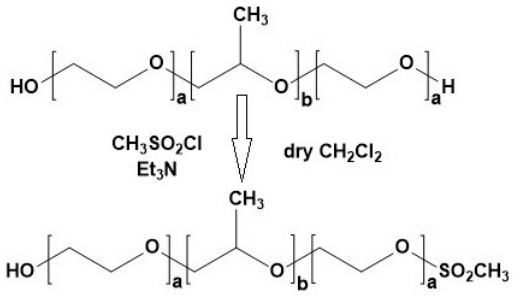

Pluronic-L64-N3. Sodium azide (195 mg, 3 mmol) was added into solution of $MeSO_2$-pluronic-L64 (3.1 g, 1.03 mmol) in dimethylformamide (DMF) (10 mL). The mixture was stirred and heated to 80 °C for 3 hours. After cooling the mix-

ture was extracted with DCM and washed with water 2 times. The organic layer was separated, dried with Na_2SO_4, filtered and evaporated under reduced pressure. Yield 2.27 g (75%), clear oil. Pluronic-L64-N3 was used in the next step without further purification. ^{1}H NMR ($CDCl_3$) δ 1.07 (m, 96H), 3.34 (m, 32H), 3.48 (m, 64H), 3.59 (m, 98H).

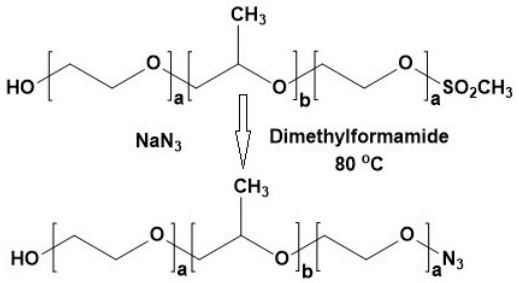

5.4.5 Nanoparticle modification

Nanoparticle modification was performed using the azide alkyne Huisgen cycloaddition reaction also known as Click chemistry. Typical procedure was used as described elsewhere [41]. Copper(II) sulfate ($CuSO_4$) (2 mg, 8 μmol) was added to the propargyl acrylate nanoparticles suspension in water (2 mL) and stirred until completely dissolved. Then solution of pluronic-L64-N3 (6) (22 mg, 7 μmol) in water (2 mL) was added. Next the solution of $CuSO_4$ (2 mg, 8 μmol) in water (2 mL) was added. The reaction was stirred and purged with nitrogen for 5 minutes, then sodium ascorbate (10 mg, 50.5 μmol) was added. The reaction continued at 28°C for 24 hours under nitrogen purge. Reaction mixture was centrifuged at 10000G for 10 minutes. Separated nanoparticles were washed with the mixture of water:Methanol 1:1 (20 mL). Then 1 mL of 0.1 M ethylenediaminetetraacetic acid (EDTA) solution was added to remove copper catalyst. Nanoparticles were re-

dispersed in 40 mL of 18.2 Megaohms water and sonicated for 3 minutes. After sonication suspension was centrifuged at 10000G for 10 minutes. This step was repeated 2 times. Next 0.1 mL of 20% sodium dodecyl sulfate (SDS) solution was added to remove any unreacted poloxamer. Nanoparticles were re-dispersed in 40 mL of 18.2 Megaohms water and sonicated for 3 minutes. After sonication suspension was centrifuged at 10000G for 10 minutes. This step was also repeated twice. Lastly nanoparticles were re-dispersed in 40 mL of 18.2 Megaohms water and sonicated for 3 minutes. After sonication suspension was centrifuged at 10000G for 10 minutes. This step was repeated 5 times to ensure that all impurities were removed. After last centrifugation nanoparticles were redispersed in 10 mL of 18.2 Megaohms water and stored in the refrigerator.

Chapter 6

Temperature triggered release of vancomycin

Vancomycin is a potent antibacterial drug that suffers from poor bioavailability due to poor water solubility and relatively high molecular weight thus limiting its application for the bacteria induced diseases. In this study propargyl acrylate - poloxamer nanocomposite (PAPN) ability to encapsulate and release when triggered various molecules is used to promote the bioavailability of the vancomycin. PAPN was prepared using emulsion polymerization of propargyl acrylate followed by surface decoration with the poloxamer to a precisely controlled grafting density level. Activity of the PAPN loaded with vancomycin was compared to the free drug and unmodified propargyl acrylate nanoparticles. Tests revealed comparable activity of PAPN loaded with vancomycin to the freshly prepared free floating vancomycin. Additionally, PAPN proved to be able to effectively encapsulate, deactivate and preserve the vancomycin until the device was heated above lower critical solution temperature (LCST) of the poloxamer used. At the temperatures above LCST PAPN was able to release vancomycin with the restoration of the vancomycin activ-

ity even after one month of storage in solution, while comparable concentration of free vancomycin became less potent against bacteria.

6.1 Introduction

Controlled release of biologically active molecules is superior to a simple injection of a drug solution because it allows us to regulate the concentration of the active components throughout the body, limiting the side effects probability and at the same time increasing the treatment efficiency [151, 152, 153, 154]. Controlled release allows researchers to achieve high concentration of the drugs at the site of interest while maintaining a safe level of the drug at other organs and systems of the body[155, 156]. One of the mechanisms used to achieve the controlled drug delivery is through the absorption-resorption of the drug into the active layer of the carrier[157, 158, 159]. Vancomycin can significantly benefit from the controlled drug delivery system due to its high activity towards multitude of gram positive bacteria but low stability in aqueous solutions[160, 161]. Various systems have been developed that are capable to encapsulate and then release vancomycin[157, 162, 163, 164, 165] but all of these approaches suffer either from the complex synthesis mechanisms, making the final price of the device too expensive for the real world applications, or the proposed systems lack in the control over the release patterns, placing strict limitations over the application conditions, making the system useful only for a narrow range of patients.

Described herein is a drug delivery device build around bio-compatible propargyl acrylate (PA) nanoparticle that was modified with poloxamer block copolymer to achieve temperature triggered drug release. PA core was shown to be a versatile build platform for the medical application [141, 40, 148]. Alkyne groups, that cover

the surface of the PA nanoparticle, serve as an anchoring points to attach various active molecules using azide alkyne cycloaddition reaction, also known as a Click reaction. Click reaction offers the ability to permanently combine two molecules under mild conditions with very high selectivity[166, 41], making Click reaction the tool of choice when biologically active molecules are involved. Mild conditions during Click reaction allows us to preserve the high biological activity of the drugs or other active molecules during synthesis steps.

Poloxamer group of copolymers is a big commercial market of surfactants and in recent years poloxamers have been demonstrated to be a potent responsive polymer for medical applications due to their ability to stabilize various active molecules in the aqueous environment[96, 98]. Poloxamers are known to form pockets that can encapsulate biologically active molecules and dimensions of these pockets are dependent on the temperature[30, 134] allowing us to use temperature differential as a trigger for the drug release mechanism. Poloxamer family of copolymers offers the ability to fine tune the temperature of the drug release simply through the selection of a correct ratio of the blocks in the copolymer[31, 34], making it possible to use the increase in the temperature at the source of inflammation as a trigger for the drug release, making targeted delivery a possibility. Decoration of PA cores with poloxamer creates an active layer on the surface of PA nanoparticle. This active layer can encapsulate drugs at the temperatures below lower critical solution temperature (LCST) of the poloxamer and when exposed to the temperature above LCST of the poloxamer the shell collapses, triggering the release of the drug.

Vancomycin is a glycopeptide antibiotic which is active towards multiple Gram positive bacteria, including *Escherichia coli* and *Staphylococcus aureus*, and is effective in the treatment of various bacterial diseases[167, 168]. This antibiotic has limited water solubility and it looses its biological activity relatively quickly

when stored as a solution, because of these two factors vancomycin has a limited range of applications and can benefit greatly when incorporated into the drug delivery device that can protect it from the environment and release it when required. Most bacteria induced diseases cause inflammation at the cite of contamination, this leads to a local increase in temperature by 2 or even 3 degrees. Based on the previous results it is expected that this difference should be sufficiently big to trigger the poloxamer collapse and thus initiating the release of vancomycin at the site of inflammation, preventing the bacteria from spreading, while maintaining low concentration of the drug in the rest of the body.

6.2 Results and Discussion

6.2.1 Characterization of propargyl acrylate poloxamer nanocomposite

Grafting density of the poloxamer on the propargyl acrylate (PA) core was determined using Fourier transform infrared spectroscopy (FTIR) as described in Chapter 4. For a set of samples with known ratios of the poloxamer to PA FTIR spectra were collected. Poloxamer has a strong peak around 1100 $cm^{-}1$ and PA has a strong peak at 1150 $cm^{-}1$, based on the ratio of this two peak a calibration curve based on a known mass ratio of the poloxamer to PA was obtained. Using this calibration curve poloxamer content in PAPN was determined. Figure 6.1 shows FTIR spectra of unmodified PA nanoparticles, poloxamer and PAPN with poloxamer content of 21 mass %. Experimentally precision of less than 1 mass % of poloxamer in the mixture was confirmed.

Based on the measured core size, grafting density of the poloxamer was de-

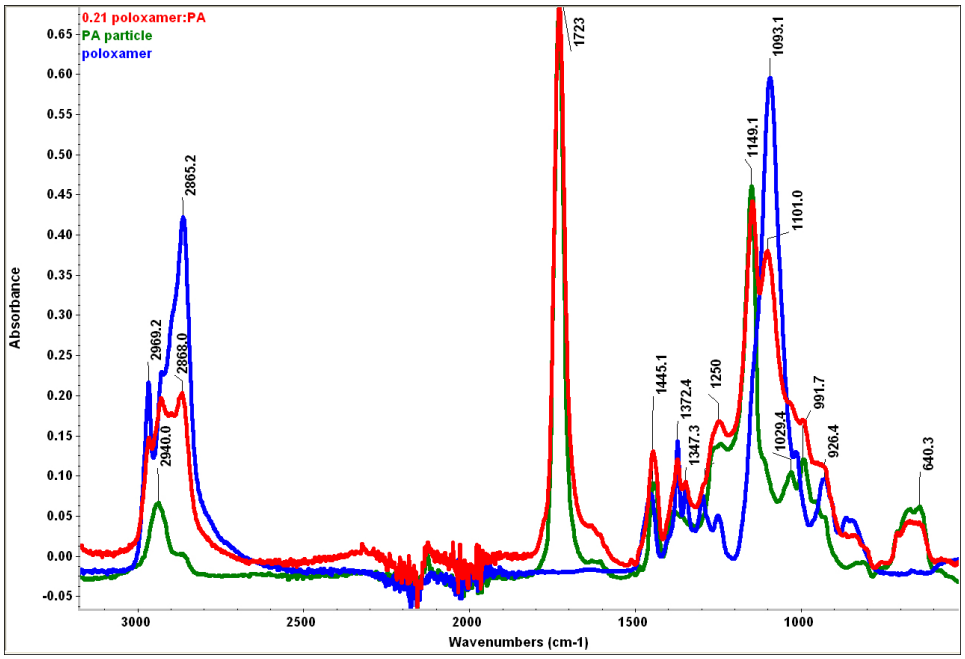

Figure 6.1: FTIR spectra of poloxamer (blue), PA particles (green) and mixture of the two (red) showing good separation of the peaks for poloxamer (1100 $cm^{-}1$) and PA particles (1150 $cm^{-}1$). Different grafting densities of poloxamer in PAPN can be distinguished through the ratio of these two peaks.

termined to be 0.29 poloxamer chains per nm^2 of PA core surface. As was shown in Chapter 5 this grafting density is close to the optimal grafting density for small molecule burst release, thus high temperature triggered release rate of the vancomycin is expected. Figure 6.2 schematically shows proposed positioning of the vancomycin inside of the poloxamer shell of the PAPN. Higher grafting densities of the poloxamer would lead to a decrease in the encapsulation capacity, while lower grafting density would limit the release rate at the elevated temperature, thus limiting the effectiveness of the system for intended use. To better match the temperature regime of the bacteria cells Pluronic-L62 version of poloxamer was used. This copolymer has LCST of 24 °C which allowed us to use 18 °C and 36 °C as the test temperatures. At this temperatures bacteria cells are not expected to be damaged from the temperature induced effects, thus observed results would indicate

influence of the device on the bacteria rather than temperature.

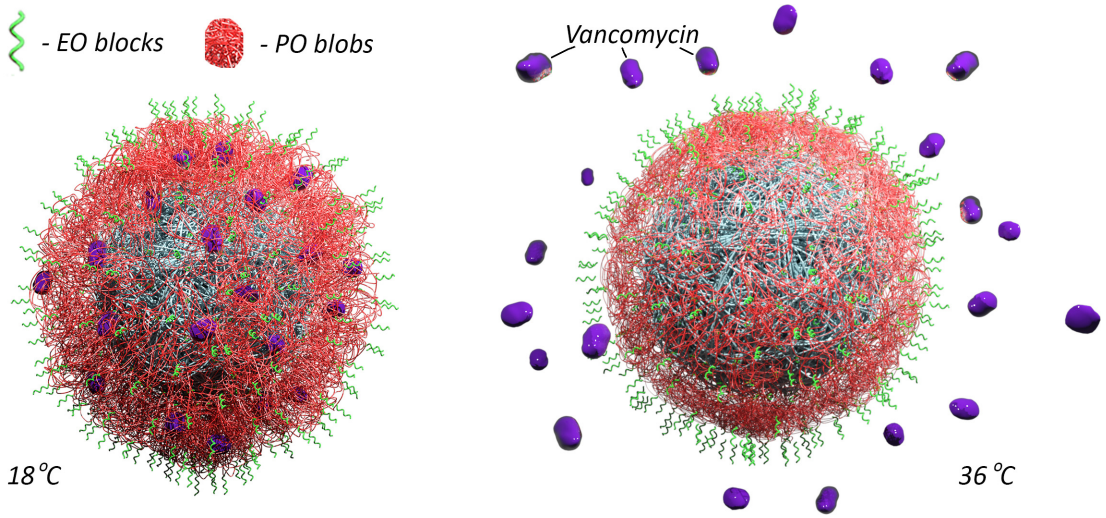

Figure 6.2: Left nanoparticle temperature is below LCST of the poloxamer, the shell is expanded and can encapsulate vancomycin. Right image nanoparticle temperature is above LCST of the poloxamer, the shell is collapsed, vancomycin is released from the shell. Image created by Olga Reukova using 3DMax software package. Dimensions of the coils on the cartoon where scaled to represent the theoretically calculated dimensions of particle and poloxamer blocks, vancomycin was not drawn to the scale for clarity.

6.2.2 Binding yield of vancomycin

Experimentally it was determined that saturation of the poloxamer shell on PAPN with vancomycin was achieved around 0.5 vancomycin molecules per nm^2 of the PAPN surface. To determine encapsulation efficiency excess of vancomycin (5 mg of vancomycin per 15 mg of cores, equivalent of 0.74 vancomycin molecules per nm^2) was added to PAPN solution at 18 °C , temperature below LCST of the poloxamer used. The mixture was kept at 18 °C for 24 hours to allow ample time for the vancomycin to penetrate into the shell and to reach the equilibrium state. After 24 hours mixture was centrifuged at 6000G for 40 minutes, maintaining the temperature at 7 °C . Vancomycin content in the supernatant was calculated based

on the molar extinction coefficient of the vancomycin and the total volume of supernatant that was collected, using same methodology as in Chapter 5. Then PAPN was re-dispersed in cooled to 5 °C deionized water and centrifuged again at 6000G for 40 minutes, while maintaining the temperature at 7 °C .

Vancomycin molar extinction coefficient was found using the same procedure as in Chapter 5 for Rhodamine. A series of vancomycin dilutions with known vancomycin concentration was prepared and UV/Vis absorbance for these samples was measured. Attempt to measure vancomycin directly on the surface of PAPN resulted in a typical scattering spectra and even through the solvent index matching procedure the scattering was dominant, no reliable measurement of vancomycin on the nanoparticles absorbance was possible.

To index match samples were dispersed in glycerin (solvent with the closest refractive index value to the polymer) and UV/Vis spectra were collected resulting in a typical scattering curve at the wavelength range of 300 nm and below, completely masking the vancomycin peak. Figure 6.3 shows absorbance of standard solutions that were prepared and a typical scattering curve that was observed when direct measurement of vancomycin on the nanoparticles was attempted.

As can be seen from the supernatant line, blue line of Figure 6.3, once the nanoparticles were removed from the suspension remaining vancomycin was detected making it possible to quantify the encapsulation efficiency. To ensure complete PAPN removal from the supernatant solution, samples were filtered through 0.2 μm filter after centrifugation. Using the peak maximum for all of the standard solutions of the vancomycin calibration curve was created, shown on Figure 6.4. All unknown samples were compared to this curve to estimate the vancomycin content in them. Based on the absorbance data for each supernatant solution the total amount of the vancomycin, that was not encapsulated by the nanoparticles or PAPN,

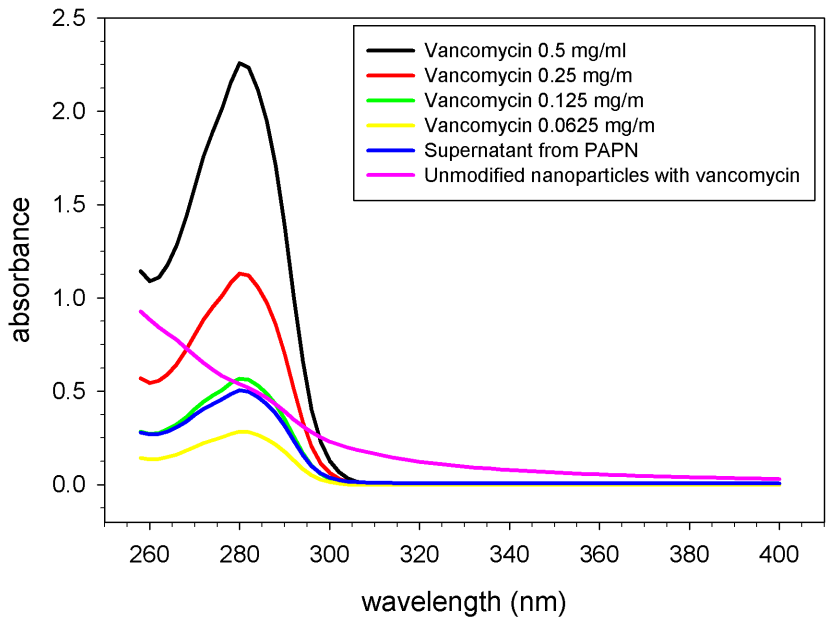

Figure 6.3: Absorbance of standard Vancomycin solutions, from supernatant after modified nanoparticles were removed from the suspension and from unmodified nanoparticles with vancomycin.

was calculated. This number was subtracted from the loading amount and encapsulation efficiency was calculated as the total amount of dye encapsulated divided by the total surface area of the particles in the sample. Unmodified nanoparticles encapsulated 0.3 mg of vancomycin per mg of dry cores or 0.67 vancomycin molecules per nm^2 of the core surface, PAPN encapsulated 0.17 mg of vancomycin per mg of dry cores or 0.38 vancomycin molecules per nm^2 of the core surface.

6.2.3 Antibacterial activity on Escherichia coli

The efficiency of the temperature triggered release of the vancomycin from PAPN was compared to the unmodified nanoparticles and to the free floating vancomycin. PAPN without drug was used as a control of the PAPN toxicity. Efficiency

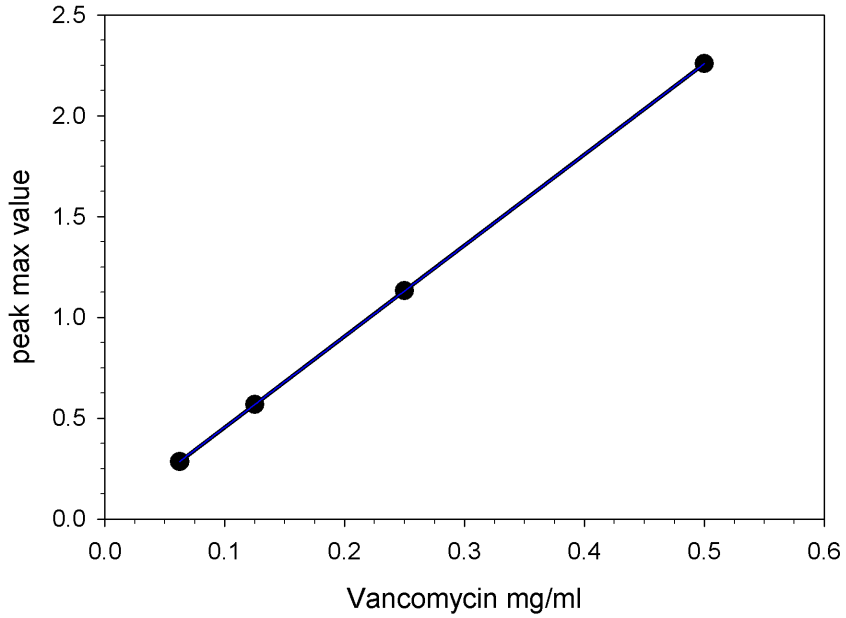

Figure 6.4: Dependence of maximum absorbance for standard vancomycin solutions on the concentration of vancomycin in solution. Line represents linear curve fit, dots actual recorded data for known concentrations.

of PAPN was tested on *Escherichia coli* and *Staphylococcus aureus* bacteria. For *Escherichia coli* experiment bacteria was incubated in the fresh media for 24 hours prior to being exposed to the PAPN and other control samples. Starting bacteria suspension, as obtained after 24 hours of growing in media, was diluted 5E-6 times. For *Staphylococcus aureus* bacteria was incubated for 17 hours and diluted to 1.5E-5.

To each vial containing 5 mL of bacteria suspension equivalent of 1.4 mg of dry cores was added. Phosphate-buffered saline (PBS) solution was used to protect bacteria cells from bursting due to osmotic pressure and to remove all sources of food for bacteria. This was done to maintain a stable number of live cells in each sample. Bacteria that was left in the growing media would have a chance to grow, thus the number of live cells in the sample would be growing over the course of

the experiment, invalidating the results. For the control sample that contained just vancomycin, 0.25 mg of vancomycin was added to 6 mL of PBS solution, this amount is roughly equivalent to the total amount of the vancomycin that was added with the PAPN sample according to the UV/Vis based calculations (1.4 mg of core * 0.17 mg/mg encapsulation efficiency = 0.238 mg).

Samples were separated into two groups and incubated for 24 hours at 18 °C or 36 °C, above and below LCST of the poloxamer used. After incubation 0.1 mL of each sample was seeded on 150 mm Petri dish with the growing agar and bacteria was allowed to grow at the optimal temperature and humidity environment (36 °C and 100% humidity) until a distinct colonies were observed on the surface of agar media. Typical time required was between 24 and 48 hours. Each sample was prepared in triplicates. Number of the colonies per Petri dish for each sample was counted and normalized according to the number of the colonies in the control sample, sample that was not treated with anything, results are shown on Figure 6.5.

As can be seen from the Figure 6.5 *0GD+vancomycin* bar - unmodified nanoparticles loaded with vancomycin had a very limited effectiveness in killing the bacteria at either temperature. PAPN that did not have any vancomycin in it, *0.29GD* bar on Figure 6.5, showed just slight toxicity towards the bacteria, which was also mostly independent from the temperature. This result also suggests that the device itself is safe enough and is not the main factor influencing the death of the bacteria. PAPN loaded with vancomycin, *0.29GD+vancomycin* bar on Figure 6.5, showed a slight increase in the number of colonies at 18°C and had the same effectiveness as the free floating vancomycin at 36°C. Very high survivability of the bacteria in the presence of the PAPN loaded with vancomycin is indicative of the PAPN ability to deactivate the drug while the drug is encapsulated in the poloxamer shell. Similar effectiveness of the PAPN to the free floating vancomycin at the elevated temper-

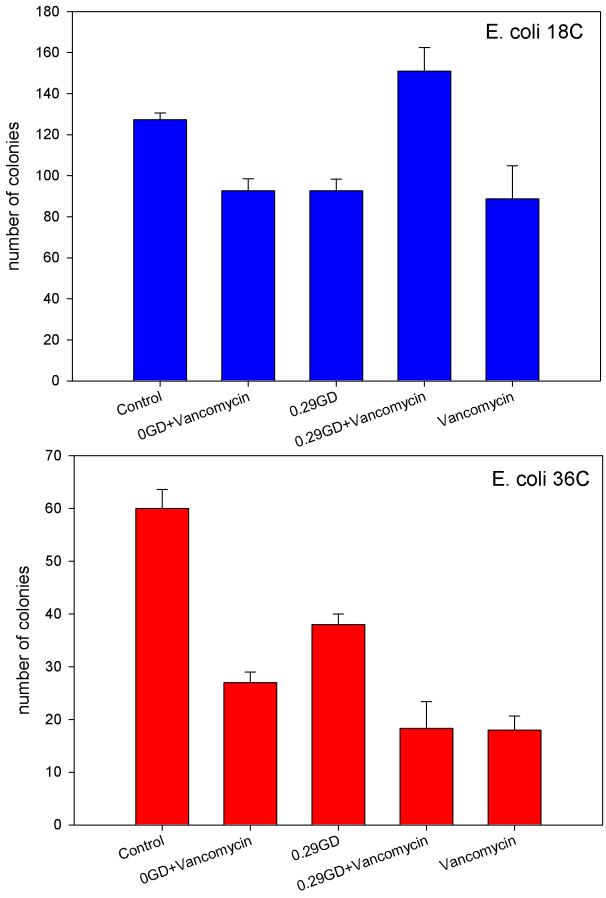

Figure 6.5: Number of colonies that has grown on petri dish after *E. coli* bacteria was exposed to PA particles with vancomycin, PAPN, PAPN with vancomycin, pure vancomycin and control in phosphate-buffered saline (PBS) solution. Top graph bacteria was incubated at 18C°C, bottom graph - at 36°C.

atures suggests that vancomycin was released from the shell and its antibacterial activity was restored, indicating that proposed system have completed its designed task: drug was encapsulate, protected and then release in a controlled manner, restoring its bio-activity.

As can be seen from the normalization of the observed number of colonies as shown on Figure 6.6. PAPN loaded with vancomycin had superior performance compared to a free floating vancomycin. PAPN loaded with vancomycin was much

more efficient in controlling the population of the bacteria compared to the unmodified propargyl acrylate nanoparticles, showing the importance of the temperature triggered mechanism introduced with the addition of the poloxamer at a correct grafting density.

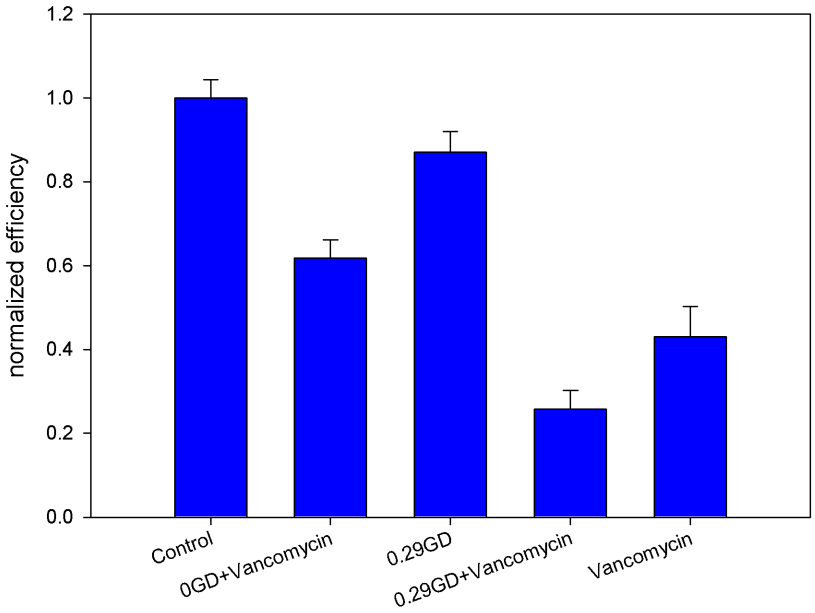

Figure 6.6: Normalized number of the colonies that survived at 36 °C compared to 18 °C . Control sample is the *Escherichia coli* bacteria that was not treated with anything and was just diluted with PBS to match bacteria concentration of other samples. The rest of the samples were normalized against the Control sample.

As a possible mechanism of the enhanced PAPN efficiency compared to the pure vancomycin a limited water solubility of the last is proposed. PAPN being decorated with the ethylene oxide groups on the outside has a much batter water compatibility thus upon heating it, facilitates a much better spreading of the vancomycin through the solution volume, enhancing vancomycin effectiveness.

The increase in the number of colonies that survived in the presence of PAPN loaded with vancomycin (Figure 6.5) demonstrates the effectiveness of the designed

system in the shielding of the drug from the environment and the shielding of the environment from the drug at temperatures below LCST. This technology has a potency to be used for both bacterial diseases and cancer treatment since it allows to deliver high concentration of active molecules to the target regions and release these molecules in the areas where there is an inflammation or actively growing tissue, resulting in the local increase in the temperature.

6.2.4 Antibacterial activity on *Staphylococcus aureus*

Escherichia coli is a good and safe test subject to work with, but for the medical application much more valuable is the data showing device efficiency against more aggressive bacteria. *Staphylococcus aureus* is often used as a test bacteria due to insufficient efficiency of the currently available methods of treatment for the patients that have been infected by this bacteria and due to the severe complications that can be caused by this bacteria. *Staphylococcus aurues* treatment is often challenging and require high doses of antibiotics thus systems that can enhance antibiotic activity are in high demand. Working with *Staphylococcus aureus* requires special care from the researcher to prevent self-contamination and to avoid release of the bacteria into the environment, that is why initial study was done on *Escherichia coli* bacteria.

Experiment protocol for *Staphylococcus aureus* was the same as for *Escherichia coli*. First bacteria was incubated in fresh media to obtain a colony at the optimal growth phase. Experimentally time needed to reach log growth phase was 18 hours at 36 °C compared to 24 hours for *Escherichia coli*. The conclusion on the time required was made based on the number of cells that were able to survive in the PBS for 6 hours. If the bacteria growth was stopped after the log growth phase the sur-

vivability of the cells in the PBS solution was much lower than for the bacteria that was taken at log growth phase, often leading to 80% or more of cell death during bacteria storage in PBS at 36°C for 6 hours. The bacteria that was taken at optimal growth phase showed only 20 to 30% cell death under the same conditions.

Staphylococcus aureus suspension was treated with freshly prepared solutions of unmodified nanoparticles with vancomycin, PAPN with vancomycin, PAPN control, and 1 month old solutions of vancomycin and PAPN with vancomycin, using the same methodology as for the *Escherichia coli* bacteria experiment. After 6 hours of incubation 0.1 mL of each sample was seeded onto agar media in 150 mm Petri dishes. Petri dishes were stored in controlled environment incubator at optimal temperature and humidity for bacteria, 100% humidity and 34°C temperature, until colonies were big enough to be clearly visible by eye. Pictures of each Petri dish were taken using 16 Megapixel Samsung camera over a black background. This pictures were magnified using Microsoft paint software package and number of colonies in each picture was counted. Control sample, bacteria in PBS, was used as a normalization sample and number of colonies for the rest samples were normalized using this number, results are shown on Figure 6.7.

As can be seen from Figure 6.7 pure vancomycin looses part of it's activity towards bacteria during storage, while vancomycin that was encapsulated in PAPN has almost the same activity after 1 month of storage in solution, both samples are not significantly different from control at 18 °C temperature, while both 32 °C temperature samples killed all bacteria, same result as for freshly prepared vancomycin. We suspect that this protection is a result of poloxamer shielding effect. Vancomycin in solution can be oxidized by diluted oxygen or hydroxyl groups present in water. Vancomycin that is encapsulated inside of the poloxamer shell is less accessible for oxygen or hydroxyl groups since it is surrounded by poloxamer

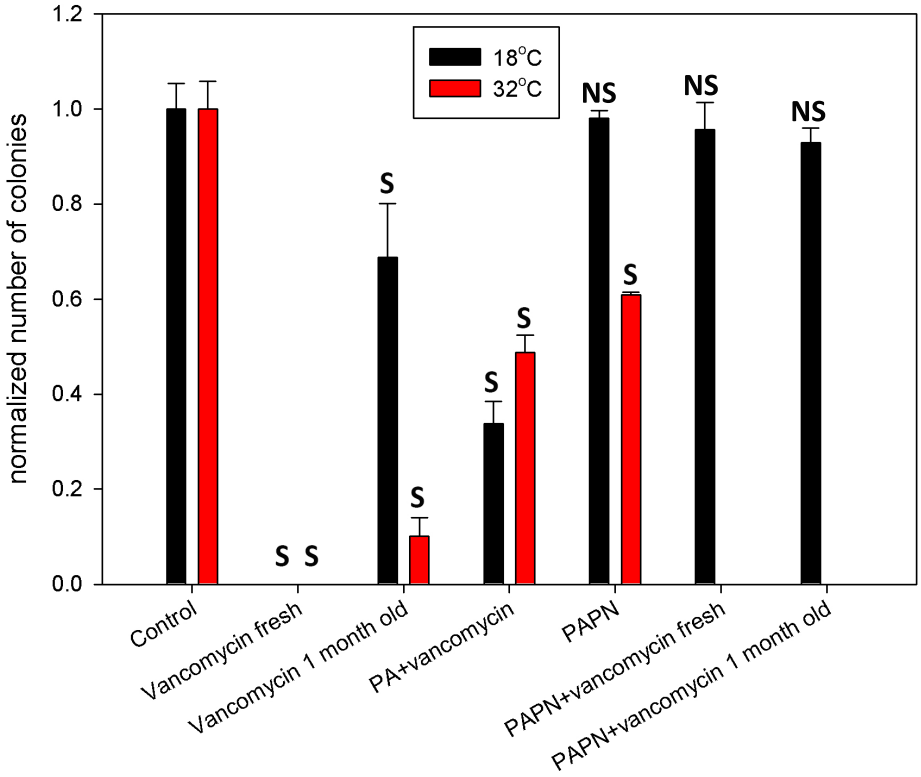

Figure 6.7: Number of the colonies that survived at 36 °Ccompared to 18 °C. Control sample is the *Staphylococcus aureus* bacteria that was not treated with anything and was just diluted with PBS to match bacteria concentration of other samples. ”S” indicates statistically significant difference from the control sample, ”NS” indicates no statistically significant difference from control according to ANOVA calculator.

chains rather than water molecules. Poloxamer vancomycin interaction is thermodynamically preferred thus other molecules has to compete with poloxamer chains to get close enough to vancomycin to cause damage, thus decreasing the probability of unwanted reactions that lead to destruction of vancomycin.

For *Staphylococcus aureus* similar to *Escherichia coli* patterns of bacteria growth were observed. As can be seen from the Figure 6.7 unmodified nanoparticles loaded with vancomycin showed some activity towards bacteria cells, but there is not enough temperature dependence for this device to make it a valuable candidate for controlled drug delivery application. More importantly vancomycin is active at

both temperatures proving that there is no control over the drug release for this simplest case, supporting the need to decorate nanoparticle surface with the poloxamer copolymer.

PAPN without vancomycin showed almost no influence on the bacteria survivability at low temperatures, not significantly different results from the control, but there was some statistical decrease in the number of cells that survived at temperature above LCST. We do not have an exact reason why this is happening, and as some of the possible reasons for this toxicity we propose effect of the loading amount of nanoparticles: at 0.233 mg/ml particle density is relatively high and can be above the toxic threshold; additionally these nanoparticles were purified 5 times in centrifuge with 1 EDTA run followed with 2 ligand exchange repetitions (ca. Chapter 4) leaving a possibility that some copper ions orother toxins were still absorbed on the PAPN. Upon statistical analysis of PAPN and PAPN with vancomycin results it was found that observed results are statistically significant and observed efficiency of PAPN with vancomycin is significantly more effective and indicates that the vancomycin was in fact released from the PAPN shell and bacteria was effected by this released vancomycin rather than PAPN itself.

Statistical significance calculations were performed using online One-Way analysis of variance using ANOVA Calculator (http://www.socscistatistics.com/tests/anova/default2.aspx). Sample variance was compered to a control sample for each group of sample at two temperatures. For the 18 °C set of samples the following parameters were calculated: the f-ratio value for fresh vancomycin is 1036.84, the p-value is < 0.00001 (significant at $p < .01$); the f-ratio value for 1 month old vancomycin is 18.93, the p-value is 0.0121 (significant at $p < .01$); the f-ratio value for PA particles with vancomycin is 259.02, the p-value is 0.000087 (significant at $p < .01$); the f-ratio value for PAPN is 0.358, the p-value is 0.58 (insignificant at $p <$

.01); the f-ratio value for fresh PAPN+vancomycin is 13.49, the p-value is 0.0349 (insignificant at $p < .01$); the f-ratio value for old PAPN+vancomycin is 11.58, the p-value is 0.0424 (insignificant at $p < .01$). For the 36 °C set of samples the following parameters were calculated: the f-ratio value for fresh vancomycin is 1036.84, the p-value is < 0.00001 (significant at $p < .01$); the f-ratio value for old vancomycin is 575.24, the p-value is 0.000018 (significant at $p < .01$); the f-ratio value for PA particles with vancomycin is 206.87, the p-value is 0.000136 (significant at $p < .01$); the f-ratio value for PAPN is 179.34, the p-value is 0.00018 (significant at $p < .01$); the f-ratio value for fresh PAPN+vancomycin is 1036.84, the p-value is < 0.00001 (significant at $p < .01$); the f-ratio value for old PAPN+vancomycin is 1036.84, the p-value is < 0.00001 (significant at $p < .01$).

6.3 Conclusion

The bio-availability of the vancomycin was improved through the use of the propargyl-acrylate poloxamer nanocomposite. Vancomycin was encapsulated in to the PAPN and remained inactive at room temperature, allowing the bacteria to grow. Poloxamer ability to change the size and shape of its coils was used to achieve a controlled release of the vancomycin at the temperature above LCST of the copolymer used. Besides being able to encapsulate and release the vancomycin upon heating, PAPN proved to be effective in protecting it's cargo from the environment deactivating the drug until the system is triggered with the temperature. PAPN offers a distinct advantage over the direct injection of the vancomycin since it allows to control the moment when the drug is activated.

6.4 Materials and Methods

6.4.1 Materials and Reagents

All reagents were purchased from Sigma-Aldrich with at least 97% purity level, solvents were purified using standard procedures.

6.4.2 Characterization

^{1}H spectra were recorded on JEOL ECX-300 spectrometers (300MHz for proton). Chemical shifts for protons are reported in parts per million downfield from tetramethylsilane and are referenced to the carbon resonances of the solvent ($CDCl_3$: δ 7.26 or DMSO-d_6: δ 2.50). Nanoparticle size was checked using Coulter N4Plus DLS using 10 mm plastic cuvette. UV/vis spectra was obtained using Perkin Elmer Lambda 850 spectrometer. Scanning electron microscopy was performed on a Hitachi S4800 FESEM at maximum accelerating voltage of 20.0 kV, images were analyzed using Quartz PCI v.8.5 software package. FTIR was done on a Nickolet Magna IR 6700 spectrometer equiped with diamond attenuated total reflectance accessory.

6.4.3 Nanoparticles preparation

Emulsion polymerization was performed in a single necked round bottom flask (250 mL equipped with the magnetic stirrer. Potassium persulfate (110 mg) was dissolved in water (80 mL) and nitrogen was purged through the solution for 15 minutes. Sodium dodecyl sulfate (90 mg) was added to the flask under nitrogen purge. Obtained solution was stirred and placed in the preheated bath at 75 °C for 3 minutes, then degassed solution of propargyl acrylate (4 mL) and divinylbenzene

(0.65 mL) were added to the main reaction flask. The mixture was stirred at 75 °C under nitrogen purge for 90 minutes. The emulsion was allowed to cool on air. Then mixture was filtered through paper filter. After filtering samples were purified by dialysis using Spectra/Por Dialysis membrane with MWCO 50000. Dialysis was performed for 3 days at 40 °C in 18.2 Megaohms water with regular water changes, typically every 8 hours. Nanoparticles were characterized using DLS analysis to determine average size. Average size of the nanoparticles was found to be 28 nm. Obtained emulsion contained 45 mg/mL of nanoparticles.

6.4.4 Poloxamer modification

$MeSO_2$-pluronic-L62: Pluronic-L62 (3.14 g, 1.086 mmol) was dissolved in dry dichloromethane (DCM) (10 mL), triethylamine (0.132 g, 1.3 mmol) was added to the solution. Obtained solution was stirred at room temperature and methanesulfonyl chloride (48 mg, 0.42 mmol) was added drop-wise. The mixture was stirred for 6 hours at room temperature, then was washed with water.The organic layer was separated, dried with Na_2SO_4, filtered and evaporated under reduced pressure. Yield 3.1 g (95%), clear oil. This product was used in the next step without further purification. ^{1}H NMR ($CDCl_3$) δ 1.11 (m, 87H), 3.06 (s, 3H), 3.38 (m, 29H), 3.52 (m, 28H), 3.63 (m, 72H).

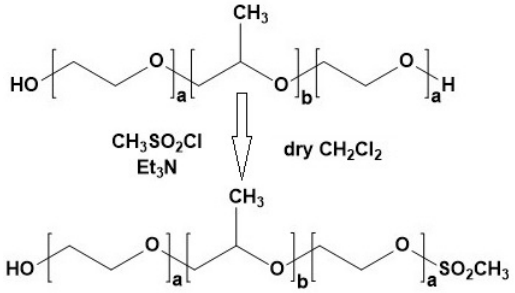

Pluronic-L62-N3. Sodium azide (195 mg, 3 mmol) was added into solution of $MeSO_2$-pluronic-L62 (3.1 g, 1.03 mmol) in dimethylformamide (DMF) (10 mL). Mixture was stirred and heated to 80 °C for 3 hours. After cooling the mixture was extracted with DCM and washed with water 2 times. The organic layer was separated, dried with Na_2SO_4, filtered and evaporated under reduced pressure. Yield 2.27 g (75%), clear oil. Pluronic-L64-N3 was used in the next step without further purification. ^{1}H NMR ($CDCl_3$) δ 1.07 (m, 87H), 3.34 (m, 29H), 3.48 (m, 59H), 3.59 (m, 72H).

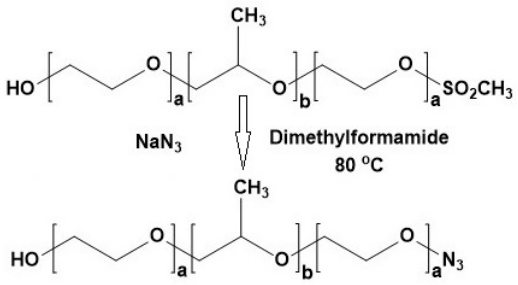

6.4.5 Nanoparticles modification

Nanoparticle modification was performed using the azide alkyne Huisgen cycloaddition reaction also known as Click chemistry. Typical procedure was used as described elsewhere [41]. Copper(II) sulfate ($CuSO_4$) (2 mg, 8 μmol) was added to the propargyl acrylate nanoparticles suspension in water (2 mL) and stirred until completely dissolved. Then solution of pluronic-L62-N3 (6) (40 mg, 16 μmol) in water (2 mL) was added. Next the solution of $CuSO_4$ (2 mg, 8 μmol) in water (2 mL) was added. The reaction was stirred and purged with nitrogen for 5 minutes, then sodium ascorbate (10 mg, 50.5 μmol) was added. The reaction continued at 28°C for 24 hours under nitrogen purge. Reaction mixture was centrifuged at

10000G for 10 minutes. Separated nanoparticles were washed with the mixture of water:Methanol 1:1 (20 mL). Then 1 mL of 0.1 M ethylenediaminetetraacetic acid (EDTA) solution was added to remove copper catalyst. Nanoparticles were re-dispersed in 40 mL of 18.2 Megaohms water and sonicated for 3 minutes. After sonication suspension was centrifuged at 10000G for 10 minutes. Next 0.1 mL of 20% sodium dodecyl sulfate (SDS) solution was added to remove any unreacted poloxamer. Nanoparticles were re-dispersed in 40 mL of 18.2 Megaohms water and sonicated for 3 minutes. After sonication suspension was centrifuged at 10000G for 10 minutes. This step was repeated one more time. Lastly nanoparticles were re-dispersed in 40 mL of 18.2 Megaohms water and sonicated for 3 minutes. After sonication suspension was centrifuged at 10000G for 10 minutes. This step was repeated 3 times to ensure that all impurities were removed. After last centrifugation nanoparticles were redispersed in 10 mL of 18.2 Megaohms water and stored in the refrigerator.

6.4.6 Molar extinction coefficient of vancomycin

Molar extinction of vancomycin was calculated in DI-H_2O to be 6.53 $M^{-1}cm^{-1}$ at 280 nm using multiple solutions of concentrations 0.5 mg/mL, 0.25 mg/mL, 0.125 mg/mL and 0.0625 mg/mL. Procedure was the similar to the Rhodamine B procedure described in Chapter 5. For each concentration UV/Vis spectra was recoded and graph of absorbance maximum versus concentration was created. Molar extinction coefficient was assumed to be equal to the slope of the line of this graph.

6.4.7 Bacteria stock preparation and mixing

Bacteria was grown in the LB Broth for 24 hours at 37 °C *Escherichia coli*, and 17 hours at 34 °C for *Staphylococcus aureus*. After initial incubation period bacteria was diluted in phosphate-buffered saline (PBS) solution to 1.5E-5 for *Staphylococcus aureus* and 5E-6 for *Escherichia coli* of the original concentration. 0.1 mL of the obtained solution was added to 5 mL of PBS in 15 mL centrifuge vial. Then nanoparticle samples were added to this vial, amount of the solution of the nanoparticles added was measured to contain 1.4 mg of dry cores equivalent, in case of free vancomycin equivalent of 0.25 mg of dry drug was added. Next volume of each sample was brought to a total of 6 mL using PBS. After this samples were left at 18 °C or 36 °C for 24 hours for *Escherichia coli*, or 6 hours for *Staphylococcus aureus* to allow ample time for the drug to kill bacteria. After 24 hours 0.1 mL of each sample was seeded on the Petri dish with LB agar. Bacteria was allowed to grow at optimal conditions (36 °C and 100 % humidity) until colonies were easy to detect by the naked eyes. Pictures of each Petri dish were taken and number of colonies per Petri dish was recorded.

Chapter 7

Concluding remarks

7.1 Summary

The objective of the presented work was to explore the possibility to use propargyl acrylate poloxamer nanocomposite (PAPN) as a temperature responsive device capable to encapsulate active molecules and perform various tasks ranging from the enhanced medical imaging to the drug delivery.

Through the combination of the propargyl acrylate core with a defined amount of the poloxamer nanocomposite of a well defined structure was synthesized. Easy and quick methods to characterize the final assembly were developed. The required tools along with the equations needed to determine the final composition of the PAPN were designed and derived.

Through the inclusion of the two dyes that form a FRET pair into the nanocomposite structure a possible mechanism of the encapsulation and the release was proposed. Poloxamer middle, PPO block, forms a favorable environment for the small molecules that have aromatic rings in their structure and helps to stabilize these molecules in the water based systems, human body being one of such sys-

tems. Changes in the poloxamer coil packing with the temperature were proposed as the main mechanism of PAPN response.

Control over the poloxamer grafting density(GD) allowed to manipulate the encapsulation efficiency and the release rate of the active molecules. The importance of the precise control over the GD was demonstrated on the example of the Rhodamine B dye.

The ability of the PAPN to encapsulate and release vancomycin was demonstrated on the example of Escherichia coli and *Staphylococcus aureus* bacteria. PAPN filled with vancomycin was successfully used to control the growth of the bacteria with the temperature. The ability of PAPN to preserve bio-activity of the vancomycin was discovered.

7.2 Recommendation for future research

Current work investigated only two of the multitude of the copolymers in the poloxamer copolymer family. Selecting a different version of the poloxamer should in theory yield a different range of the temperature response allowing researcher to fine tune the system to a desired applications. Two poloxamers used in this work had an LCST of 24 °C and 58 °C which is below and above the normal human body temperature range. The most value for the medical application would have a system with the poloxamer that has LCST of 37.5 °C, unfortunately there is no commercially available version of the poloxamer currently available on the market with 37.5 °C temperature of response. Poloxamer family of copolymers was extensively studied over the past few decades and current synthetic techniques allow the researcher to synthesize any copolymer composition. Available knowledge about the dependence of the LCST temperature on the block length and ratio makes it

possible to predict the correct structure of the poloxamer that is needed to achieve LCST of 37.5 °C, though additional research is required in this direction.

Next phase for the project would involve testing of the PAPN on a cancer cells eventually moving all the way to the human trials. Substitution of vancomycin with doxorubicin or other anticancer drug would be required in order to test the system for the anticancer activity.

Another area of possible application for the PAPN is in the waste water treatment plants. PAPN's ability to trap organic molecules and then release them upon heating can be used to remove toxic waste from the water supply system and to concentrate this waste for further processing. Since the poloxamer temperature induced changes are reversible it is expected that system based on the PAPN can be reused multiple times making it cost effective alternative to the currently available filtration systems.

Bibliography

[1] O. Veiseh, J. W. Gunn, and M. Q. Zhang. Design and fabrication of magnetic nanoparticles for targeted drug delivery and imaging. *Advanced Drug Delivery Reviews*, 62(3):284–304, 2010.

[2] S. M. Moghimi, A. C. Hunter, and J. C. Murray. Long-circulating and target-specific nanoparticles: Theory to practice. *Pharmacological Reviews*, 53(2):283–318, 2001.

[3] A. Kumari, S. K. Yadav, and S. C. Yadav. Biodegradable polymeric nanoparticles based drug delivery systems. *Colloids and Surfaces B-Biointerfaces*, 75(1):1–18, 2010.

[4] M. E. Davis, Z. Chen, and D. M. Shin. Nanoparticle therapeutics: an emerging treatment modality for cancer. *Nature Reviews Drug Discovery*, 7(9):771–782, 2008.

[5] K. S. Soppimath, T. M. Aminabhavi, A. R. Kulkarni, and W. E. Rudzinski. Biodegradable polymeric nanoparticles as drug delivery devices. *Journal of Controlled Release*, 70(1-2):1–20, 2001.

[6] D. E. Owens and N. A. Peppas. Opsonization, biodistribution, and pharmacokinetics of polymeric nanoparticles. *International Journal of Pharmaceutics*, 307(1):93–102, 2006.

[7] K. Kataoka, A. Harada, and Y. Nagasaki. Block copolymer micelles for drug delivery: design, characterization and biological significance. *Advanced Drug Delivery Reviews*, 47(1):113–131, 2001.

[8] E. S. Gil and S. M. Hudson. Stimuli-reponsive polymers and their bioconjugates. *Progress in Polymer Science*, 29(12):1173–1222, 2004.

[9] R. A. Petros and J. M. DeSimone. Strategies in the design of nanoparticles for therapeutic applications. *Nature Reviews Drug Discovery*, 9(8):615–627, 2010.

[10] X. H. Gao, Y. Y. Cui, R. M. Levenson, L. W. K. Chung, and S. M. Nie. In vivo cancer targeting and imaging with semiconductor quantum dots. *Nature Biotechnology*, 22(8):969–976, 2004.

[11] A. C. Balazs, T. Emrick, and T. P. Russell. Nanoparticle polymer composites: Where two small worlds meet. *Science*, 314(5802):1107–1110, 2006.

[12] M. Liong, J. Lu, M. Kovochich, T. Xia, S. G. Ruehm, A. E. Nel, F. Tamanoi, and J. I. Zink. Multifunctional inorganic nanoparticles for imaging, targeting, and drug delivery. *Acs Nano*, 2(5):889–896, 2008.

[13] B. Sahoo, K. S. P. Devi, R. Banerjee, T. K. Maiti, P. Pramanik, and D. Dhara. Thermal and ph responsive polymer-tethered multifunctional magnetic nanoparticles for targeted delivery of anticancer drug. *Acs Applied Materials and Interfaces*, 5:3884–3893, 2013.

[14] A. Popat, J. Liu, G. Q. Lu, and S. Z. Qiao. A ph-responsive drug delivery system based on chitosan coated mesoporous silica nanoparticles. *Journal of Materials Chemistry*, 22(22):11173–11178, 2012.

[15] S. Trabulo, A. M. Cardoso, T. Santos-Ferreira, A. L. Cardoso, S. Simoes, and M. C. P. de Lima. Survivin silencing as a promising strategy to enhance the sensitivity of cancer cells to chemotherapeutic agents. *Molecular Pharmaceutics*, 8(4):1120–1131, 2011.

[16] A. M. Malekzadeh, A. Ramazani, S. J. T. Rezaei, and H. Niknejad. Design and construction of multifunctional hyperbranched polymers coated magnetite nanoparticles for both targeting magnetic resonance imaging and cancer therapy. *Journal of Colloid and Interface Science*, 490:64–73, 2017.

[17] Y. Hu, R. Z. Wang, J. C. Li, L. Ding, X. L. Wang, X. Y. Shi, and M. W. Shen. Facile synthesis of lactobionic acid-targeted iron oxide nanoparticles with ultrahigh relaxivity for targeted mr imaging of an orthotopic model of human hepatocellular carcinoma. *Particle and Particle Systems Characterization*, 34(1), 2017.

[18] G. D. Nandagopal, P. Periyathambi, and T. P. Sastry. Fabrication of a multifunctional nanocomposite containing inp coated with chitosan coupled with folic acid and loaded with quercetin in diagnosis and its possible treatment of cancer. *Rsc Advances*, 6(101):99514–99523, 2016.

[19] Z. H. Zhai, X. H. Yu, B. Yang, Y. J. Zhang, L. Zhang, X. L. Li, and H. Z. Sun. Colorectal cancer heterogeneity and targeted therapy: Clinical implications, challenges and solutions for treatment resistance. *Seminars in Cell and Developmental Biology*, 64:107–115, 2017.

[20] D. E. Discher and A. Eisenberg. Polymer vesicles. *Science*, 297(5583):967–973, 2002.

[21] S. Ganta, H. Devalapally, A. Shahiwala, and M. Amiji. A review of stimuli-responsive nanocarriers for drug and gene delivery. *Journal of Controlled Release*, 126(3):187–204, 2008.

[22] Y. Maeda, T. Higuchi, and I. Ikeda. Change in hydration state during the coil-globule transition of aqueous solutions of poly(n-isopropylacrylamide) as evidenced by ftir spectroscopy. *Langmuir*, 16(19):7503–7509, 2000.

[23] Y. Xia, N. A. D. Burke, and H. D. H. Stover. End group effect on the thermal response of narrow-disperse poly(n-isopropylacrylamide) prepared by atom transfer radical polymerization. *Macromolecules*, 39(6):2275–2283, 2006.

[24] O. J. Cayre, N. Chagneux, and S. Biggs. Stimulus responsive core-shell nanoparticles: synthesis and applications of polymer based aqueous systems. *Soft Matter*, 7(6):2211–2234, 2011.

[25] Kewal K. Jain. Drug delivery system. *Humana Press, New York, NY*, 1141:280, 2014.

[26] T. Maeda, T. Kanda, Y. Yonekura, K. Yamamoto, and T. Aoyagi. Hydroxylated poly(n-isopropylacrylamide) as functional thermoresponsive materials. *Biomacromolecules*, 7(2):545–549, 2006.

[27] Y. Chen and W. J. Xu. The evolution of structure and properties of pnipa/clay nanocomposite hydrogels with the freezing time in polymerization. *Journal of Materials Research*, 29(6):820–832, 2014.

[28] B. C. Choi, S. Choi, and D. E. Leckband. Poly(n-isopropyl acrylamide) brush topography: Dependence on grafting conditions and temperature. *Langmuir*, 29(19):5841–5850, 2013.

[29] J. F. Lutz, O. Akdemir, and A. Hoth. Point by point comparison of two thermosensitive polymers exhibiting a similar lcst: Is the age of poly(nipam) over? *Journal of the American Chemical Society*, 128(40):13046–13047, 2006.

[30] P. Alexandridis and T. A. Hatton. Poly(ethylene oxide)-poly(propylene oxide)-poly(ethylene oxide) block-copolymer surfactants in aqueous-solutions and at interfaces - thermodynamics, structure, dynamics, and modeling. *Colloids and Surfaces a-Physicochemical and Engineering Aspects*, 96:1–46, 1995.

[31] P. Alexandridis, J. F. Holzwarth, and T. A. Hatton. Micellization of poly(ethylene oxide)-poly(propylene oxide)-poly(ethylene oxide) triblock copolymers in aqueous-solutions - thermodynamics of copolymer association. *Macromolecules*, 27:2414–2425, 1994.

[32] T. Niidome, M. Yamagata, Y. Okamoto, Y. Akiyama, H. Takahashi, T. Kawano, Y. Katayama, and Y. Niidome. Peg-modified gold nanorods with a stealth character for in vivo applications. *Journal of Controlled Release*, 114(3):343–347, 2006.

[33] S. Stolnik, L. Illum, and S. S. Davis. Long circulating microparticulate drug carriers. *Advanced Drug Delivery Reviews*, 16(2-3):195–214, 1995.

[34] E. V. Batrakova and A. V. Kabanov. Pluronic block copolymers: Evolution of drug delivery concept from inert nanocarriers to biological response modifiers. *Journal of Controlled Release*, 130(2):98–106, 2008.

[35] H. C. Kolb, M. G. Finn, and K. B. Sharpless. Click chemistry: Diverse chemical function from a few good reactions. *Angewandte Chemie-International Edition*, 40(11):2004–+, 2001.

[36] R. D. Roeder, P. Rungta, V. Tsyalkovskyy, Y. Bandera, and S. H. Foulger. Colloidal templating: seeded emulsion polymerization of a soluble shell with a controlled alkyne surface density. *Soft Matter*, 8(20):5493–5500, 2012.

[37] R. K. Jain. Transport of molecules, particles, and cells in solid tumors. *Annual Review of Biomedical Engineering*, 1:241–263, 1999.

[38] L. W. Seymour. Passive tumor targeting of soluble macromolecules adn drug conjugates. *Critical Reviews in Therapeutic Drug Carrier Systems*, 9(2):135–187, 1992.

[39] D. V. McAllister, M. G. Allen, and M. R. Prausnitz. Microfabricated microneedles for gene and drug delivery. *Annual Review of Biomedical Engineering*, 2:289–313, 2000.

[40] R. Jenkins, Y. P. Bandera, M. A. Daniele, L. L. Ledford, A. Tietje, A. A. Kelso, M. G. Sehorn, Y. Z. Wei, M. Chakrabarti, S. K. Ray, and S. H. Foulger. Sequestering survivin to functionalized nanoparticles: a strategy to enhance apoptosis in cancer cells. *Biomaterials Science*, 4(4):614–626, 2016.

[41] Parul Rungta, Yuriy P. Bandera, Volodymyr Tsyalkovsky, and Stephen H. Foulger. Designing fluoroprobes through forster resonance energy transfer: surface modification of nanoparticles through ”click” chemistry. *Soft Matter*, 6:6083–6095, 2010.

[42] D. D. Evanoff, S. E. Hayes, Y. Ying, G. H. Shim, J. R. Lawrence, J. B. Carroll, R. D. Roeder, J. M. Houchins, C. E. Huebner, and S. H. Foulger. Functionalization of crystalline colloidal arrays through click chemistry. *Advanced Materials*, 19(21):3507–+, 2007.

[43] J. G. Paez, P. A. Janne, J. C. Lee, S. Tracy, H. Greulich, S. Gabriel, P. Herman, F. J. Kaye, N. Lindeman, T. J. Boggon, K. Naoki, H. Sasaki, Y. Fujii, M. J. Eck, W. R. Sellers, B. E. Johnson, and M. Meyerson. Egfr mutations in lung cancer: Correlation with clinical response to gefitinib therapy. *Science*, 304(5676):1497–1500, 2004.

[44] M. Maemondo, A. Inoue, K. Kobayashi, S. Sugawara, S. Oizumi, H. Isobe, A. Gemma, M. Harada, H. Yoshizawa, I. Kinoshita, Y. Fujita, S. Okinaga, H. Hirano, K. Yoshimori, T. Harada, T. Ogura, M. Ando, H. Miyazawa, T. Tanaka, Y. Saijo, K. Hagiwara, S. Morita, T. Nukiwa, and N. E. Japan Study Grp. Gefitinib or chemotherapy for non-small-cell lung cancer with mutated egfr. *New England Journal of Medicine*, 362(25):2380–2388, 2010.

[45] J. C. Riboh, A. J. Haes, A. D. McFarland, C. R. Yonzon, and R. P. Van Duyne. A nanoscale optical biosensor: Real-time immunoassay in physiological buffer enabled by improved nanoparticle adhesion. *Journal of Physical Chemistry B*, 107(8):1772–1780, 2003.

[46] C. R. Yonzon, D. A. Stuart, X. Y. Zhang, A. D. McFarland, C. L. Haynes, and R. P. Van Duyne. Towards advanced chemical and biological nanosensors - an overview. *Talanta*, 67(3):438–448, 2005.

[47] C. C. Huang and H. T. Chang. Selective gold-nanoparticle-based "turn-on" fluorescent sensors for detection of mercury(ii) in aqueous solution. *Analytical Chemistry*, 78(24):8332–8338, 2006.

[48] X. Peng, Q. Long, H. T. Li, Y. Y. Zhang, and S. Z. Yao. "turn on-off" fluorescent sensor for protamine and heparin based on label-free silicon quantum dots coupled with gold nanoparticles. *Sensors and Actuators B-Chemical*, 213:131–138, 2015.

[49] I. L. Medintz, A. R. Clapp, H. Mattoussi, E. R. Goldman, B. Fisher, and J. M. Mauro. Self-assembled nanoscale biosensors based on quantum dot fret donors. *Nature Materials*, 2:630–638, 2003.

[50] K. E. Sapsford, L. Berti, and I. L. Medintz. Materials for fluorescence resonance energy transfer analysis: Beyond traditional donor-acceptor combinations. *Angewandte Chemie-International Edition*, 45:4562–4588, 2006.

[51] M. P. Robin and R. K. O'Reilly. Strategies for preparing fluorescently labelled polymer nanoparticles. *Polymer International*, 64(2):174–182, 2015.

[52] M. Pastore and F. De Angelis. First-principles computational modeling of fluorescence resonance energy transfer in co-sensitized dye solar cells. *Journal of Physical Chemistry Letters*, 3(16):2146–2153, 2012.

[53] S. Laurent, D. Forge, M. Port, A. Roch, C. Robic, L. V. Elst, and R. N. Muller. Magnetic iron oxide nanoparticles: Synthesis, stabilization, vectorization, physicochemical characterizations, and biological applications. *Chemical Reviews*, 108(6):2064–2110, 2008.

[54] N. Dejaeger, H. Demeyere, R. Finsy, R. Sneyers, J. Vanderdeelen, P. Vandermeeren, and M. Vanlaethem. Particle sizing by photon-correlation spectroscopy .1. monodisperse lattices - influence of scattering angle and concentration of dispersed material. *Particle and Particle Systems Characterization*, 8(3):179–186, 1991.

[55] H. J. Dai, J. H. Hafner, A. G. Rinzler, D. T. Colbert, and R. E. Smalley. Nanotubes as nanoprobes in scanning probe microscopy. *Nature*, 384(6605):147–150, 1996.

[56] H. J. Dai and C. M. Lieber. Scanning-tunneling-microscopy studies of low-dimensional materials - charge-density-wave pinning and melting in 2 dimensions. *Annual Review of Physical Chemistry*, 44:237–263, 1993.

[57] Ford NC Asch R. Design of an ideal digital correlation computer. *Rev Sci Inst*, 44:506–508, 1973.

[58] Evans K Bott S. Measurement and methods for measuring alpha and beta using a coulter n4 submicron particle sizer. *Langley Ford Instruments*, N4(Reprint T105), 1984.

[59] B. Schuler, E. A. Lipman, and W. A. Eaton. Probing the free-energy surface for protein folding with single-molecule fluorescence spectroscopy. *Nature*, 419:743–747, 2002.

[60] P. Carriba, G. Navarro, F. Ciruela, S. Ferre, V. Casado, L. Agnati, A. Cortes, J. Mallol, K. Fuxe, E. I. Canela, C. Lluis, and R. Franco. Detection of heteromerization of more than two proteins by sequential bret-fret. *Nature Methods*, 5:727–733, 2008.

[61] L. Stryer. Fluorescence energy-transfer as a spectroscopic ruler. *Annual Review of Biochemistry*, 47:819–846, 1978.

[62] S. Buhbut, S. Itzhakov, E. Tauber, M. Shalom, I. Hod, T. Geiger, Y. Garini, D. Oron, and A. Zaban. Built-in quantum dot antennas in dye-sensitized solar cells. *Acs Nano*, 4:1293–1298, 2010.

[63] V. Vohra, G. Calzaferri, S. Destri, M. Pasini, W. Porzio, and C. Botta. Toward white light emission through efficient two-step energy transfer in hybrid nanofibers. *Acs Nano*, 4:1409–1416, 2010.

[64] H. Langhals, A. J. Esterbauer, A. Walter, E. Riedle, and I. Pugliesi. Forster resonant energy transfer in orthogonally arranged chromophores. *Journal of the American Chemical Society*, 132:16777–16782, 2010.

[65] K. Ray and T. N. Mishra. Energy transfer between carbazole and anthracene moieties organised in langmuir-blodgett films. *Journal of Physics and Chemistry of Solids*, 60:401–405, 1999.

[66] F. Pinaud, R. Millereux, P. Vialar-Trarieux, B. Catargi, S. Pinet, I. Gosse, N. Sojic, and V. Ravaine. Differential photo luminescent and electrochemiluminescent behavior for resonance energy transfer processes in thermoresponsive microgels. *Journal of Physical Chemistry B*, 119:12954–12961, 2015.

[67] T. Desmettre, J. M. Devoisselle, and S. Mordon. Fluorescence properties and metabolic features of indocyanine green (icg) as related to angiography. *Survey of Ophthalmology*, 45:15–27, 2000.

[68] R. Philip, A. Penzkofer, W. Baumler, R. M. Szeimies, and C. Abels. Absorption and fluorescence spectroscopic investigation of indocyanine green. *Journal of Photochemistry and Photobiology A-Chemistry*, 96:137–148, 1996.

[69] S. A. Soper and Q. L. Mattingly. Steady-state and picosecond laser fluorescence studies of nonradiative pathways in tricarbocyanine dyes - implications to the design of near-ir fluorochromes with high fluorescence efficiencies. *Journal of the American Chemical Society*, 116:3744–3752, 1994.

[70] T. J. Muckle. Plasma-proteins binding of indocyanine green. *Biochemical Medicine*, 15:17–21, 1976.

[71] M. Chalfie, Y. Tu, G. Euskirchen, W. W. Ward, and D. C. Prasher. Green fluorescent protein as a marker for gene-expression. *Science*, 263:802–805, 1994.

[72] R. Y. Tsien. The green fluorescent protein. *Annual Review of Biochemistry*, 67:509–544, 1998.

[73] N. C. Shaner, P. A. Steinbach, and R. Y. Tsien. A guide to choosing fluorescent proteins. *Nature Methods*, 2:905–909, 2005.

[74] P. Sharma, S. Brown, G. Walter, S. Santra, and B. Moudgil. Nanoparticles for bioimaging. *Advances in Colloid and Interface Science*, 123:471–485, 2006.

[75] S. Jin and K. M. Ye. Nanoparticle-mediated drug delivery and gene therapy. *Biotechnology Progress*, 23:32–41, 2007.

[76] J. Yu, M. A. Yaseen, B. Anvari, and M. S. Wong. Synthesis of near-infrared-absorbing nanoparticle-assembled capsules. *Chemistry of Materials*, 19:1277–1284, 2007.

[77] A. C. Bhasikuttan, J. Mohanty, W. M. Nau, and H. Pal. Efficient fluorescence enhancement and cooperative binding of an organic dye in a supramolecular host-protein assembly. *Angewandte Chemie-International Edition*, 46:4120–4122, 2007.

[78] R. Zadmard and T. Schrader. Nanomolar protein sensing with embedded receptor molecules. *Journal of the American Chemical Society*, 127:904–915, 2005.

[79] R. Jenkins, M. K. Burdette, and S. H. Foulger. Mini-review: fluorescence imaging in cancer cells using dye-doped nanoparticles. *Rsc Advances*, 6:65459–65474, 2016.

[80] J. R. Babendure, S. R. Adams, and R. Y. Tsien. Aptamers switch on fluorescence of triphenylmethane dyes. *Journal of the American Chemical Society*, 125:14716–14717, 2003.

[81] V. S. Jisha, K. T. Arun, M. Hariharan, and D. Ramaiah. Site-selective interactions: Squaraine dye-serum albumin complexes with enhanced fluorescence and triplet yields. *Journal of Physical Chemistry B*, 114:5912–5919, 2010.

[82] V. S. Jisha, K. T. Arun, M. Hariharan, and D. Ramaiah. Site-selective binding and dual mode recognition of serum albumin by a squaraine dye. *Journal of the American Chemical Society*, 128:6024–6025, 2006.

[83] A. P. Alivisatos, W. W. Gu, and C. Larabell. *Quantum dots as cellular probes*, volume 7 of *Annual Review of Biomedical Engineering*, pages 55–76. Annual Reviews, Palo Alto, 2005.

[84] S. N. Baker and G. A. Baker. Luminescent carbon nanodots: Emergent nanolights. *Angewandte Chemie-International Edition*, 49:6726–6744, 2010.

[85] K. P. Loh, Q. L. Bao, G. Eda, and M. Chhowalla. Graphene oxide as a chemically tunable platform for optical applications. *Nature Chemistry*, 2:1015–1024, 2010.

[86] X. Q. Ge, L. N. Sun, L. Y. Shi, and R. Y. Wei. The modified upconversion nanomaterials (ucnms) for multimodal imaging and therapies. *Biomedical Spectroscopy and Imaging*, 4:391–412, 2015.

[87] V. Muhr, S. Wilhelm, T. Hirsch, and O. S. Wolfbeis. Upconversion nanoparticles: From hydrophobic to hydrophilic surfaces. *Accounts of Chemical Research*, 47:3481–3493, 2014.

[88] D. A. Chiappetta and A. Sosnik. Poly(ethylene oxide)-poly(propylene oxide) block copolymer micelles as drug delivery agents: Improved hydrosolubility, stability and bioavailability of drugs. *European Journal of Pharmaceutics and Biopharmaceutics*, 66:303–317, 2007.

[89] G. Bonacucina, M. Cespi, G. Mencarelli, G. Giorgioni, and G. F. Palmieri. Thermosensitive self-assembling block copolymers as drug delivery systems. *Polymers*, 3:779–811, 2011.

[90] A. V. Kabanov, E. V. Batrakova, and V. Y. Alakhov. Pluronic (r) block copolymers as novel polymer therapeutics for drug and gene delivery. *Journal of Controlled Release*, 82:189–212, 2002.

[91] B. Foster, T. Cosgrove, and B. Hammouda. Pluronic triblock copolymer systems and their interactions with ibuprofen. *Langmuir*, 25:6760–6766, 2009.

[92] X. M. Li, L. Y. Ding, Y. L. Xu, Y. L. Wang, and Q. N. Ping. Targeted delivery of doxorubicin using stealth liposomes modified with transferrin. *International Journal of Pharmaceutics*, 373:116–123, 2009.

[93] R. Basak and R. Bandyopadhyay. Encapsulation of hydrophobic drugs in pluronic f127 micelles: Effects of drug hydrophobicity, solution temperature, and ph. *Langmuir*, 29:4350–4356, 2013.

[94] Dennis E. Discher, Vanessa Ortiz, Goundla Srinivas, Michael L. Klein, Younghoon Kim, David Christian, Shenshen Cai, Peter Photos, and Fariyal Ahmed. Emerging applications of polymersomes in delivery: From molecular dynamics to shrinkage of tumors. *Progress in Polymer Science*, 32:838–857, 2007.

[95] M. Chiper, K. H. Aubert, A. Auge, J. F. Fouquenet, M. Souce, and I. Chourpa. Colloidal stability and thermo-responsive properties of iron oxide nanoparticles coated with polymers: advantages of pluronic (r) f68-peg mixture. *Nanotechnology*, 24:605–616, 2013.

[96] V. Alakhov, E. Klinski, S. M. Li, G. Pietrzynski, A. Venne, E. Batrakova, T. Bronitch, and A. Kabanov. Block copolymer-based formulation of doxorubicin. from cell screen to clinical trials. *Colloids and Surfaces B-Biointerfaces*, 16:113–134, 1999.

[97] V. Y. Erukova, O. O. Krylova, Y. N. Antonenko, and N. S. Melik-Nubarov. Effect of ethylene oxide and propylene oxide block copolymers on the permeability of bilayer lipid membranes to small solutes including doxorubicin. *Biochimica Et Biophysica Acta-Biomembranes*, 1468:73–86, 2000.

[98] A. V. Kabanov, E. V. Batrakova, and V. Y. Alakhov. Pluronic((r)) block copolymers for overcoming drug resistance in cancer. *Advanced Drug Delivery Reviews*, 54:759–779, 2002.

[99] L. Tavano, R. Muzzalupo, L. Mauro, M. Pellegrino, S. Ando, and N. Picci. Transferrin-conjugated pluronic niosomes as a new drug delivery system for anticancer therapy. *Langmuir*, 29:12638–12646, 2013.

[100] P. Rungta, Y. P. Bandera, R. D. Roeder, Y. C. Li, W. S. Baldwin, D. Sharma, M. G. Sehorn, I. Luzinov, and S. H. Foulger. Selective imaging and killing of cancer cells with protein-activated near-infrared fluorescing nanoparticles. *Macromolecular Bioscience*, 11:927–937, 2011.

[101] F. Alexis, E. Pridgen, L. K. Molnar, and O. C. Farokhzad. Factors affecting the clearance and biodistribution of polymeric nanoparticles. *Molecular Pharmaceutics*, 5:505–515, 2008.

[102] F. Alexis, J. W. Rhee, J. P. Richie, A. F. Radovic-Moreno, R. Langer, and O. C. Farokhzad. New frontiers in nanotechnology for cancer treatment. *Urologic Oncology-Seminars and Original Investigations*, 26:74–85, 2008.

[103] W. H. De Jong, W. I. Hagens, P. Krystek, M. C. Burger, Ajam Sips, and R. E. Geertsma. Particle size-dependent organ distribution of gold nanoparticles after intravenous administration. *Biomaterials*, 29(12):1912–1919, 2008.

[104] P. Jani, G. W. Halbert, J. Langridge, and A. T. Florence. Nanoparticle uptake by the rat gastrointestinal mucosa - quantitation and particle-size dependency. *Journal of Pharmacy and Pharmacology*, 42(12):821–826, 1990.

[105] L.H. Sperling. Introduction to physical polymer science 4th edition. *Introduction to Physical Polymer Science*, 4th edition:845, 2006.

[106] J. R. Lakowicz. Principles of fluorescence spectroscopy. *Kluwer Academic/Plenum Press*, 2nd edition:923, 1999.

[107] E. G. Kelley, J. N. L. Albert, M. O. Sullivan, and T. H. Epps. Stimuli-responsive copolymer solution and surface assemblies for biomedical applications. *Chemical Society Reviews*, 42:7057–7071, 2013.

[108] A. G. Denkova, E. Mendes, and M. O. Coppens. Non-equilibrium dynamics of block copolymer micelles in solution: recent insights and open questions. *Soft Matter*, 6:2351–2357, 2010.

[109] G. Fleischer. Micellization in aqueous-solution of a poly(ethylene oxide) poly(propylene oxide) poly(ethylene oxide) triblock copolymer investigated with pulsed field gradient nmr. *Journal of Physical Chemistry*, 97:517–521, 1993.

[110] I. R. Schmolka. *Physical basis for poloxamer interactions*, volume 720 of *Annals of the New York Academy of Sciences*, pages 92–97. New York Acad Sciences, New York, 1994.

[111] R. Muzzalupo, L. Tavano, S. Trombino, R. Cassano, N. Picci, and C. La Mesa. Niosomes from alpha,omega-trioxyethylene-bis(sodium 2-dodecyloxy-propylenesulfonate): Preparation and characterization. *Colloids and Surfaces B-Biointerfaces*, 64:200–207, 2008.

[112] J. Ren, X. L. Zhao, Q. C. Wang, C. F. Ku, D. H. Qu, C. P. Chang, and H. Tian. Synthesis and fluorescence properties of novel co-facial folded naphthalimide dimers. *Dyes and Pigments*, 64:179–186, 2005.

[113] M. Karimi, P. S. Zangabad, A. Ghasemi, M. Amiri, M. Bahrami, H. Malekzad, H. G. Asl, Z. Mandieh, M. Bozorgomid, A. Ghasemi, Mrrt Boyuk, and M. R. Hamblin. Temperature-responsive smart nanocarriers for delivery of therapeutic agents: Applications and recent advances. *Acs Applied Materials and Interfaces*, 8(33):21107–21133, 2016.

[114] C. E. Mora-Huertas, H. Fessi, and A. Elaissari. Polymer-based nanocapsules for drug delivery. *International Journal of Pharmaceutics*, 385(1-2):113–142, 2010.

[115] L. F. Zhang, J. M. Chan, F. X. Gu, J. W. Rhee, A. Z. Wang, A. F. Radovic-Moreno, F. Alexis, R. Langer, and O. C. Farokhzad. Self-assembled lipid-polymer hybrid nanoparticles: A robust drug delivery platform. *Acs Nano*, 2(8):1696–1702, 2008.

[116] M. C. Branco and J. P. Schneider. Self-assembling materials for therapeutic delivery. *Acta Biomaterialia*, 5(3):817–831, 2009.

[117] M. Muratalin, P. F. Luckham, A. Esimova, S. Aidarova, B. Mutaliyeva, G. Madybekova, A. Sharipova, and A. Issayeva. Study of n-isopropylacrylamide-based microgel particles as a potential drug delivery agents. *Colloids and Surfaces a-Physicochemical and Engineering Aspects*, 532:8–17, 2017.

[118] A. Klaikherd, C. Nagamani, and S. Thayumanavan. Multi-stimuli sensitive amphiphilic block copolymer assemblies. *Journal of the American Chemical Society*, 131(13):4830–4838, 2009.

[119] Y. Z. You, K. K. Kalebaila, S. L. Brock, and D. Oupicky. Temperature-controlled uptake and release in pnipam-modified porous silica nanoparticles. *Chemistry of Materials*, 20(10):3354–3359, 2008.

[120] S. T. Sun and P. Y. Wu. A one-step strategy for thermal- and ph-responsive graphene oxide interpenetrating polymer hydrogel networks. *Journal of Materials Chemistry*, 21(12):4095–4097, 2011.

[121] M. Asai, D. Zhao, and S. K. Kumar. Role of grafting mechanism on the polymer coverage and self-assembly of hairy nanoparticles. *Acs Nano*, 11(7):7028–7035, 2017.

[122] T. Soulestin, V. Ladmiral, F. D. Dos Santos, and B. Ameduri. Vinylidene fluoride- and trifluoroethylene-containing fluorinated electroactive copolymers. how does chemistry impact properties? *Progress in Polymer Science*, 72:16–60, 2017.

[123] B. Jeong, Y. H. Bae, D. S. Lee, and S. W. Kim. Biodegradable block copolymers as injectable drug-delivery systems. *Nature*, 388(6645):860–862, 1997.

[124] K. S. Soppimath, T. M. Aminabhavi, A. R. Kulkarni, and W. E. Rudzinski. Biodegradable polymeric nanoparticles as drug delivery devices. *Journal of Controlled Release*, 70(1-2):1–20, 2001.

[125] Q. Y. Hu, T. Kang, J. X. Feng, Q. Q. Zhu, T. Z. Jiang, J. H. Yao, X. G. Jiang, and J. Chen. Tumor microenvironment and angiogenic blood vessels dual-targeting for enhanced anti-glioma therapy. *Acs Applied Materials and Interfaces*, 8(36):23568–23579, 2016.

[126] M. Lattuada and T. A. Hatton. Functionalization of monodisperse magnetic nanoparticles. *Langmuir*, 23(4):2158–2168, 2007.

[127] Y. L. Hsin, K. C. Hwang, and C. T. Yeh. Poly(vinylpyrrolidone)-modified graphite carbon nanofibers as promising supports for ptru catalysts in direct methanol fuel cells. *Journal of the American Chemical Society*, 129(32):9999–10010, 2007.

[128] R. De Palma, S. Peeters, M. J. Van Bael, H. Van den Rul, K. Bonroy, W. Laureyn, J. Mullens, G. Borghs, and G. Maes. Silane ligand exchange to make hydrophobic superparamagnetic nanoparticles water-dispersible. *Chemistry of Materials*, 19(7):1821–1831, 2007.

[129] D. Ciprari, K. Jacob, and R. Tannenbaum. Characterization of polymer nanocomposite interphase and its impact on mechanical properties. *Macromolecules*, 39(19):6565–6573, 2006.

[130] B. Sarmento, D. Ferreira, F. Veiga, and A. Ribeiro. Characterization of insulin-loaded alginate nanoparticles produced by ionotropic pre-gelation through dsc and ftir studies. *Carbohydrate Polymers*, 66(1):1–7, 2006.

[131] S. S. Feng, L. Mu, K. Y. Win, and G. F. Huang. Nanoparticles of biodegradable polymers for clinical administration of paclitaxel. *Current Medicinal Chemistry*, 11(4):413–424, 2004.

[132] Z. P. Zhang and S. S. Feng. Nanoparticles of poly(lactide)/vitamin e tpgs copolymer for cancer chemotherapy: Synthesis, formulation, characterization and in vitro drug release. *Biomaterials*, 27(2):262–270, 2006.

[133] J. D. Blando, R. J. Porcja, and B. J. Turpin. Issues in the quantitation of functional groups by ftir spectroscopic analysis of impactor-collected aerosol samples. *Aerosol Science and Technology*, 35(5):899–908, 2001.

[134] Q. T. H. Shubhra, J. Toth, J. Gyenis, and T. Feczko. Poloxamers for surface modification of hydrophobic drug carriers and their effects on drug delivery. *Polymer Reviews*, 54(1):112–138, 2014.

[135] Marcel Dekker J Bicerano. Prediction of polymer properties. *John Wiley and Sons*, 1:728, 2003.

[136] B. Zhao and W. J. Brittain. Polymer brushes: surface-immobilized macromolecules. *Progress in Polymer Science*, 25(5):677–710, 2000.

[137] Paul J. Flory. Principles of polymer chemistry. *Cornell University Press, Ithaca, NY*, 1981.

[138] K. S. Iyer, B. Zdyrko, H. Malz, J. Pionteck, and I. Luzinov. Polystyrene layers grafted to macromolecular anchoring layer. *Macromolecules*, 36(17):6519–6526, 2003.

[139] M. A. C. Stuart, W. T. S. Huck, J. Genzer, M. Muller, C. Ober, M. Stamm, G. B. Sukhorukov, I. Szleifer, V. V. Tsukruk, M. Urban, F. Winnik, S. Zauscher, I. Luzinov, and S. Minko. Emerging applications of stimuli-responsive polymer materials. *Nature Materials*, 9(2):101–113, 2010.

[140] R. Jenkins, M. K. Burdette, and S. H. Foulger. Mini-review: fluorescence imaging in cancer cells using dye-doped nanoparticles. *Rsc Advances*, 6(70):65459–65474, 2016.

[141] M. K. Burdette, R. Jenkins, Y. Bandera, R. R. Powell, T. F. Bruce, X. Yang, Y. Z. Wei, and S. H. Foulger. Bovine serum albumin coated nanoparticles for in vitro activated fluorescence. *Nanoscale*, 8(48):20066–20073, 2016.

[142] J. X. Li, L. Yang, X. G. Fan, J. Zhang, F. Wang, and Z. Y. Wang. Temperature and glucose dual-responsive carriers bearing poly(n-isopropylacrylamide) and phenylboronic acid for insulin-controlled release: A review. *International Journal of Polymeric Materials and Polymeric Biomaterials*, 66(11):577–587, 2017.

[143] X. Q. Jin, Q. Wang, J. H. Sun, H. Panezail, X. Wu, and S. Y. Bai. Dual temperature- and ph-responsive ibuprofen delivery from poly(n-isopropylacrylamide-co-acrylic acid) nanoparticles and their fractal features. *Polymer Bulletin*, 74(9):3619–3638, 2017.

[144] X. Chen, P. Y. Yuan, Z. N. Liu, Y. K. Bai, and Y. S. Zhou. Dual responsive hydrogels based on functionalized mesoporous silica nanoparticles as an injectable platform for tumor therapy and tissue regeneration. *Journal of Materials Chemistry B*, 5(30):5968–5973, 2017.

[145] J. Skvarla, R. K. Raya, M. Uchman, J. Zednik, K. Prochazka, V. M. Garamus, A. Meristoudi, S. Pispas, and M. Stepanek. Thermoresponsive behavior of poly(n-isopropylacrylamide)s with dodecyl and carboxyl terminal groups in aqueous solution: ph-dependent cloud point temperature. *Colloid and Polymer Science*, 295(8):1343–1349, 2017.

[146] E. Khodaverdi, M. Gharechahi, M. Alibolandi, F. S. M. Tekie, B. Z. Khashyarmanesh, and F. Hadizadeh. Self-assembled supramolecular hydrogel based on pcl-peg-pcl triblock copolymer and -cyclodextrin inclusion complex for sustained delivery of dexamethasone. *International Journal of Pharmaceutical Investigation*, 6(2):78–85, 2016.

[147] I. Roy and M. N. Gupta. Smart polymeric materials: Emerging biochemical applications. *Chemistry and Biology*, 10(12):1161–1171, 2003.

[148] M. A. Daniele, Y. P. Bandera, D. Sharma, P. Rungta, R. Roeder, M. G. Sehorn, and S. H. Foulger. Substrate-baited nanoparticles: A catch and release strategy for enzyme recognition and harvesting. *Small*, 8(13):2083–2090, 2012.

[149] K. Brozewicz and J. Slawinski. 1-(2-mercaptobenzenesulfonyl)-3-hydroxyguanidines - novel potent antiproliferatives, synthesis and in vitro biological activity. *European Journal of Medicinal Chemistry*, 55:384–394, 2012.

[150] B. Zdyrko and I. Luzinov. Polymer brushes by the ”grafting to” method. *Macromolecular Rapid Communications*, 32(12):859–869, 2011.

[151] S. Radin, T. Chen, and P. Ducheyne. The controlled release of drugs from emulsified, sol gel processed silica microspheres. *Biomaterials*, 30(5):850–858, 2009.

[152] Peppas Langer R. Advances in biomaterials, drug delivery, and biotechnology. *AIChE J*, 12(49):2990–3006, 2003.

[153] P. Kortesuo, M. Ahola, M. Kangas, T. Leino, S. Laakso, L. Vuorilehto, A. Yli-Urpo, J. Kiesvaara, and M. Marvola. Alkyl-substituted silica gel as a carrier in the controlled release of dexmedetomidine. *Journal of Controlled Release*, 76(3):227–238, 2001.

[154] M. A. Rauschmann, T. A. Wichelhaus, V. Stirnal, E. Dingeldein, L. Zichner, R. Schnettler, and V. Alt. Nanocrystalline hydroxyapatite and calcium sulphate as biodegradable composite carrier material for local delivery of antibiotics in bone infections. *Biomaterials*, 26(15):2677–2684, 2005.

[155] S. Radin and P. Ducheyne. *Nanostructural control of implantable xerogels for the controlled release of biomolecules*, volume 171. Springer, Dordrecht, 2004.

[156] S. Radin, P. Ducheyne, T. Kamplain, and B. H. Tan. Silica sol-gel for the controlled release of antibiotics. i. synthesis, characterization, and in vitro release. *Journal of Biomedical Materials Research*, 57(2):313–320, 2001.

[157] K. E. Anderson, L. A. Eliot, B. R. Stevenson, and J. A. Rogers. Formulation and evaluation of a folic acid receptor-targeted oral vancomycin liposomal dosage form. *Pharmaceutical Research*, 18(3):316–322, 2001.

[158] A. Baral, S. Roy, A. Dehsorkhi, I. W. Hamley, S. Mohapatra, S. Ghosh, and A. Banerjee. Assembly of an injectable noncytotoxic peptide-based hydrogelator for sustained release of drugs. *Langmuir*, 30(3):929–936, 2014.

[159] F. Ye, H. F. Guo, H. J. Zhang, and X. L. He. Polymeric micelle-templated synthesis of hydroxyapatite hollow nanoparticles for a drug delivery system. *Acta Biomaterialia*, 6(6):2212–2218, 2010.

[160] G. M. Sheldrick, P. G. Jones, O. Kennard, D. H. Williams, and G. A. Smith. Structure of vancomycin and its complex with acetyl-d-alanyl-d-alanine. *Nature*, 271(5642):223–225, 1978.

[161] M. Ge, Z. Chen, H. R. Onishi, J. Kohler, L. L. Silver, R. Kerns, S. Fukuzawa, C. Thompson, and D. Kahne. Vancomycin derivatives that inhibit peptidoglycan biosynthesis without binding d-ala-d-ala. *Science*, 284(5413):507–511, 1999.

[162] H. R. Bakhsheshi-Rad, E. Hamzah, A. F. Ismail, M. Aziz, Z. Hadisi, M. Kashefian, and A. Najafinezhad. Novel nanostructured baghdadite-vancomycin scaffolds: In-vitro drug release, antibacterial activity and biocompatibility. *Materials Letters*, 209:369–372, 2017.

[163] E. Cevher, Z. Orhan, L. Mulazimoglu, D. Sensoy, M. Alper, A. Yildiz, and Y. Ozsoy. Characterization of biodegradable chitosan microspheres containing vancomycin and treatment of experimental osteomyelitis caused by methicillin-resistant staphylococcus aureus with prepared microspheres. *International Journal of Pharmaceutics*, 317(2):127–135, 2006.

[164] H. W. Kim, J. C. Knowles, and H. E. Kim. Hydroxyapatite porous scaffold engineered with biological polymer hybrid coating for antibiotic vancomycin release. *Journal of Materials Science-Materials in Medicine*, 16(3):189–195, 2005.

[165] A. M. Le Ray, S. Chiffoleau, P. Iooss, G. Grimandi, A. Gouyette, G. Daculsi, and C. Merle. Vancomycin encapsulation in biodegradable poly(epsilon-caprolactone) microparticles for bone implantation. influence of the formulation process on size, drug loading, in vitro release and cytocompatibility. *Biomaterials*, 24(3):443–449, 2003.

[166] D. D. Evanoff, S. E. Hayes, Y. Ying, G. H. Shim, J. R. Lawrence, J. B. Carroll, R. D. Roeder, J. M. Houchins, C. E. Huebner, and S. H. Foulger. Functionalization of crystalline colloidal arrays through click chemistry. *Advanced Materials*, 19(21):3507–+.

[167] L. Rumian, H. Tiainen, U. Cibor, M. Krok-Borkowicz, M. Brzychczy-Wloch, H. J. Haugen, and E. Pamula. Ceramic scaffolds with immobilized vancomycin-loaded poly(lactide-co-glycolide) microparticles for bone defects treatment. *Materials Letters*, 190:67–70, 2017.

[168] M. Parent, A. Magnaudeix, S. Delebassee, E. Sarre, E. Champion, M. V. Trecant, and C. Damia. Hydroxyapatite microporous bioceramics as vancomycin reservoir: Antibacterial efficiency and biocompatibility investigation. *Journal of Biomaterials Applications*, 31(4):488–498, 2016.

Appendices

Appendix A BET analysis

Quantachrome® ASiQwin™- Automated Gas Sorption Data
Acquisition and Reduction
© 1994-2014, Quantachrome Instruments
version 4.0

Analysis				**Report**			
Operator:	qa	**Date:**	2017/01/05	**Operator:**	qa	**Date:**	2017/01/05
Sample ID:	oleksak 20nm second run	**Filename:**		Oleksak 20170105.qps			
Sample Desc:	using sample mass as specified by customer	**Comment:**		Oleksandr Klep BET Sample 20nm particles second run			
Sample Weight:	0.009 g	**Instrument:**		Autosorb iQ Station 1			
Outgas Time:	10.0 hrs	**Outgas Temp.:**		70 °C			
Analysis gas:	Nitrogen	**Non-ideality:**		6.58e-05 1/Torr	**CellType:**		6mm w/o rod
Analysis Time:	1:52 hr:min	**Bath temp.:**		77.35 K			
Analysis Mode:	Standard				**VoidVol Remeasure:**		off
VoidVol. Mode:	He Measure	**Cold Zone V:**		6.47467 cc	**Warm Zone V:**		7.56042 cc

Multi-Point BET

Data Reduction Parameters Data

Adsorbate model	**Thermal Transpiration:** on	**Eff. mol. diameter (D):** 3.54 Å		**Eff. cell stem diam. (d):** 4.0000 mm	
	Nitrogen	**Temperature**	77.350K		
	Molec. Wt.: 28.013	**Cross Section:**	16.200 Å²	**Liquid Density:**	0.808 g/cc

Multi-Point BET Data

Relative Pressure [P/Po]	Volume @ STP [cc/g]	1 / [W((Po/P) - 1)] [1/g]	Relative Pressure [P/Po]	Volume @ STP [cc/g]	1 / [W((Po/P) - 1)] [1/g]
1.28746e-01	33.5789	3.5210e+00	2.28716e-01	44.8970	5.2846e+00
1.53710e-01	36.5363	3.9775e+00	2.53726e-01	47.6130	5.7133e+00
1.78667e-01	39.4598	4.4108e+00	2.78792e-01	50.3100	6.1478e+00
2.03906e-01	42.2978	4.8450e+00			

BET summary

Slope =	17.460 1/g
Intercept =	1.285e+00 1/g
Correlation coefficient, r =	0.999970
C constant=	14.583
Surface Area =	185.783 m²/g

Appendix B Poloxamer modification two end probability table

A	B	C	D	E	F	G
MeSO3	unmod OH	unmod react probab	1 mod react probab	unmod chains left	end amount with 1 mod	end amount with 2 mod
40	200	0	0	100	0	0
39	198	1	0	99	1	0
38	197.0050251	0.994974874	0.005025126	98.00502513	1.989949749	0.005025126
37	196.0150251	0.99	0.01	97.01502513	2.969949749	0.015025126
36	195.0299506	0.985074502	0.014925498	96.02995062	3.940098754	0.029950623
35	194.0497531	0.980197528	0.019802472	95.04975309	4.90049381	0.049753095
34	193.0743849	0.975368245	0.024631755	94.07438485	5.8512303	0.07438485
33	192.103799	0.970585838	0.029414162	93.10379901	6.792401975	0.103799012
32	191.1379495	0.965849514	0.034150486	92.1379495	7.724101003	0.137949499
31	190.176791	0.961158497	0.038841503	91.176791	8.646417996	0.176791002
30	189.220279	0.956512029	0.043487971	90.22027897	9.559442054	0.220278973
29	188.2683696	0.95190937	0.04809063	89.2683696	10.46326079	0.268369603
28	187.3210198	0.947349796	0.052650204	88.32101981	11.35796039	0.321019807
27	186.3781872	0.942832602	0.057167398	87.37818721	12.24362559	0.378187205
26	185.4398301	0.938357095	0.061642905	86.43983011	13.12033978	0.43983011
25	184.5059075	0.9339226	0.0660774	85.50590751	13.98818498	0.50590751
24	183.5763791	0.929528457	0.070471543	84.57637905	14.84724189	0.576379053
23	182.651205	0.92517402	0.07482598	83.65120503	15.69758993	0.651205033
22	181.7303464	0.920858657	0.079141343	82.73034638	16.53930725	0.730346376
21	180.8137646	0.916581751	0.083418249	81.81376462	17.37247075	0.813764625
20	179.9014219	0.912342698	0.087657302	80.90142193	18.19715615	0.901421927
19	178.993281	0.908140905	0.091859095	79.99328102	19.01343796	0.993281022
18	178.0893052	0.903975794	0.096024206	79.08930523	19.82138954	1.089305228
17	177.1894584	0.899846799	0.100153201	78.18945843	20.62108314	1.189458429
16	176.2937051	0.895753366	0.104246634	77.29370506	21.41258987	1.293705063
15	175.4020101	0.891694951	0.108305049	76.40201011	22.19597978	1.402010111
14	174.5143391	0.887671024	0.112328976	75.51433909	22.97132183	1.514339087
13	173.630658	0.883681065	0.116318935	74.63065802	23.73868396	1.630658022
12	172.7509335	0.879724563	0.120275437	73.75093346	24.49813308	1.75093346
11	171.8751324	0.875801019	0.124198981	72.87513244	25.24973512	1.875132441
10	171.0032225	0.871909945	0.128090055	72.0032225	25.99355501	2.003222496
9	170.1351716	0.868050862	0.131949138	71.13517163	26.72965673	2.135171634
8	169.2709483	0.8642233	0.1357767	70.27094833	27.45810333	2.270948334
7	168.4105215	0.8604268	0.1395732	69.41052153	28.17895693	2.410521534
6	167.5538606	0.85666091	0.14333909	68.55386062	28.89227875	2.553860624
5	166.7009354	0.852925189	0.147074811	67.70093543	29.59812913	2.700935435
4	165.8517162	0.849219204	0.150780796	66.85171623	30.29656754	2.85171623
3	165.0061737	0.845542531	0.154457469	66.0061737	30.9876526	3.0061737
2	164.1642789	0.841894752	0.158105248	65.16427895	31.6714421	3.164278948
1	163.3260035	0.838275459	0.161724541	64.32600349	32.34799302	3.326003489
0	162.4913192	0.834684252	0.165315748	63.49131924	33.01736153	3.491319237

B45=B44-C45 C45=A44*B44/(A44*B44+C44*A44) D45=F44*A44/(A44*B44+F44*A44) E45=E44-C45 F45=F44+C45-D45 G45=G44+D45

Figure 1: Probability of one and two end modification with azide group for poloxamer as described in Chapter 4, probability calculations are based on the loading ratio that was used for the reaction, higher loading ratio would lead to a much higher probability of dual end modified poloxamer creating a high probability to crosslink multiple particles together.

Appendix C NMR data

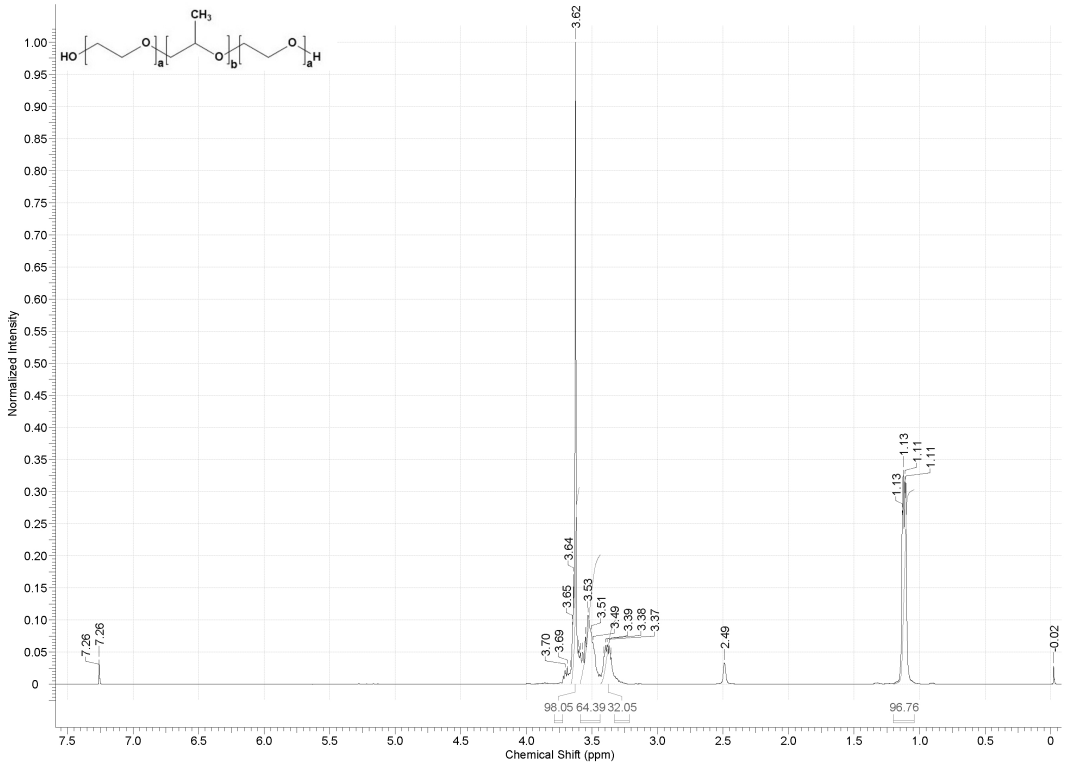

Figure 2: ^{1}HNMR spectra of Pluronic L64 as received. δ 1.11 (32) CH_3 groups from PPO block, δ 3.38 (32) CH groups in PPO block, δ 3.53 (32) CH_2 groups from PPO block, δ 3.64 (48) CH_2 groups from both PEO blocks.

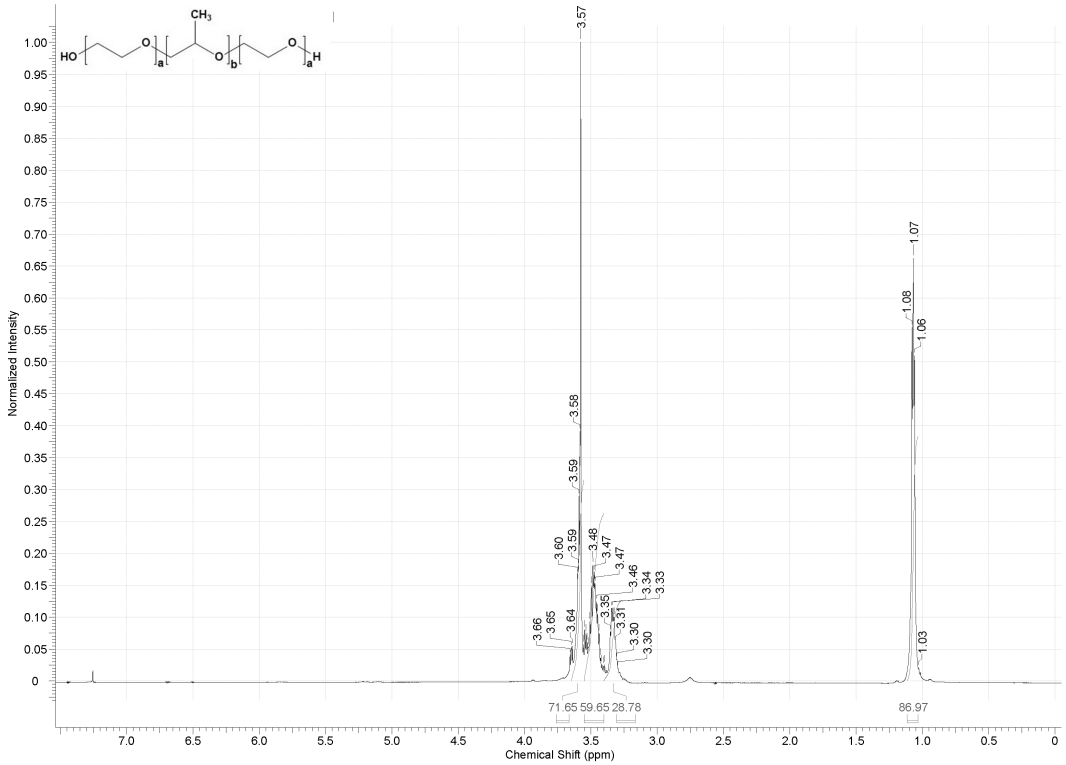

Figure 3: ^{1}HNMR spectra of Pluronic L64 as received. δ 1.07 (29) CH_3 groups from PPO block, δ 3.33 (29) CH groups in PPO block, δ 3.47 (29) CH_2 groups from PPO block, δ 3.57 (36) CH_2 groups from both PEO blocks.

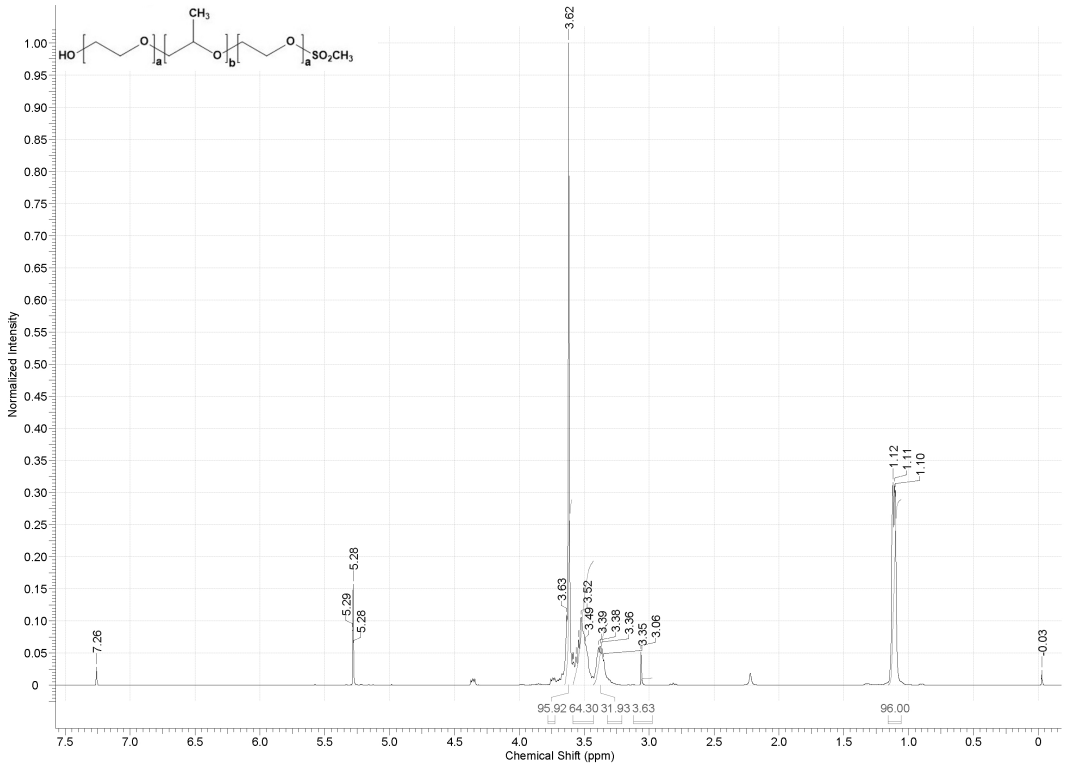

Figure 4: ^{1}HNMR spectra of Pluronic L64 as received. δ 1.11 (32) CH_3 groups from PPO block, δ 3.06 (1) CH_3 group from $MeSO_2$ group, δ 3.38 (32) CH groups in PPO block, δ 3.52 (32) CH_2 groups from PPO block, δ 3.62 (48) CH_2 groups from both PEO blocks.

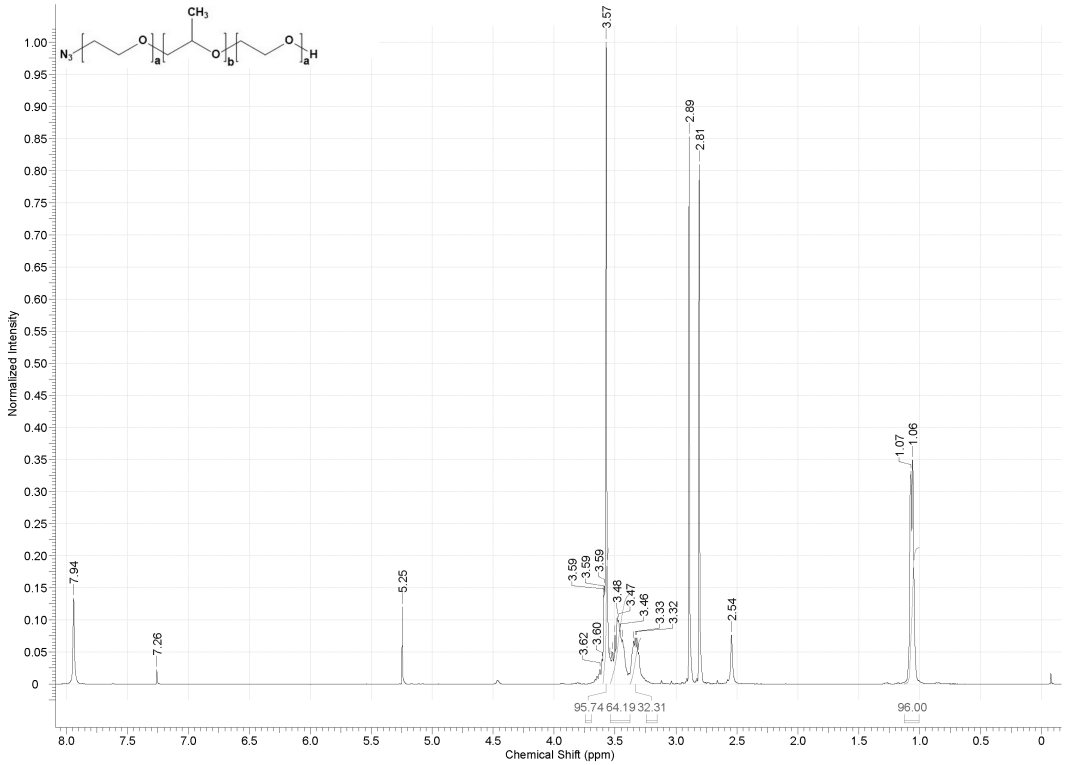

Figure 5: ^{1}HNMR spectra of Pluronic L64 as received. δ 1.06 (32) CH_3 groups from PPO block, δ 3.33 (32) CH groups in PPO block, δ 3.47 (32) CH_2 groups from PPO block, δ 3.57 (48) CH_2 groups from both PEO blocks.

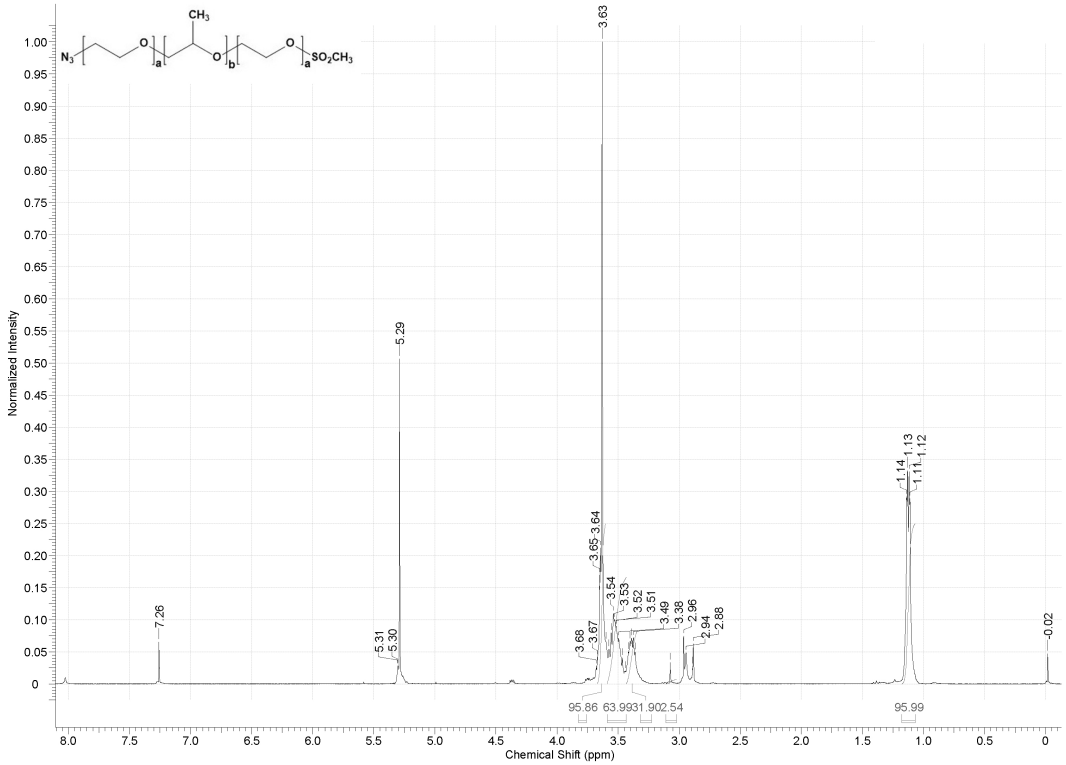

Figure 6: [1]HNMR spectra of Pluronic L64 as received. δ 1.13 (32) CH_3 groups from PPO block, δ 3.07 (1) CH_3 group from $MeSO_2$ group, δ 3.38 (32) CH groups in PPO block, δ 3.54 (32) CH_2 groups from PPO block, δ 3.63 (48) CH_2 groups from both PEO blocks.

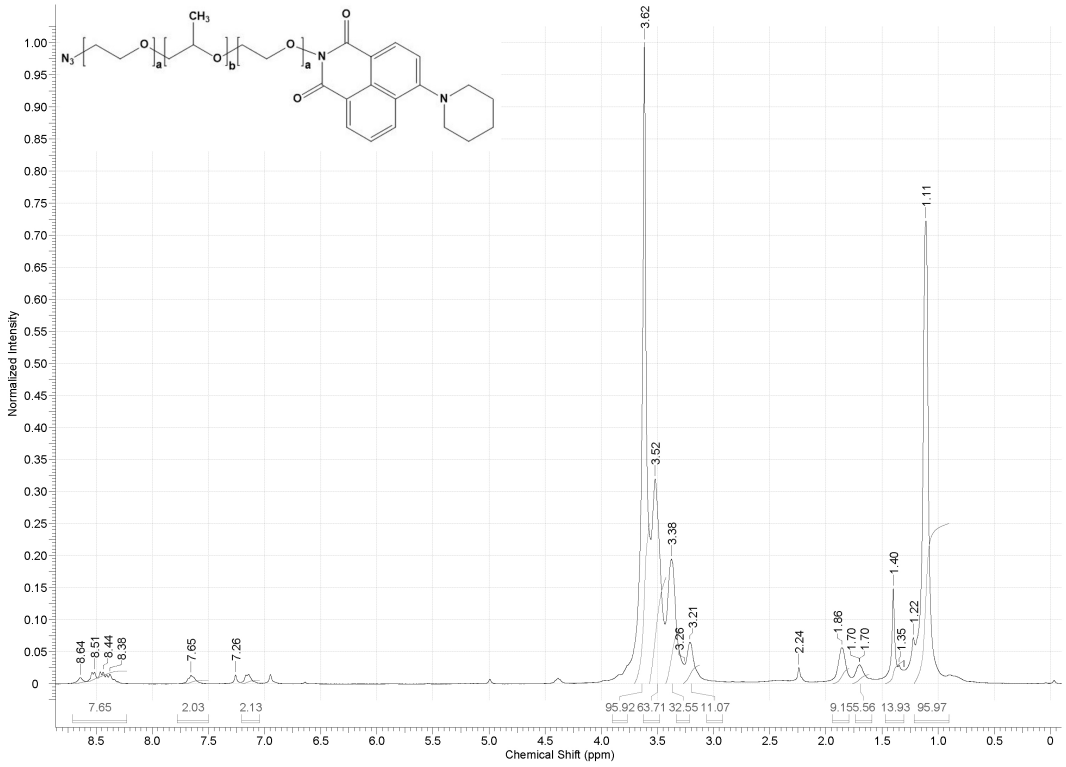

Figure 7: ^{1}HNMR spectra of Pluronic L64 as received. δ 1.11 (32) CH_3 groups from PPO block, δ 3.38 (32) CH groups in PPO block, δ 3.52 (32) CH_2 groups from PPO block, δ 3.62 (48) CH_2 groups from both PEO blocks, δ 1.40, 1.70, 1.86, 3.21, 7,14, 7.65, 8.38-8.64 Naphthalimide signals .

Appendix D Copyright permission

ELSEVIER LICENSE
TERMS AND CONDITIONS

Mar 05, 2018

This Agreement between Clemson University -- Oleksandr Klep ("You") and Elsevier ("Elsevier") consists of your license details and the terms and conditions provided by Elsevier and Copyright Clearance Center.

License Number	4302590603673
License date	Mar 05, 2018
Licensed Content Publisher	Elsevier
Licensed Content Publication	Advanced Drug Delivery Reviews
Licensed Content Title	Design and fabrication of magnetic nanoparticles for targeted drug delivery and imaging
Licensed Content Author	Omid Veiseh,Jonathan W. Gunn,Miqin Zhang
Licensed Content Date	Mar 8, 2010
Licensed Content Volume	62
Licensed Content Issue	3
Licensed Content Pages	21
Start Page	284
End Page	304
Type of Use	reuse in a thesis/dissertation
Portion	figures/tables/illustrations
Number of figures/tables/illustrations	1
Format	both print and electronic
Are you the author of this Elsevier article?	No
Will you be translating?	No
Original figure numbers	Figure 3 on page 288. (Fig. 3. Illustration of multifunctional imaging/therapeutic MNPs anatomy.....)
Title of your thesis/dissertation	PROGRAMMING OF RETENTION CAPACITY AND RELEASE CAPABILITIES OF PROPARGYL ACRYLATE NANOPARTICLES DECORATED WITH POLOXAMER COPOLYMER
Expected completion date	Apr 2018
Estimated size (number of pages)	120
Requestor Location	Clemson University 91 Technology dr. Office 149 EVERGREEN HILLS, SC 29625 United States Attn: Oleksandr Klep
Publisher Tax ID	98-0397604
Total	0.00 USD

Terms and Conditions

INTRODUCTION

1. The publisher for this copyrighted material is Elsevier. By clicking "accept" in connection with completing this licensing transaction, you agree that the following terms and conditions apply to this transaction (along with the Billing and Payment terms and conditions established by Copyright Clearance Center, Inc. ("CCC"), at the time that you opened your Rightslink account and that are available at any time at http://myaccount.copyright.com).

GENERAL TERMS

2. Elsevier hereby grants you permission to reproduce the aforementioned material subject to the terms and conditions indicated.

3. Acknowledgement: If any part of the material to be used (for example, figures) has appeared in our publication with credit or acknowledgement to another source, permission must also be sought from that source. If such permission is not obtained then that material may not be included in your publication/copies. Suitable acknowledgement to the source must be made, either as a footnote or in a reference list at the end of your publication, as follows:

"Reprinted from Publication title, Vol /edition number, Author(s), Title of article / title of chapter, Pages No., Copyright (Year), with permission from Elsevier [OR APPLICABLE SOCIETY COPYRIGHT OWNER]." Also Lancet special credit - "Reprinted from The Lancet, Vol. number, Author(s), Title of article, Pages No., Copyright (Year), with permission from Elsevier."

4. Reproduction of this material is confined to the purpose and/or media for which permission is hereby given.

5. Altering/Modifying Material: Not Permitted. However figures and illustrations may be altered/adapted minimally to serve your work. Any other abbreviations, additions, deletions and/or any other alterations shall be made only with prior written authorization of Elsevier Ltd. (Please contact Elsevier at permissions@elsevier.com). No modifications can be made to any Lancet figures/tables and they must be reproduced in full.

6. If the permission fee for the requested use of our material is waived in this instance, please be advised that your future requests for Elsevier materials may attract a fee.

7. Reservation of Rights: Publisher reserves all rights not specifically granted in the combination of (i) the license details provided by you and accepted in the course of this licensing transaction, (ii) these terms and conditions and (iii) CCC's Billing and Payment terms and conditions.

8. License Contingent Upon Payment: While you may exercise the rights licensed immediately upon issuance of the license at the end of the licensing process for the transaction, provided that you have disclosed complete and accurate details of your proposed use, no license is finally effective unless and until full payment is received from you (either by publisher or by CCC) as provided in CCC's Billing and Payment terms and conditions. If full payment is not received on a timely basis, then any license preliminarily granted shall be deemed automatically revoked and shall be void as if never granted. Further, in the event that you breach any of these terms and conditions or any of CCC's Billing and Payment terms and conditions, the license is automatically revoked and shall be void as if never granted. Use of materials as described in a revoked license, as well as any use of the materials beyond the scope of an unrevoked license, may constitute copyright infringement and publisher reserves the right to take any and all action to protect its copyright in the materials.

9. Warranties: Publisher makes no representations or warranties with respect to the licensed material.

10. Indemnity: You hereby indemnify and agree to hold harmless publisher and CCC, and their respective officers, directors, employees and agents, from and against any and all claims arising out of your use of the licensed material other than as specifically authorized pursuant to this license.

11. No Transfer of License: This license is personal to you and may not be sublicensed, assigned, or transferred by you to any other person without publisher's written permission.
12. No Amendment Except in Writing: This license may not be amended except in a writing signed by both parties (or, in the case of publisher, by CCC on publisher's behalf).
13. Objection to Contrary Terms: Publisher hereby objects to any terms contained in any purchase order, acknowledgment, check endorsement or other writing prepared by you, which terms are inconsistent with these terms and conditions or CCC's Billing and Payment terms and conditions. These terms and conditions, together with CCC's Billing and Payment terms and conditions (which are incorporated herein), comprise the entire agreement between you and publisher (and CCC) concerning this licensing transaction. In the event of any conflict between your obligations established by these terms and conditions and those established by CCC's Billing and Payment terms and conditions, these terms and conditions shall control.
14. Revocation: Elsevier or Copyright Clearance Center may deny the permissions described in this License at their sole discretion, for any reason or no reason, with a full refund payable to you. Notice of such denial will be made using the contact information provided by you. Failure to receive such notice will not alter or invalidate the denial. In no event will Elsevier or Copyright Clearance Center be responsible or liable for any costs, expenses or damage incurred by you as a result of a denial of your permission request, other than a refund of the amount(s) paid by you to Elsevier and/or Copyright Clearance Center for denied permissions.

LIMITED LICENSE

The following terms and conditions apply only to specific license types:
15. **Translation**: This permission is granted for non-exclusive world **English** rights only unless your license was granted for translation rights. If you licensed translation rights you may only translate this content into the languages you requested. A professional translator must perform all translations and reproduce the content word for word preserving the integrity of the article.
16. **Posting licensed content on any Website**: The following terms and conditions apply as follows: Licensing material from an Elsevier journal: All content posted to the web site must maintain the copyright information line on the bottom of each image; A hyper-text must be included to the Homepage of the journal from which you are licensing at http://www.sciencedirect.com/science/journal/xxxxx or the Elsevier homepage for books at http://www.elsevier.com; Central Storage: This license does not include permission for a scanned version of the material to be stored in a central repository such as that provided by Heron/XanEdu.
Licensing material from an Elsevier book: A hyper-text link must be included to the Elsevier homepage at http://www.elsevier.com . All content posted to the web site must maintain the copyright information line on the bottom of each image.

Posting licensed content on Electronic reserve: In addition to the above the following clauses are applicable: The web site must be password-protected and made available only to bona fide students registered on a relevant course. This permission is granted for 1 year only. You may obtain a new license for future website posting.
17. **For journal authors:** the following clauses are applicable in addition to the above:
Preprints:
A preprint is an author's own write-up of research results and analysis, it has not been peer-reviewed, nor has it had any other value added to it by a publisher (such as formatting, copyright, technical enhancement etc.).
Authors can share their preprints anywhere at any time. Preprints should not be added to or enhanced in any way in order to appear more like, or to substitute for, the final versions of articles however authors can update their preprints on arXiv or RePEc with their Accepted Author Manuscript (see below).

If accepted for publication, we encourage authors to link from the preprint to their formal publication via its DOI. Millions of researchers have access to the formal publications on ScienceDirect, and so links will help users to find, access, cite and use the best available version. Please note that Cell Press, The Lancet and some society-owned have different preprint policies. Information on these policies is available on the journal homepage.
Accepted Author Manuscripts: An accepted author manuscript is the manuscript of an article that has been accepted for publication and which typically includes author-incorporated changes suggested during submission, peer review and editor-author communications.
Authors can share their accepted author manuscript:

- immediately
  - via their non-commercial person homepage or blog
  - by updating a preprint in arXiv or RePEc with the accepted manuscript
  - via their research institute or institutional repository for internal institutional uses or as part of an invitation-only research collaboration work-group
  - directly by providing copies to their students or to research collaborators for their personal use
  - for private scholarly sharing as part of an invitation-only work group on commercial sites with which Elsevier has an agreement
- After the embargo period
  - via non-commercial hosting platforms such as their institutional repository
  - via commercial sites with which Elsevier has an agreement

In all cases accepted manuscripts should:

- link to the formal publication via its DOI
- bear a CC-BY-NC-ND license - this is easy to do
- if aggregated with other manuscripts, for example in a repository or other site, be shared in alignment with our hosting policy not be added to or enhanced in any way to appear more like, or to substitute for, the published journal article.

Published journal article (JPA): A published journal article (PJA) is the definitive final record of published research that appears or will appear in the journal and embodies all value-adding publishing activities including peer review co-ordination, copy-editing, formatting, (if relevant) pagination and online enrichment.
Policies for sharing publishing journal articles differ for subscription and gold open access articles:
Subscription Articles: If you are an author, please share a link to your article rather than the full-text. Millions of researchers have access to the formal publications on ScienceDirect, and so links will help your users to find, access, cite, and use the best available version.
Theses and dissertations which contain embedded PJAs as part of the formal submission can be posted publicly by the awarding institution with DOI links back to the formal publications on ScienceDirect.
If you are affiliated with a library that subscribes to ScienceDirect you have additional private sharing rights for others' research accessed under that agreement. This includes use for classroom teaching and internal training at the institution (including use in course packs and courseware programs), and inclusion of the article for grant funding purposes.
Gold Open Access Articles: May be shared according to the author-selected end-user license and should contain a CrossMark logo, the end user license, and a DOI link to the formal publication on ScienceDirect.
Please refer to Elsevier's posting policy for further information.
18. **For book authors** the following clauses are applicable in addition to the above:
Authors are permitted to place a brief summary of their work online only. You are not

allowed to download and post the published electronic version of your chapter, nor may you scan the printed edition to create an electronic version. **Posting to a repository:** Authors are permitted to post a summary of their chapter only in their institution's repository.
19. **Thesis/Dissertation**: If your license is for use in a thesis/dissertation your thesis may be submitted to your institution in either print or electronic form. Should your thesis be published commercially, please reapply for permission. These requirements include permission for the Library and Archives of Canada to supply single copies, on demand, of the complete thesis and include permission for Proquest/UMI to supply single copies, on demand, of the complete thesis. Should your thesis be published commercially, please reapply for permission. Theses and dissertations which contain embedded PJAs as part of the formal submission can be posted publicly by the awarding institution with DOI links back to the formal publications on ScienceDirect.

Elsevier Open Access Terms and Conditions
You can publish open access with Elsevier in hundreds of open access journals or in nearly 2000 established subscription journals that support open access publishing. Permitted third party re-use of these open access articles is defined by the author's choice of Creative Commons user license. See our open access license policy for more information.
Terms & Conditions applicable to all Open Access articles published with Elsevier:
Any reuse of the article must not represent the author as endorsing the adaptation of the article nor should the article be modified in such a way as to damage the author's honour or reputation. If any changes have been made, such changes must be clearly indicated.
The author(s) must be appropriately credited and we ask that you include the end user license and a DOI link to the formal publication on ScienceDirect.
If any part of the material to be used (for example, figures) has appeared in our publication with credit or acknowledgement to another source it is the responsibility of the user to ensure their reuse complies with the terms and conditions determined by the rights holder.
Additional Terms & Conditions applicable to each Creative Commons user license:
CC BY: The CC-BY license allows users to copy, to create extracts, abstracts and new works from the Article, to alter and revise the Article and to make commercial use of the Article (including reuse and/or resale of the Article by commercial entities), provided the user gives appropriate credit (with a link to the formal publication through the relevant DOI), provides a link to the license, indicates if changes were made and the licensor is not represented as endorsing the use made of the work. The full details of the license are available at http://creativecommons.org/licenses/by/4.0.
CC BY NC SA: The CC BY-NC-SA license allows users to copy, to create extracts, abstracts and new works from the Article, to alter and revise the Article, provided this is not done for commercial purposes, and that the user gives appropriate credit (with a link to the formal publication through the relevant DOI), provides a link to the license, indicates if changes were made and the licensor is not represented as endorsing the use made of the work. Further, any new works must be made available on the same conditions. The full details of the license are available at http://creativecommons.org/licenses/by-nc-sa/4.0.
CC BY NC ND: The CC BY-NC-ND license allows users to copy and distribute the Article, provided this is not done for commercial purposes and further does not permit distribution of the Article if it is changed or edited in any way, and provided the user gives appropriate credit (with a link to the formal publication through the relevant DOI), provides a link to the license, and that the licensor is not represented as endorsing the use made of the work. The full details of the license are available at http://creativecommons.org/licenses/by-nc-nd/4.0.
Any commercial reuse of Open Access articles published with a CC BY NC SA or CC BY NC ND license requires permission from Elsevier and will be subject to a fee.
Commercial reuse includes:

- Associating advertising with the full text of the Article
- Charging fees for document delivery or access

- Article aggregation
- Systematic distribution via e-mail lists or share buttons

Posting or linking by commercial companies for use by customers of those companies.

20. **Other Conditions**:

v1.9

Questions? customercare@copyright.com or +1-855-239-3415 (toll free in the US) or +1-978-646-2777.